An Experimental/Modeling Study of Jet Attachment during Counterflow Thrust Vectoring

* FINAL REPORT *
NASA/NAG1-1736

Grant Period
1 July, 1995 — 30 June, 1996

Principal Investigator
Paul J. Strykowski
Associate Professor

An Experimental/Modeling Study of Jet Attachment during Counterflow Thrust Vectoring

* FINAL REPORT *
NASA/NAG1-1736

Grant Period
1 July, 1995 — 30 June, 1996

Principal Investigator
Paul J. Strykowski
Associate Professor

An Experimental/Modeling Study of Jet Attachment during Counterflow Thrust Vectoring

* FINAL REPORT *

Principal Investigator:	Paul J. Strykowski, Associate Professor
Grant Period:	1 July, 1995 — 30 June, 1996
Institution Address:	Department of Mechanical Engineering 125 Mech. Engr. 111 Church Street SE University of Minnesota Minneapolis, MN 55455

NASA AGENCY:	NASA — Langley
GRANT NO:	NASA/NAG1-1736
Technical Officer:	David J. Wing
Grants Officer:	Joseph Murray

Executive Summary

A joint modeling and experimental study was carried out to examine the jet attachment process which exists during CounterFlow Thrust Vectoring (CFTV). The primary jet operating conditions investigated were for jet exit Mach numbers less than 0.5 and for jet stagnation temperatures near ambient conditions (nominally 300 Kelvin). Modeling of the jet attachment process assumed the flow to be ideally two dimensional. The theoretical findings were then compared to experimental results obtained in a 4-to-1 aspect ratio rectangular jet which was shown to be nominally two-dimensional. Comparisons between the model predictions and experiment, as summarized below, were quite satisfactory, but were limited to shock free flow. Extensions of the modeling and experimental work to shock containing flows is highly desirable, but was not addressed in detail during the course of this study.

Experimental studies of jet behavior in the proximity to a curved Coanda surface, performed in our laboratory and summarized in Section §1 of this report, indicated that the streamwise development of the attached jet (relative to its curved path) was not significantly affected by the presence of the wall. This observation lead to the model simplification that the streamwise jet development would be assumed to follow that of free turbulent jets, for which significant data were available. Consequently, the jet was modeled as consisting of a potential core surrounded by compressible turbulent shear layers, which experienced transverse growth depending on the velocity ratio, density ratio and convective Mach number of the shear layer. After the shear layer merging process, coincident with the termination of the jet potential core, the jet undergoes transition to its far field turbulent state. Modeling of this transitional regime was found to be unnecessary in the present investigation since jet attachment occurred upstream of this region.

Conservative equations of mass and momentum were used to evaluate the location where the subsonic jet would attach to the adjacent surface as a function of a number of geometrical parameters including: 1) the radius of curvature of the curved surface; 2) the downstream extent of the surface; and 3) the transverse displacement of the surface relative to the jet axis. Modeling of jet attachment was

formulated through a coupled set of nonlinear equations which were solved iteratively using the EES software package. The model was used to predict the distance downstream of the jet exit where attachment occurred on the curved surface, as well as the "bubble" pressure developed in the region of separation immediately downstream and off-axis of the jet exit. The model also accommodated input parameters including jet Mach number, jet stagnation temperature, and secondary mass flow ratio, where both coflowing and counterflowing conditions could be studied. A summary of jet modeling can be found in Section §2 of this report.

The experimental apparatus and facilities used to examine jet attachment are described in Section §3 of this report. Identifying the location of jet attachment to the curved collar surface was done through two independent means, first through a flow visualization study using oil and lamp-black and, second using surface pressure surveys. Surface pressures were particularly useful in identifying a local peak in the wall pressure due to stagnation of the jet fluid on the collar. Comparisons of the experimental results to model predictions were quite encouraging, as were model-experimental comparisons of bubble pressure for various levels of counterflow. A collar-truncation study was also performed to assess whether the analytical model could successfully predict the effect of shortening the collar — an important consideration from an external drag standpoint. In all aspects, the jet attachment model proved to be quite robust and predictive of the experimental trends, but limited at this time to shock free flow fields. The study suggested that the jet attachment process could be avoided by two principal means, namely collar truncation and pressure release. In the first method, attachment can be avoided if the collar is truncated at a length less than L_{att}, which is the streamwise distance at which jet attachment would occur. This approach is undoubtedly conservative, but is passive and hence attractive from an operational standpoint. The second approach requires that a pressure release system be designed which will prevent the bubble pressure from exceeding a critical vacuum level. During attachment, the jet fluid must turn over a relatively small radius of curvature, giving rise to a significant vacuum pressure relative to the pressures experienced during unattached operation. If fluid is bled into the bubble region — either by passive or active control means — to

prevent large vacuum pressures, jet attachment will not occur. A complete description of the model and experimental results can be found in Section §4.

Designing an optimal nozzle-collar system to avoid jet attachment is necessarily subjective owing to the rather large parametric space involved. Although collar optimization was not a primary objective of this research, a design study was undertaken to evaluate a candidate collar which minimized external drag power and secondary pumping power, while maintaining attachment free jet vectoring; see Section §5. One of the difficult modeling issues encountered was the accurate assessment of pressure drop experienced by the secondary fluid passing along the collar surface. This pressure drop is dominated by the turbulent shear stresses along the countercurrent mixing layer. Although pumping power is increased by shear and turbulent stresses, the frictional nature of the fluid in the secondary flow path is vital to avoid choking, which would occur at a pressure ratio near two for isentropic flow conditions; significantly higher pressure ratios can be supported by frictional Fanno flow along the secondary flow path. Much more extensive research of the mean and turbulent flow field characteristics of curved countercurrent shear layers needs to be done to address this question.

This research has attempted to provide a more complete fundamental understanding of the fluid mechanical and geometrical parameters responsible for the attachment of a jet stream to an adjacent Coanda surface. The agreement between model predictions and experiments was quite encouraging, but it must be remembered that only preliminary results were provided in the shock-containing flow regime, which from a practical standpoint is where more fundamental understanding is critical to further development of CFTV control. In the closing period of our work, we began to understand the nature of the overall design process which we believe is needed to properly design a CFTV system. In particular, the designer must be able to exploit the collar geometry to attain attachment free operation over a significant range of flow conditions, while providing a high level of confidence that jet attachment can be avoided. The proper design must incorporate the following fundamental nature of CFTV operation. The primary jet which exhausts along the extended collar surface is itself a pump capable of either entraining large amounts of secondary fluid or generating vacuum, or combinations thereof, depending on flow and geometric conditions. Working against the pumping action of the

primary jet, is the secondary vacuum system (which itself may be driven by e.g. a jet ejector pump). Hence, one must property match the performance curves of *continuous* CFTV and that of *attached* CFTV, with the vacuum pump performance characteristics. One can then envision a family of such design curves which could be applied over a wide range of nozzle pressure ratios, or jet operating temperatures as the system requirements demand.

Abstract:

Recent studies, have shown the applicability of vectoring rectangular jets using asymmetrically applied counterflow in the presence of a short collar. This novel concept has applications in the aerospace industry where counterflow can be used to vector the thrust of a jet's exhaust, shortening take-off and landing distances and enhancing in-flight maneuverability of the aircraft. Counterflow thrust vectoring, "CFTV", is desirable due to its fast time response, low thrust loss, and absence of moving parts. However, implementation of a CFTV system is only possible if bistable jet attachment can be prevented. This can be achieved by properly designing the geometry of the collar. An analytical model is developed herein to predict the conditions under which a two-dimensional jet will attach to an offset curved wall. Results from this model are then compared with experiment; for various jet exit Mach numbers, collar offset distances, and radii of curvature. Their excellent correlation permits use of the model as a tool for designing a CFTV system.

Table of Contents

List of Figures

Figure 2.5 Experimentally measured, bubble pressure, P_B, and collar stagnation pressure, P_I, averaged over a range of Mach numbers from 0.15 to 0.52, and plotted vs. gap width, G/H, for a R/H = 5 collar. Plotted using solid lines are the predictions given by the model.

Figure 2.6 Experimentally measured axial velocity distribution for unvectored jet M=0.5 jet. Velocity measurements were taken along the centerline of the jet using a pitot tube. It is difficult to obtain precise values of c_L, using this plot, due to ambiguities about the definition. Subsequent measurements using entrainment data give c_L = 7.3.

Figure 2.7 Diagram illustrating the definition of vorticity based shear layer thickness δ_ω, which is the thickness an equivalent layer would be if it had a uniform shear stress equal in magnitude to the shear layer in question.

Figure 2.8 Schematic of the secondary flow passage. To compute the level of counterflow, the flow is treated as a turbulent channel flow. Pipe geometry is a function of the geometry of the collar and the exit vector angle. An empirically determined friction factor, f, is used to characterize the shear stress imparted on the flow by its surroundings.

Figure 2.9 Experimental data relating the secondary mass flowrate, normalized by the primary mass flowrate, to the plenum pressure, P_B. Data for M = 2.0 flow was taken from Strykowski et. al. [2]. Collar geometry: L/H=6.9, R/H=15, G/H=0.385. For M=0.5 flow, collar geometry: L/H=1.15, R/H=6, G/H=0.2. The M=0.5 data is best matched using f=0.1; M=2.0 data is best matched using f=0.3.

List of Symbols:

AR	Aspect ratio of the jet.
c_L	The dimensionless measure of the core length region: $= x_c/H$
c_D	The coefficient of drag for skin friction acting on the collar surface.
D_H	Hydraulic diameter, used in calculating the mass flow rate through the secondary flow channel.
Drag	The total additional drag which results from the installation of the collar surface.
$F_{c,x}$	The force per unit depth exerted on the fluid control volume by the pressure forces on the collar, in the Cartesian x direction.
$F_{c,y}$	The force per unit depth exerted on the fluid control volume by the pressure forces on the collar, in the Cartesian y direction.
F_{gap}	The force per unit depth exerted on the fluid control volume by the pressure forces and secondary momentum flux, in the gap region.
F_{jet}	The force per unit depth exerted on the fluid control volume by the pressure forces and the primary momentum flux in the jet exit plane.
F_{out}	The force per unit depth exerted on the fluid control volume by the pressure forces and the momentum flux leaving the control volume.
G	The distance between the lip of the nozzle, off which the primary flow passes, and the collar surface.
G_{min}	The lower limit on the gap spacing where jet to collar interference becomes a limitation.

H	The small dimension of the nozzle exit.
J	The primary momentum flow per unit depth of the jet, $J = \rho_1 u_1^2 H$.
J_{in}	The effective momentum per unit depth flowing into the control volume, accounting for momentum augmentation
J_c	The momentum per unit depth of the secondary flow stream.
J_{out}	The momentum per unit depth leaving the control volume.
L_{att}	The axial length, measured from the exit plane of the jet, where the attaching streamline intersects the collar surface.
L_c	The axial length of the collar.
L_{max}	The maximum length of the collar surface, after which jet attachment is possible.
M	The Mach number of the primary flow, in the exit plane of the jet.
M_c	The convective Mach number in the vectoring jet.
$\dot{m}_1$	The mass flow rate of the primary jet.
$\dot{m}_2$	The mass flow rate of the secondary flow.
NPR	The nozzle pressure ratio: the ratio between the stagnation pressure and nozzle exit pressure
P_B	The absolute pressure in the recirculating region.
P_{exit}	The static pressure in the exit plane of the jet.

P_I The absolute pressure on the surface of the collar at the attachment point.

P_0 The stagnation pressure in the exit plane of the jet.

P_∞ Absolute atmospheric pressure.

Q The mass flow rate per unit depth of the primary jet, at the nozzle exit.

Q_c The mass flow rate per unit depth of the secondary flow.

R The radius of curvature of the collar surface.

R' The radius of curvature of the jet, as it arcs towards the wall.

t A convenient way to express the parametric equation of the attaching streamline.

u_1 The exit plane velocity of the primary jet, assumed to be uniform in the exit plane.

u_2 The mean velocity of the counterflowing stream in the exit plane of the jet.

u_p The velocity of the airplane.

w The large dimension of the nozzle exit.

w_c The ratio of secondary mass flow rate to primary mass flow rate.

W_{pump} The power required to operate the secondary pump.

x The streamwise coordinate measured along the jet's centerline, originating in the jet exit plane.

x_{att} The streamwise location at which the attaching streamline intersects the wall.

x_c The axial extent of the potential core length.

y The transverse coordinate measured normally from the centerline of the jet.

y_{collar} The transverse coordinate used to measure the position the collar.

y_{jet} The transverse coordinate used to measure the outer boundary of the shear layer.

$Y(x)$ The transverse location of the attaching streamline.

α The angle on the collar, measure from the exit plane of the jet, where the attaching streamline intersects the collar.

χ The total power penalty associated with the addition of the collar surfaces. Includes drag and pumping losses.

δ_v The vector angle.

$\delta_{v,max}$ The maximum desired vector angle.

Δ Channel width, used in secondary mass flowrate model.

ϕ The empirically determined weighting factor used in evaluating the angle at which the momentum exits the control volume.

γ The angle subtended by the jet centerline, at which attachment occurs.

θ The included angle of the collar surface.

ρ Fluid density.

ρ_1 Density of primary jet.

ρ_2 Density of secondary flow stream.

σ The dimensionless spreading rate parameter, used in evaluating the jet velocity profile.

ψ The angle at which the flow exits the momentum control volume.

Section 1: Introduction

The ability to redirect the thrust of an aircraft engine offers several advantages to the aerospace industry. It provides the potential for a vertical component of thrust which may be used, especially at low speeds, to augment the lift force generated by the wings. This allows the aircraft to take off in a shorter distance, and ascend at a higher rate. During landing, downward thrust can be used to supplement the lift force generated by the wings, and approach speeds may be reduced without changing the rate of descent. This allows the pilot to approach the runway at a slower speed, reducing the distance required to stop the plane. The benefits of short take off and landing (STOL) aircraft are especially attractive for landing on aircraft-carriers or at damaged airfields. Currently, the wings are the sole mechanism for generating lift. To accommodate changing flight conditions, the wings are equipped with movable control surfaces that alter the flow pattern around the wing, and hence its aerodynamic characteristics. These control surfaces are used to steer, generate additional lift during take-off, and generate additional drag during landing. However they have aerodynamic limitations; namely airfoil stall, which refers to the condition in which the flow separates from the top surface of the airfoil. Stall causes a dramatic decrease in airfoil performance and must be avoided to maintain adequate control of the aircraft. Thrust vectoring can be used to maintain (or re-establish) control

under stalled conditions, thus enhancing the overall maneuverability of the plane [1].

There are various methods to vector the exhaust thrust of a jet engine. One way is to tilt the whole exit plane of the nozzle. While this generally requires complex actuation hardware, it has been implemented successfully on the Harrier jet for several years. Upon take-off, the thrust in directed almost fully downwards, allowing for vertical take-offs. Once in flight, the nozzle locks in place horizontally and the plane performs in a conventional manner. Another method which has been employed in the Lockheed X-31 and the NASA F-18 H.A.R.V (High Alpha Research Vehicle), among others, employs hinged turning vanes downstream of the nozzle exit. The exhaust impinges on these mechanically actuated vanes and is deflected. This method has proven to greatly enhance the maneuverability of the test aircraft [1], as well as considerably shorten the take-off and landing distance. However, these advantages come at the expense of additional weight and reduced thrust due to the wall interaction. Similar advantages can be achieved, in principle, without the intricate mechanical control systems and with improved thrust recovery, by fluidically vectoring the jet.

The present study centers around a method of fluidic vector control using counterflow. Counter-Flow Thrust Vectoring, or "CFTV", has been demonstrated experimentally for subsonic as well as supersonic jets. Van der Veer [2], was able to vector a subsonic (M = 0.5) jet continuously up to angles of 20°. Strykowski, Krothapalli, and Forliti [3] achieved similar performance

from a supersonic (M = 2) jet. A schematic of the CFTV process is illustrated in Figure 1.1. CFTV works on the principle of asymmetric mass entrainment. Strykowski and Niccum [4] have shown that counterflow, when applied to the periphery of an axisymmetric jet, greatly enhances the mixing characteristics of the shear layer. Strykowski and Khemakhem [5] have shown this to be the case in a planar shear layer as well. By applying counterflow on only one side of the jet, the excited shear layer mixes much more rapidly than the opposing free shear layer. This imbalance in entrainment causes a cross-jet pressure gradient, which bends the jet in the direction of the applied counterflow, resulting in a vectored primary flow.

With CFTV, no moving parts are directly required to steer the jet. Consequently, reliability is greatly enhanced. There are no surfaces in direct contact with the high temperature, high velocity exhaust gases. This eliminates the need for expensive materials or exotic cooling schemes, which is necessary with turning vanes. Furthermore, since the jet is steering itself, via an entrainment induced pressure differential, rather than being forced to steer, by deflection, there is a much greater percentage of the thrust recovered [3]; increasing overall performance. Because of the minimal weight addition, the CFTV system may be retrofitted into an existing aircraft's engine without significant structural alteration of the airframe. The result is a reliable, robust system with a relatively low initial cost, and minimized maintenance costs.

1.1 CFTV Operating Curve

The operation of a CFTV system has been qualitatively described above. However, for purposes of design and optimization, a quantitative description is necessary as well. The exit vector angle, δ_v, depends on the length of the collar surface, L, the forward momentum flow of the jet, J^*, and the pressure distribution on the collar surface. Experimental work [2] has shown that the pressure distribution on the collar surface is nominally uniform during vectoring, and may be proportionally controlled by varying the plenum pressure P_B. The relationship between the control pressure and the vector angle is critically important for design. This relationship defines the operating curve of a CFTV system. Characterization of the CFTV operating curve has been the subject of numerous experiments [2], [3] over a wide range of jet operating conditions; at vector angles up to 20°. However until now, no analytical explanation has been offered.

Examination of the two-dimensional, radial momentum equation in polar coordinates gives us insight into the fluid mechanics which affect the relationship of δ_v with P_B.

---

* The Jet's momentum, $J = \rho_1 u_1^2 H$, is taken per unit depth throughout this analysis.

$$\rho\left(\frac{\partial u_r}{\partial t}+u_r\frac{\partial u_r}{\partial r}+\frac{u_\theta}{r}\frac{\partial u_r}{\partial \theta}-\frac{u_\theta{}^2}{r}\right)=$$

$$-\frac{\partial P}{\partial r}+\mu\left(\frac{\partial^2 u_r}{\partial r^2}+\frac{1}{r}\frac{\partial u_r}{\partial r}-\frac{u_r{}^2}{r}+\frac{1}{r^2}\frac{\partial^2 u_r}{\partial \theta^2}-\frac{2}{r^2}\frac{\partial u_\theta}{\partial \theta}\right) \qquad (1.1)$$

Recognizing that viscous terms are small compared to inertial effects in a free jet, and assuming the flow is nominally parallel in the streamwise direction (i.e. $u_\theta \approx u_\theta(r)$, and $u_r \approx 0$), the momentum equation can be simplified to:

$$\frac{\partial P}{\partial r}=\frac{\rho u_\theta{}^2}{r.} \qquad (1.2)$$

This differential equation can be evaluated by integrating both sides. To evaluate this expression, it is assumed that the jet uniformly arcs at a constant radius of curvature, R'. This assumption is fairly accurate, so long as the jet is far enough away from the collar surface to have little interaction, and that R' is significantly larger than the jet thickness (≈ H). In other words, this analysis applies for small vector angles.

$$\int dP=\frac{1}{R'}\int \rho u_\theta{}^2 dr \qquad (1.3)$$

Integrating from one side of the jet to the other, the right hand side represents the streamwise momentum. Since streamwise momentum is conserved in a

free jet flow, this quantity is identically equal to the momentum flow (per unit depth) in the jet exit plane, J. The integral on the left hand side is known from the boundary conditions. On the radially outward shear layer, the pressure is equal to that of the ambient, P_∞, on the inner shear layer, the pressure is approximately that of the control stream P_B. Thus (1.3) becomes:

$$P_\infty - P_B = \frac{J}{R'} \tag{1.4}$$

Upon reaching the extent of the collar, the mechanism for sustaining the cross-jet pressure gradient, namely the parallel counterflow, dies off. As a result the jet exits straight into the atmosphere, at an angle δ_v, refer to Figure 1.1. The jet curvature, R', can be related to the exit vector angle and the length of the collar, L, using the following expression.

$$R' = \frac{L}{\sin\delta_v} \tag{1.5}$$

Substituting (1.5) into (1.4) and solving for the vector angle in terms of the control pressure, we have:

$$\sin\delta_v = \frac{(P_\infty - P_B)L}{J} \tag{1.6}$$

Experimental observation shows that this expression holds true, to a good approximation, over a wide range of flow conditions and collar geometries. Figure 1.2 illustrates the relationship between equilibrium vector angle δ_v and the dimensionless control variable in equation (1.6). The data points that are plotted [2], [3] represent a wide range of collar geometries and jet operating conditions: from M=0.2 to 2.0; from R/H=2 to 15; from G/H=0.1 to 0.75; from L/H=1 to 7; and from $T_{0,jet}$ = 300K to 600K.

1.2 Jet Attachment

Due to the entrainment differential, a small degree of jet turning is possible without a collar surface, however it is the addition of an extended collar surface that makes CFTV a viable technology. First, it channels the secondary flow in parallel with the primary flow, effectively inducing a countercurrent mixing layer over the entire length of the collar. Second, it restricts the natural entrainment of the jet, intensifying the cross stream pressure gradient. Finally, it gives the pressure forces a surface over which to act. A longer collar has more surface area for the pressure forces to act on; thus a smaller pressure differential will impart an equal transverse force on the jet. In other words, with a longer collar, the same vector angle is achievable with a smaller amount of vacuum from the secondary flow system. The net effect is a reduction in pumping power losses.

While the collar is vital to the efficiency of the CFTV system, it poses a potential problem that can disrupt the continuity of the operating surface. This condition, a result of the bistable interaction between a free jet and a wall, is one in which the jet attaches to, and reaches a stable equilibrium on, the wall. It has been observed, under certain operating conditions, by previous CFTV investigators [2], [3] that the jet attaches to the collar surface during vectoring. This is unacceptable from a design standpoint as, in a flight situation, this may cause a loss of control. Furthermore, to release the jet from the collar, the control pressure must be reduced beyond that which was required to cause attachment. This hysteretic behavior makes a continuous vector-control system very difficult (if not impossible) to implement. Fortunately, this situation can be prevented by correctly tailoring the geometry of the collar. The primary focus of this study was the prevention of jet attachment; a phenomenon that is also commonly referred to as the "Coanda effect*."

When a jet issues into a surrounding fluid, its shear layers experience rapid spatial growth and soon become turbulent. The effect of this shear layer growth, and accompanying vortical structure, is to diffuse momentum into the surrounding stationary fluid (primary due to turbulent transport

* This effect refers to the low pressure field caused by entrainment of a jet. In the vicinity of a wall, the low pressure field acts to pull the jet off axis, causing attachment to the wall . Although this was first observed by Young, in 1800, it is named after Henri Coanda, a French engineer who patented the effect in 1932. He was working on an exhaust gas scavenging device, for internal combustion engines, at the time.

mechanisms) and to entrain mass from the surroundings. This is done in a way such that the total streamwise momentum is conserved. The presence of a collar inhibits this free-entrainment process, resulting in reduced pressures on, and in the vicinity of, the collar surface. The transverse pressure field causes the jet to bend towards the surface. This process is unstable since this bending of the jet further inhibits the shear layer's entrainment and, consequently, leads to further surface pressure reductions. This transient phenomenon continues until the jet reaches a stable equilibrium. If the geometry of the collar surface permits, the jet will attach to the wall, as shown in Figure 1.3. For this to occur, the conditions necessary for stable equilibrium at the wall must be satisfied. In equilibrium, the transverse pressure forces across the jet must balance with the centrifugal forces demanded by the jet's curvature; this is essentially a macroscopic satisfaction of the differential momentum equation. The pressure force per unit depth acting transversely is approximated by (1.7a). The centrifugal force generated by the bending jet is approximately (1.7b).

$$\text{Transverse Force} \approx (P_\infty - P_B)L_{att} \qquad (1.7a)$$

$$\text{Centrifugal Force} \approx J/R' \qquad (1.7b)$$

The important thing to bear in mind when designing a CFTV system is that wall attachment can only occur if equilibrium can be sustained. This

means that the entrainment mechanisms within the jet must be able to sustain the low pressure necessary to hold the jet attached to the wall. The shorter the collar, the sharper the jet must turn in order to attach; thus a lower bubble pressure will be required. Furthermore, with a short collar, the shear layer has less contact with the bubble region. This makes it more difficult for the pumping mechanism within the jet to generate the low pressure required to hold itself to the wall. Consequently, if the collar is sufficiently short, attachment will not occur.

There is a unique equilibrium location where the attaching streamline intersects the collar. This location depends on the gap width, the mixing dynamics of the shear layer, and the amount of secondary flow leaving (or entering) the recirculation zone. A large gap places the collar surface farther away from the jet, resulting in a longer attachment length. Enhanced shear layer growth rate means the jet is more effective in sustaining the low pressure within the bubble region. Likewise, counterflow being drawn from the bubble region by a secondary pump assists the jet in sustaining the low pressure necessary to hold itself to the wall. These two latter conditions enable the jet to turn with a tighter radius of curvature, resulting in a shorter attachment length.

If the collar is longer than this equilibrium attachment length, the jet will merely attach at the designated location, and follow the contour of the wall until boundary layer separation occurs. However, if the collar is shorter than the equilibrium attachment length, the jet will not attach to wall. When

designing a collar, it is important to be able to estimate the attachment length based on the intended operating conditions. To safeguard against jet attachment, the collar should always be made shorter than this critical length, enabling smooth and continuous operation of the CFTV system. It is clear that to effectively implement a CFTV system, jet attachment must be avoided under all circumstances. To do this, we must gain a better understanding of the physics behind jet attachment, and the operating conditions under which it occurs.

1.3 Previous Jet Attachment Studies

The concept of jet attachment has been employed in the past for applications related to controllable fluidic switching, [6], [7] and [8]. A typical switch design consisted of a rectangular jet exiting in the vicinity of two adjacent walls, symmetrically offset from the lip of the nozzle. The walls were sufficiently long to insure that the jet would attach, rather than exiting straight; thus the device would be bistable. The wall to which the jet attached was varied by opening or closing pressure relief vents located on each wall. Due to the robust nature of fluidics, no moving parts, etc., these switches were investigated for their functionality as logic elements for use in computers. They have the desirable characteristic that the high momentum primary jet can be manipulated using very low energy input. This characteristic warranted the name "fluid amplifier", by which they were commonly

referred. Considerable research in this field was performed in the 1960's by Bourque [9], Newman [9], [11], Perry [12], Sawyer [13], Mueller [14], Olson [15], and numerous others. Prior to the inception of reliable semi-conductor technology, which took over in the early 1970's, working computers were constructed solely using fluidic logic elements. In the interest of optimizing the performance of these logic elements, and reducing their physical size, it became necessary to study, and model, the jet attachment process. Modeling efforts focused on adjacent parallel walls, and diverging flat walls in both subsonic and supersonic environments.

Bourque and Newman [9] began in 1959 by developing a model to predict the point at which an incompressible, planar jet would reattach to an offset parallel wall. Their solution approach was to draw a control volume around the features of the flow, see Figure 1.4. By applying the conservation of mass and momentum equations to this control volume, the important features of the flow, specifically the attachment location, could be determined. To do this, the pressure distribution on the boundaries of this control volume, must be characterized. Further, the net momentum inflow, outflow, and their respective vector directions must be evaluated. Bourque and Newman assumed that the pressure on the adjacent surface was constant until intersected by the extrapolated centerline of the jet. The pressure on the wall was then assumed to jump discontinuously to that of the ambient, which it was taken to equal on the outer lateral boundary as well. In order to obtain the momentum flux in and out of the control volume, the velocity

profile was integrated at the corresponding location. The profile was described mathematically using Görtler's self-similar planar jet solution, as outlined in Schlichting [10]. The spreading rate parameter, σ, used by Görtler, was evaluated empirically by comparing the predictions of the model to experiments conducted for various wall offset distances. The match of experimental data was quite good. This model, and modeling procedure, was held up to be more or less the standard, through the years, though it underwent various modifications. Newman [11] extended this analysis, using the identical control volume technique, to account for diverging walls. Perry [12] concluded that the pressure in the recirculating zone was indeed not constant, as was being assumed by Bourque and Newman, and that experiment could be matched better by altering the pressure distribution in this region. He did so by assuming a sinusoidal wall pressure distribution, whose magnitude was described by an empirical pressure coefficient in the model. Sawyer [13] used the same pressure assumptions as Bourque and Newman, but modified the velocity profile to account for the jet's curvature. He skewed the velocity profile in favor of the inner half using physical justifications set forth by Schlicting [10]. The degree to which the profiles were skewed by the bending jet was calculated by an empirically determined constant. McCree and Moses [14] studied the effects of three dimensionality on attaching flow in an incompressible jet. They performed attachment studies using rectangular jets of various aspect ratios attaching to angled walls. They concluded that for aspect ratios greater than 2:1, attachment

characteristics are independent of aspect ratio, and that the jet may be modeled as two-dimensional.

Studies regarding supersonic flow were conducted by Mueller [15], who performed experiments at various Mach numbers, with a two-dimensional jet attaching to a diverging flat plate. In addition to performing experiments in a supersonic flow, Olson [16] developed a control-volume based model to account for the nature of the supersonic flow. In many ways, the methodology was similar to that used in the Bourque and Newman model, however the velocity profile was modified to account for a constant velocity core region, which extends farther in supersonic jets than it does in subsonic jets, due to the change in shear layer growth rate.

The techniques that have been employed in the past, with regards to fluidic switching studies are all very valuable. However the geometry which was investigated differs significantly from that being proposed for a CFTV system. With fluid amplifiers, the offset distances were large compared to the nozzle width; usually in the ballpark of $G/H = 3$. As a result, the attachment locations occurred well downstream of the potential core region (except in supersonic cases). This allowed the use of Görtler's self-similar jet profile solution. To preserve the aerodynamic nature of a CFTV system, the gap width must be made small ($G/H \approx 0.3$). Thus attachment occurs farther upstream, within the potential core region. Moreover, in each of the previous attachment studies, the adjacent surface was flat. As a result, the flow direction leaving the control volume was unambiguously chosen to be

parallel to the wall, and the pressure on the wall, after attachment, was equal to that of the atmosphere. For reasons that will be discussed later, the adjacent walls for a CFTV system are curved. This does not enable a simple extrapolation from the fluid amplifier attachment models to a CFTV attachment model, rather it will be necessary to make some changes in the modeling methodology.

Our approach to this problem is to develop a simple analytical model that will allow the accurate prediction of the conditions necessary and sufficient for jet attachment. This will be accompanied by an experimental study using a subsonic ($M \leq 0.5$) jet facility, similar to that described in [2]. Both studies focused on determining where the jet would attach to an adjacent collar surface, and how the operating conditions affect attachment. As mentioned above, the attachment location depends on the shear layer mixing dynamics, the amount of mass flow leaving (or entering) the bubble region, and the geometry of the collar (the gap width and collar radius). Whether the jet attaches to the wall depends on whether the pressure in the bubble region, required to hold it there, can be sustained by the pumping mechanism of the jet. Attachment can be avoided by making the collar length shorter than the attachment length. In the following section, a method to model this attachment process is proposed. Ultimately, this model can be used as a tool to optimize the design of a CFTV system.

Section 2: Model Study

Often the most useful way to tackle a problem in fluid mechanics is to apply the conservation equations to a control volume. This method is especially attractive with regards to jet attachment, because all of the relevant parameters can be captured within a single control volume. In addition, the boundary conditions can be evaluated with relative ease. Since this development is meant only as an engineering design model, exact solutions to the Navier-Stokes equations are not necessary. However, empiricism has been avoided wherever possible.

2.1 Geometry

Previous counterflow thrust vectoring, CFTV, studies have utilized truncated circular-arc collars offset from the lip of the nozzle. Consequently, we have chosen to investigate this specific geometry for its attachment characteristics. It should be noted that any mathematically descriptive geometry, such as a flat wall, elliptic or parabolic arcs, could be modeled in a similar manner. Upon deciding the geometry of the collar, a control volume is drawn from the exit plane of the nozzle to the point of attachment; bounded by the collar surface, see Figure 2.1. The radially outward boundary extends sufficiently far to insure that there is no significant pressure gradient across it, and the momentum flow across the boundary is negligible.

We assume that the centerline of the jet arcs towards the wall at a constant radius, R'. The streamwise coordinate, x, originates at the exit plane of the jet, and designates the axial distance along the jet's centerline. The variable x_{att} denotes the streamwise position, as measured along the centerline, at which the attaching streamline intersects the wall. The transverse coordinate, y, is everywhere orthogonal to the streamwise coordinate (identical to the r - θ coordinate system), and measures the distance from the centerline. The following geometric relationships, which correspond to the variables shown in Figure 2.1a, can be written:

$$R' = \frac{x_{att}}{\gamma} \tag{2.1}$$

$$R\sin\alpha = \left[R' - Y(x_{att})\right]\sin\gamma \tag{2.2}$$

$$R(1-\cos\alpha) + G + \frac{H}{2} = R'(1-\cos\gamma) + Y(x_{att})\cos\gamma \tag{2.3}$$

2.2 Velocity Profile Assumption

Before the conservation equations can be applied (mass and momentum), an adequate mathematical description of the jet's behavior must be developed. Because we are using a control volume solution procedure, the details of the velocity field are less important than the integral quantities which are used in evaluating mass and momentum fluxes. However, the features of the actual

velocity profile are to be matched as closely as possible. Nearly without exception, the attachment models used in the past, see Section 1.2, made the assumption that the jet behaved consistent with Görtler's incompressible solution for the self-similar regime [10]. For the geometries under consideration in this study, offset distances will be relatively small, and thus attachment will likely occur within the core region of the jet. This requires a "top-hat" velocity profile assumption.

The jet issues into a quiescent fluid having a velocity in the exit plane which is uniformly equal to u_1. Owing to viscosity, and turbulent transport mechanisms, the jet imparts shear forces on the surrounding stationary fluid. These shear forces act to accelerate, or entrain, the stationary fluid and decelerate the high speed fluid within the jet; all the while, the jet's axial momentum is conserved. The portion of the high speed flow which is unaffected by this shearing action is known as the potential, or inviscid core region. The general character of the jet is depicted in Figure 2.2. The width of the potential core clearly decreases as a function of streamwise position. Initially, only an infinitesimal portion of the jet is affected by the surrounding fluid. At some distance downstream, six to eight jet diameters for a subsonic planar jet, the growing shear layers merge, and the potential core vanishes. There is then a short period of transition flow, followed by a self-similar regime in which Görtler's analysis applies. As mentioned above, in the case of CFTV, the collar generally will not extend past the core region, thus we will focus our modeling efforts there.

Owing to the fact that a turbulent shear layer grows linearly with axial position [10], we assume the potential core width decays linearly with axial position. Thus the half width of the potential core, Δy, is given by equation 2.4.

$$\Delta y = \frac{1}{2}\left(H - \frac{x}{x_c/H} \right) \tag{2.4}$$

We further assume that Görtler's solution of an incompressible flow in the self-similar regime of the jet [10], applies for the shear layers. Thus the velocity profile can be characterized by equation 2.5:

$$u(x,y) = u_1' \qquad \text{Where } |y| < \Delta y \tag{2.5a}$$

$$u(x,y) = u_1 \operatorname{sech}^2\left(\frac{\sigma(y - \Delta y)}{x} \right) \qquad \text{Where } |y| \geq \Delta y \tag{2.5b}$$

By conserving axial momentum, Görtler's spreading rate parameter, σ, in equation (2.5b) can be written in terms of the core length.

$$\frac{\rho u_1^2 H}{2} = \int_0^{\Delta y} \rho u_1^2 dy + \int_{\Delta y}^{\infty} \rho u_1^2 \operatorname{sech}^4\left(\frac{\sigma(y - \Delta y)}{x} \right) dy \tag{2.6}$$

Since the exit plane momentum flux, ρu_1^2, is a constant, it can be taken out of the integrand and thus canceled out. The resulting integration, leaves:

$$\frac{H}{2} = \frac{2}{3(\sigma/x)} + \Delta y \qquad (2.7)$$

Combining with equation (2.4),

$$\frac{H}{2} = \frac{2}{3(\sigma/x)} + \frac{1}{2}\left(H - \frac{x}{x_c/H}\right) \qquad (2.8)$$

Which simplifies to:

$$\sigma = \frac{4}{3} c_L \qquad (2.9)$$

Where $c_L = x_C/H$. Substituting this expression into equation (2.5), we get:

$$u(x,y) = u_1 \qquad \text{Where } |y| < \Delta y \qquad (2.10a)$$

$$u(x,y) = u_1 \,\text{sech}^2\left(\frac{4c_L(y-\Delta y)}{3x}\right) \qquad \text{Where } |y| \geq \Delta y \qquad (2.10b)$$

We now have the velocity profile in terms of one parameter, the non-dimensional core length. The core length is the sole descriptor of the jet's mixing layer dynamics, and may be evaluated experimentally, using a variety of methods, which will be discussed later. Inside the potential core region, $x < x_c$, the centerline velocity is equal to the exit plane velocity u_1. Outside the potential core region in the axial direction, $x \geq x_c$, the centerline velocity decays like $x^{-1/2}$. This is determined by conserving axial momentum , see Appendix A1.

2.3 Conservation of Mass

As is the case for any control volume, mass and momentum flow must be conserved. We begin by applying the principle of mass conservation. This is done by postulating a mean-flow streamline which exits from the jet and intersects the wall; i.e. the attaching streamline. By definition, no mass can cross a streamline or the solid boundary of the collar. In the absence of counterflow, the attaching streamline must originate at the lip of the nozzle. The mass flow on one side of the streamline is from the primary jet. The flow on the bubble side is entrained from the surroundings, then as the jet impinges on the wall it is turned back and recirculated into the bubble region. Counterflow, when applied, is ultimately drawn from the primary jet. Thus the attaching streamline originates at some position within the exit plane of the jet. Accounting for the possibility of counterflow, Q_c, an integral equation can be written to mathematically describe this attaching streamline Y(x):

$$\underbrace{\frac{Q}{2} - Q_c}_{\substack{\text{Net\_Inflow} \\ \text{at\_x=0}}} = \underbrace{\int_0^{Y(x)} \rho u(x,y) \cdot dy}_{\substack{\text{Outflow} \\ \text{at\_any\_x}}} \tag{2.11}$$

Substituting our velocity profile assumption, we get:

$$\frac{Q}{2} - Q_c = \int_0^{\Delta y} \rho u_1 dy + \int_{\Delta y}^{Y(x)} \rho u_1 \, \text{sech}^2\left(\frac{4c_L(y-\Delta y)}{3x}\right) \cdot dy \tag{2.12}$$

Integrating, and combining with equation (2.4):

$$\frac{Q}{2} - Q_c = \frac{\rho u_1}{2}\left(H - \frac{x}{c_L}\right) + \frac{3\rho u_1 x}{4c_L} \tanh\left(\frac{4c_L(Y(x)-\Delta y)}{3x}\right) \tag{2.13}$$

Dividing through by $Q = \rho u_1 H$ and rearranging, we get an explicit form of the streamfunction Y(x), which is convenient to write in the following manner:

$$t = \tanh\left(\frac{4c_L(Y(x)-\Delta y)}{3x}\right) = \frac{2}{3} - \frac{4c_L H}{3x}\frac{Q_c}{Q} \tag{2.14}$$

Since the right side is known, this becomes the defining parametric equation for the attaching streamline Y(x). In the absence of counterflow, it diverges linearly

away from the jet centerline; its slope dependent on the core length. With counterflow the streamfunction becomes a more complex hyperbolic function.

2.4 Conservation of Momentum

To apply conservation of momentum to the control volume shown in Figure 2.1, we need some information about the pressure distributions on the boundaries. Our pressure field assumptions, outlined in the following sub-sections, will be based on physical arguments, and will be validated by experimental measurements wherever possible. Once all the forces* acting on the control volume are evaluated, the unknown variables appearing in Figure 2.1 can be evaluated.

2.4.1 Collar Pressure Profile

The bubble region originates at the exit plane of the jet and continues to the angular location, a, where the attaching streamline intersects the wall, refer to Figure 2.1a. Due to the nature of a recirculatory region, our first approximation was that the pressure would be constant in the bubble region. This is true within the first half, however owing to fluid impingement on the wall, the pressure rises in the downstream half of the bubble until it reaches a local maximum at the streamline intersection point. We thus assume that the pressure is constant, and

* All of the forces described in this analysis are calculated on a per-unit-depth basis.

equal to P_B, until it reaches an angular location of $\alpha/2$, and then decreases linearly to a stagnation pressure, P_I, at the angular attachment location α. Mathematically:

$$0 \le \theta < \alpha/2: \qquad P(\theta) = P_B \tag{2.15}$$

$$\alpha/2 \le \theta < \alpha: \qquad P(\theta) = P_B + \left(\frac{2\theta}{\alpha} - 1\right)(P_I - P_B) \tag{2.16}$$

The shape of this assumed collar pressure profile is confirmed by numerous experimental measurements. Figure 2.3 shows a typical experimental collar pressure profile plotted against the predictions of the model. Though the profiles are not linear in a latter half of the bubble, they can be adequately modeled as such with reasonable accuracy. Evaluation of the bubble pressure, P_B, and the stagnation point pressure, P_I, are outlined in Sub-Section 2.4.5.

To obtain the force exerted by the wall on the control volume, the pressure profile is integrated in scalar form.

$$F_{c,x} = \int_0^{\alpha} (P(\theta) - P_\infty) R \sin\theta d\theta \tag{2.17}$$

and

$$F_{c,y} = \int_0^{\alpha} (P(\theta) - P_\infty) R \cos\theta d\theta \tag{2.18}$$

Substituting equations (2.15) and (2.16); the integrals in (2.17) and (2.18) may be evaluated.

$$F_{c,x} = (P_B - P_\infty)R(1-\cos\alpha) + R(P_I - P_B)\left[\frac{2}{\alpha}(\sin\alpha - \sin\alpha/2) - \cos\alpha\right] \quad (2.19)$$

$$F_{c,y} = (P_B - P_\infty)R\sin\alpha + R(P_I - P_B)\left[\frac{2}{\alpha}(\cos\alpha - \cos\alpha/2) + \sin\alpha\right] \quad (2.20)$$

2.4.2 Gap Region

Due to the recirculatory nature of the flow within the bubble region, the pressure on the gap boundary is assumed to be constant and equal to the bubble pressure, P_B. The pressure force per unit depth exerted on the control volume by the gap region boundary is simply the bubble pressure (minus P_∞) times the projected area per unit depth.

$$F_{gap} = (P_B - P_\infty)\, G \quad (2.21)$$

2.4.3 Jet Exit Plane

With the jet attached to the wall, there is a significant pressure gradient across the nozzle exit plane. On one side of the jet, the pressure is equal to that of the ambient, on the other side, the pressure is equal to the recirculating bubble

pressure, P_B. For subsonic flow, we will assume the pressure varies linearly across the exit plane of the jet from P_∞ at y = -H/2, to P_B at y= H/2. Mathematically:

$$P(y) = \frac{P_\infty + P_B}{2} + (P_B - P_\infty)\frac{y}{H} \tag{2.22}$$

To find the pressure force, we integrate this pressure distribution (minus P_∞) across the jet exit plane; the linear term disappears, and we are left with the following expression:

$$F_{jet} = (P_B - P_\infty)\frac{H}{2} \tag{2.23}$$

The formulation of this force term only applies to subsonic flow. A formulation for supersonic flow is described in Appendix A2.

2.4.4 Momentum Inflow

A free jet, with stagnation pressure P_0, exhausts into the atmosphere, at P_∞, with a more or less uniform velocity. If we assume this is done in an

isentropic manner, Bernoulli's equation could be employed to calculate the exit plane velocity*.

$$\frac{1}{2}\rho u_1^2 = P_0 - P_\infty \tag{2.24}$$

However, for an attached jet, the pressure in the exit plane is non-uniform. In subsonic flow, this transverse pressure variation will lead to a skewed velocity distribution. Since the bubble pressure is sub-atmospheric, this effect actually augments the momentum flux entering the control volume, as illustrated by Figure 2.4. Again, the exit plane velocity, which is now a function of y, can be calculated by applying Bernoulli's equation to each individual streamline.

$$\frac{1}{2}\rho u(y)^2 = P_0 - P(y) \tag{2.25}$$

Substituting the exit plane pressure distribution, equation (2.22), and simplifying, we get:

$$\rho u(y)^2 = (P_0 - P_\infty) + (P_0 - P_B) + 2(P_\infty - P_B)\frac{y}{H} \tag{2.26}$$

* Due to the mathematical complexity associated with the compressible regime, we will carry out this analysis assuming incompressible flow, and assume that the discrepancies associated with compressibility are small.

The momentum entering the control volume is found by integrating (2.26) from -H/2 to H/2. When this is done, the linear term cancels out, and we're left with the following expression:

$$J_{in} = \int_{-H/2}^{H/2} \rho u(y)^2 dy = (P_0 - P_\infty)H + (P_0 - P_B)H \qquad (2.27)$$

Which can be written as:

$$J_{in} = [(P_0 - P_\infty) + (P_0 - P_\infty) + (P_\infty - P_B)]H \qquad (2.28)$$

Substituting in equation (2.24), we clearly see that the effective momentum influx is considerably greater than the free jet momentum, J.

$$J_{in} = \underbrace{\rho u_1^2 H}_{\substack{\text{Free\_Jet} \\ \text{Momentum}}} + \underbrace{(P_\infty - P_B)H}_{\substack{\text{Augmented} \\ \text{Momentum}}} \qquad (2.29)$$

The degree of augmentation depends on the magnitude of the bubble pressure. For the collars used in this study, augmented momentum accounts for 10% to 20% of the total jet momentum.

In supersonic flow, there is no skewing of the velocity profile, nor is there any momentum augmentation. The momentum inflow to the control volume is

identically equal to the free jet momentum. This formulation is shown in Appendix A2.

2.4.5 Momentum Outflow

As the jet attaches to the wall, a certain fraction of its momentum is turned back. The fluid that turns back due to the wall, recirculates into the bubble region, and is either re-entrained by the jet, or pumped out by the secondary flow system. The flow that continues on, leaves the control volume at an angle ψ, refer to Figure 2.1b (the computation of this angle will be discussed later). The attaching streamline Y(x), is the dividing line between the flow that gets turned back, and the flow that continues in a "forward" direction. Thus the magnitude of this forward momentum can be computed by integrating from $-\infty$ to the location of the attaching streamline Y(x) at the streamwise attachment location, x_{att}.

$$J_{out} = \int_{-\infty}^{Y(x_{att})} \rho u(x_{att}, y)^2 \, dy \qquad (2.30)$$

Substituting in the velocity profile assumption, developed in Section 2.2, J_{out} becomes:

$$J_{out} = \underbrace{\frac{\rho u_1^2 H}{2}}_{\substack{\text{Momentum} \\ \text{of\_Half\_Jet}}} + \underbrace{\int_0^{\Delta y} \rho u_1^2 dy}_{\text{Core\_Region}} + \underbrace{\int_{\Delta y}^{Y(x_{att})} \rho u_1^2 \, \text{sech}^4\left(\frac{4c_L(y-\Delta y)}{3x_{att}}\right) \cdot dy}_{\text{Shear\_Layer\_Region}} \tag{2.33}$$

Integrating, and simplifying:

$$J_{out} = \rho u_1^2 \left(H - \frac{x_{att}}{2c_L}\right) + \frac{3\rho u_1^2 x_{att}}{4c_L}\left(t(x_{att}) - \frac{t(x_{att})^3}{3}\right) \tag{2.34}$$

Where t is the hyperbolic tangent function, given by (2.14). It is convenient to non-dimensionalize this by the primary momentum.

$$\frac{J_{out}}{J} = 1 + \frac{3\,x_{att}/H}{4c_L}\left(t(x_{att}) - \frac{t(x_{att})^3}{3} - \frac{2}{3}\right) \tag{2.35}$$

For the geometries modeled in this study, this dimensionless quantity varies from 90% to 95%.

The other momentum outflow from the control volume is from the counterflow being drawn through the gap region. The direction of the counterflow is opposite to the main flow; the magnitude is given by the following expression:

$$J_c = \rho_2 u_2^2 G \tag{2.36}$$

For purposes of comparison, it is again useful to normalize the secondary momentum by primary momentum, which is expressed here in terms of the secondary mass flow ratio, w_C; ρ_1 and ρ_2 are the mean densities in the primary and secondary flow streams, respectively.

$$\frac{J_c}{J} = \frac{{w_c}^2}{G/H}\frac{\rho_1}{\rho_2} \tag{2.37}$$

Even with moderate amounts of counterflow, $w_C \approx 10\%$, this quantity was less than 3% for the experiments conducted in this study.

2.4.6 Evaluation of Pressure Terms.

The bubble pressure, P_B, is evaluated using the same physical arguments used in Section 1.1 to develop an equation for the CFTV operating curve. The radial momentum equation for two dimensional flow is given in equation 1.1, and rewritten here.

$$\rho\left(\frac{\partial u_r}{\partial t} + u_r\frac{\partial u_r}{\partial r} + \frac{u_\theta}{r}\frac{\partial u_r}{\partial \theta} - \frac{{u_\theta}^2}{r}\right) =$$

$$-\frac{\partial P}{\partial r} + \mu\left(\frac{\partial^2 u_r}{\partial r^2} + \frac{1}{r}\frac{\partial u_r}{\partial r} - \frac{{u_r}^2}{r} + \frac{1}{r^2}\frac{\partial^2 u_r}{\partial \theta^2} - \frac{2}{r^2}\frac{\partial u_\theta}{\partial \theta}\right) \tag{1.1}$$

In the bubble region, the flow is not yet bounded by the wall, therefore viscous effects are small. The flow is nominally parallel in the streamwise direction, meaning that radial velocity is negligible, as are the gradients in the streamwise direction (i.e. $u_r \approx 0$, and $u_\theta \approx u_\theta(r)$ only). Thus the same simplifications that applied to the CFTV operating curve model, apply to the attached flow. Therefore the flow is approximately governed by equation (1.2).

$$\frac{\partial P}{\partial r} = \frac{\rho u_\theta^2}{r} \tag{1.2}$$

This differential equation can be solved by separating both parts and integrating. We have already made the assumption that the jet is bending at a constant radius of curvature, R′, towards the wall. Therefore equation (1.3) remains valid.

$$\int dP = \frac{1}{R'} \int \rho u_\theta^2 dr \tag{1.3}$$

On the radially outward shear layer, the pressure is equal to that of the ambient, P_∞, on the inner shear layer, the pressure is equal to that of the bubble, P_B. The integral on the right hand side of (1.3) is just the streamwise momentum of the jet, J. Therefore equation (1.4) is also applicable.

$$P_\infty - P_B = \frac{J}{R'} \tag{1.4}$$

This analysis breaks down as the flow approaches the wall, but is valid in the first half of the bubble region (where it is being applied).

In the downstream half of the bubble region, the pressure increases (we assume it to be a linear variation) to a maximum value, P_I, where the attaching streamline stagnates on the wall. The velocity of a fluid particle traveling on this streamline, u_Y, can be computed using the velocity profile assumption presented in Section 2.2.

$$u_Y = u(x_{att}, Y(x_{att})) = u_1 \operatorname{sech}^2\left(\frac{4c_L(Y(x_{att}) - \Delta y)}{3x_{att}}\right) \tag{2.38}$$

However at the wall, the no slip boundary condition must hold. Assuming the fluid on that streamline decelerates isentropically, then:

$$P_I = P_B + \frac{1}{2}\rho u_Y^2 \tag{2.39}$$

Substituting in equation (2.38):

$$P_I - P_B = \frac{1}{2}\rho u_1^2 \operatorname{sech}^4\left(\frac{4c_L(Y(x_{att}) - \Delta y)}{3x_{att}}\right) \tag{2.40}$$

Figure 2.5, illustrates how well these pressure relationships correlate with experiment. Although there are many simplifications made, the pressure predictions work out to be fairly close to experimental values over a wide range of geometric configurations.

2.4.7 Summation of Forces

Thus far, each individual component of force that acts on the fluid control volume has been evaluated, with the exception of F_{out}, which is the pressure force acting over the outflow control volume boundary.

$$\bar{F}_{out} = \int_A P(r,\theta)\bar{n}\cdot d\bar{A} \tag{2.41}$$

We have no reliable source of information about the pressure field in the exit plane, and the momentum equations provide little useful insight, due to their complexity in the vicinity of the wall. Nevertheless, we can combine all of the forces acting on the control volume into two scalar equations, and leave F_{out} as an unknown.

$$\sum F_x = \underbrace{F_{jet} + F_{gap} + F_{c,x} - F_{out}\cos\psi}_{External\_Pressure\_Forces} = \underbrace{J_{out}\cos\psi - J_c}_{Momentum\_Out} - \underbrace{J_{in}}_{Momentum\_In} \tag{2.42}$$

$$\sum F_y = \underbrace{F_{c,y} + F_{out}\sin\psi}_{External\_Pressure\_Forces} = \underbrace{-J_{out}\sin\psi}_{Momentum\_Out} \qquad (2.43)$$

Combining these equations, we obtain the following expressions:

$$\tan\psi = \frac{-F_{c,y}}{J_{in} + J_c + F_{jet} + F_{gap} + F_{c,x}} \qquad (2.44)$$

$$F_{out} + J_{out} = \sqrt{\left(F_{jet} + F_{gap} + F_{c,x} + J_{in} + J_c\right)^2 + F_{c,y}{}^2} \qquad (2.45)$$

The angle ψ, given by equation 2.44, measures the direction in which the flow leaves the control volume, refer to Figure 2.1b. It can be predicted empirically in terms of the attachment angle, α, and the turning angle of the jet, γ.

$$\psi = \phi\alpha + (1-\phi)\gamma \qquad (2.46)$$

Where ϕ is an empirically determined weighting factor. A value of $\phi = 0$ would correspond to the flow leaving the control volume at an angle γ, which is the turning angle of the jet centerline, refer to Figure 2.1. A value of $\phi = 1$ would correspond to the flow leaving the control volume at an angle α, which is the angle tangent to the wall. However due to the interaction with the wall, and high pressure recovery on the surface, the flow is deflected and, on average, exits

the control volume at an angle smaller than both α and γ. This deflection effect has been widely observed in previous wall attachment studies [7]-[9], [11]. Using a value of $\phi = 1.3$ gives the best agreement with experimental attachment data, so that is the value chosen throughout. With that, the momentum balance is complete. The only remaining unknown is the non-dimensional potential core length, c_L, which is used to characterize the mixing characteristics of the jet.

2.5 Evaluation of Core Length

Several strategies may be employed in order to evaluate the dimensionless core length, c_L. One option would be to estimate the core length based on axial centerline velocity profiles, such as that shown in Figure 2.6. However, the value of c_L, using this approach, is subject to various interpretations. It is therefore desirable to use entrainment rate data to define this core length parameter. This seems the most useful, since the model's results depend only on integral quantities, and the entrainment rate is critical in mathematically defining the attachment streamline.

The fact that the two-dimensional velocity profile can be written as a single function allows the entrainment rate to be computed directly, and written in terms of the dimensionless core length, c_L. The flow rate at any axial position is written as follows:

$$\frac{Q(x)}{2} = \int_{\Delta y}^{\infty} \rho u_1 \operatorname{sech}^2\left(\frac{4c_L(y-\Delta y)}{3x}\right)dy + \int_{0}^{\Delta y} \rho u_1 dy \tag{2.47}$$

Integrating, we get:

$$\frac{Q(x)}{2} = \frac{3\rho u_1 x}{4c_L} + \frac{\rho u_1 H}{2} - \frac{\rho u_1 x}{2c_L} \tag{2.48}$$

Which simplifies to:

$$Q(x) = Q\left(1 + \frac{x/H}{2c_L}\right) \tag{2.49}$$

Where Q is given as $\rho u_1 H$. We can then differentiate this expression to get:

$$\frac{dQ(x)}{dx} = \frac{Q}{2c_L H} \tag{2.50}$$

The non-dimensional entrainment rate, which will be used in evaluating c_L, is written as:

$$\frac{d(Q(x)/Q)}{d(x/H)} = \frac{1}{2c_L} \tag{2.51}$$

By doing this, we have an unambiguous method by which to experimentally evaluate the potential core length of the jet. When this core length, c_L, is used in our velocity profile formulation (Section 2.2), we are insured that the entrainment rate used in the model matches that of experiment. The location of the attaching streamline is computed based on the principles of mass conservation, see Section 2.3. Therefore it is of primary importance to accurately characterize the mass entrainment characteristics of the jet. The experimental methods used to do this will be outlined in Section 3.

2.6 Shear Layer Dynamics

The mixing characteristics of a shear layer may be characterized by its spatial growth rate. An advantage of this model is that the details of the velocity field, as posed by Section 2.2, can be manipulated to relate the shear layer growth rate to the potential core length, c_L. This is necessary to predict how c_L changes with changing flow variables; such as Mach number, density ratio, and velocity ratio, which will be invaluable in extending the attachment model to jets operating at high temperature and high Mach numbers.

Mathematically, we define a vorticity based shear layer thickness, δ_ω, as the thickness that the layer would take if it had a uniform shear stress (or vorticity) equal to that of the maximum shear stress, see Figure 2.7.

$$\delta_\omega = \frac{u_{max}}{\left.\frac{\partial u}{\partial y}\right|_{max}} \tag{2.52}$$

Using the velocity profile for the shear layer, given by equation 2.10b, the transverse velocity gradient can be readily computed as a function of spatial position.

$$\frac{\partial u(x,y)}{\partial y} = \frac{\partial}{\partial y}\left(u_1 \operatorname{sech}^2\left(\frac{4c_L y}{3x}\right)\right) = -2u_1 \frac{4c_L}{3x} \operatorname{sech}^2\left(\frac{4c_L y}{3x}\right)\tanh\left(\frac{4c_L y}{3x}\right) \tag{2.53}$$

The maximum shear stress resides at the point of inflection in the velocity profile, which is found by setting the second partial derivative (with respect to y) equal to zero.

$$\frac{\partial^2 u}{\partial y^2} = 0$$

$$= -2u_1 \frac{4c_L}{3x}\left(-2\frac{4c_L}{3x}\operatorname{sech}^2\left(\frac{4c_L y}{3x}\right)\tanh^2\left(\frac{4c_L y}{3x}\right) + \frac{4c_L}{3x}\operatorname{sech}^4\left(\frac{4c_L y}{3x}\right)\right) \tag{2.54}$$

Canceling like terms, this reduces to:

$$\operatorname{sech}^2\left(\frac{4c_L y}{3x}\right) = 2\tanh^2\left(\frac{4c_L y}{3x}\right) \tag{2.55}$$

Which is satisfied only when:

$$\frac{4c_L y}{3x} = 0.6585 \tag{2.56}$$

Plugging this value into equation (2.53), the maximum gradient is computed to be:

$$\left.\frac{\partial u}{\partial y}\right|_{max} = 1.0264 \frac{u_1 c_L}{x} \tag{2.57}$$

Thus the expression for the vorticity thickness becomes:

$$\delta_\omega = 0.9743 \frac{x}{c_L} \tag{2.58}$$

The axial growth rate of the shear layer can be found by differentiation.

$$\frac{d\delta_\omega}{dx} = \frac{0.9743}{c_L} \tag{2.59}$$

It is convenient to compute the shear layer growth rate, because there are theoretical relationships, developed by Papamoshou [17], to relate the growth rate to the velocity ratio, density ratio, and convective Mach number.

$$\frac{d\delta_\omega}{dx} = \frac{c(M_c)\left(1+\sqrt{\frac{\rho_2}{\rho_1}}\right)\left(1-\frac{u_2}{u_1}\right)}{1+\frac{u_2}{u_1}\sqrt{\frac{\rho_2}{\rho_1}}} \qquad (2.60)$$

The subscripts 1 and 2 refer to the primary and secondary flow streams, respectively. The secondary velocity u_2, is in the opposite direction to the primary flow velocity u_1. The empirically determined constant, c, is a function of convective Mach number, which is defined as follows:

$$M_c = \frac{u_1 - u_2}{a_1 + a_2} \qquad (2.61)$$

It is constant for convective Mach numbers up to about 0.4, then drops by roughly a factor of three at convective Mach numbers greater than 0.9. There is considerable scatter in the data throughout the transonic regime, though it is thought to drop in a more or less linear fashion from $M_c = 0.4$ to $M_c = 0.9$ [18]. Based on the experimental core length measurements made for our M = 0.5, unheated (T_0 = 300K) jet , in the absence of counterflow, the value of this constant was determined to be 0.067. Equation

(2.60) allows us to predict how the core length, and thus the predicted velocity field, is affected by different jet operating conditions.

2.7 Secondary Mass Flow Rate

Thus far in the development of this jet attachment model, the secondary mass flow rate has been treated as if it were an independent variable. However, under real CFTV operating circumstances, it would not be known *a priori*. Under the intended operating conditions of a CFTV system, the jet is vectored to some angle, δ_v, by controlling the pressure in the gap region, refer to Figure 1.1. Hence the pressure is really the relevant independent variable. The amount of secondary flow required to generate this control pressure varies with geometry. For large gap widths, more mass flow is required to sustain a given pressure differential. To adequately evaluate the equilibrium attachment length under "real" jet operating conditions, it is necessary to predict the amount of secondary mass flow as a function of control pressure. To do this, we treat the secondary flow passage as if it were turbulent flow through a channel, see Figure 2.8. Thus the following equation applies:

$$(P_\infty - P_B) = \frac{4fL_s}{D_H}\frac{\rho u_2^2}{2} \qquad (2.62)$$

The secondary flow velocity, u_2, can be related to the secondary mass flow ratio, w_C, and the primary flow velocity, u_1.

$$u_2 = u_1 \frac{w_c}{G/H} \tag{2.63}$$

The length of the secondary flow channel, L_s, is related to the collar length, L, and the vector angle of the jet, δ_v.

$$L_s = L \frac{\delta_v}{\sin \delta_v} \tag{2.64}$$

The hydraulic diameter for the flow channel, D_H, is four times the area divided by the wetted perimeter. This can be written as a function of the nozzle aspect ratio, AR, and the channel width Δ.

$$D_H = \frac{4\Delta(AR \cdot H)}{2(\Delta + AR \cdot H)} \tag{2.65}$$

The distance between the collar and the edge of the primary jet, Δ, is defined as the channel width. It varies with axial position, collar geometry, and vector angle.

$$\Delta = \left[G + R\left(1 - \cos\left(\sin^{-1}\frac{x}{R}\right)\right) - \frac{L}{\delta_v}\left(1 - \cos\frac{x\delta_v}{L} + \frac{x\delta_v}{2c_L L}\frac{1}{\cos\frac{x\delta_v}{L}}\right)\right]\cos\frac{x\delta_v}{L} \quad (2.66)$$

To calculate the hydraulic diameter, an average channel width will be employed. The average channel width is taken at the collar's axial midpoint.

$$\bar{\Delta} = \left[G + R\left(1 - \cos\left(\sin^{-1}\frac{L}{2R}\right)\right) - \frac{L}{\delta_v}\left(1 - \cos\frac{\delta_v}{2} + \frac{\delta_v}{4c_L}\frac{1}{\cos\frac{\delta_v}{2}}\right)\right]\cos\frac{\delta_v}{2} \quad (2.67)$$

Equation (2.67) represents the main jet's position with respect to the collar. Embedded in this variable is the relationship between control pressure and vector angle, as given by equation (1.6).

The friction coefficient, f, is a dimensionless measure of the amount of shear stress imparted on the fluid by its surroundings. In our flow situation, the bulk of the shear stress comes from the interaction of the secondary flow with the primary flow, thus it would follow that f would vary linearly with primary flow velocity u_1. It will be evaluated empirically by taking counterflow measurements at various geometric configurations. Experimental data is best satisfied for a M = 0.5 jet (≈ 170 m/s) by using f = 0.1. Counterflow data taken from Strykowski et. al. [3] for a M = 2.0 jet (≈ 517 m/s) are matched best using f = 0.3. The results of this prediction are shown in Figure 2.9. This supports a linear dependence

between f, a measure of shear stress, and primary flow velocity u_1, given by the following empirical relationship.

$$f = (5.9e\text{-}4)u_1 \tag{2.68}$$

Plugging equations (2.63), (2.64), (2.65), (2.67), and (2.68) into equation (2.62); the relationship between the control pressure and the secondary mass flow ratio, although complex, may be evaluated.

2.8 Modeling Summary

There are now an equal number of equations as there are unknowns, thus the system of equations can be solved. This is done using a commercially available non-linear equation solver, Engineering Equation Solver, "EES". The set of equations are written to a worksheet, and iteratively solved until convergence is reached. A copy of this worksheet is shown in Appendix B1.

The inputs to the modeling program are as follows:

1) The collar geometry; characterized by G, R, and L.

2) The jet operating conditions; described by M, T_0, H, and P_∞ (and nozzle pressure ratio, NPR for supersonic flows).

3) The secondary mass flow ratio, w_C.

4) Empirical variables; friction factor, f, and exit angle coefficient, ϕ.

Using these variable inputs, peripheral variables such as jet momentum, primary and secondary velocity, shear layer growth rate, and potential core length are directly computed. Since the secondary flow rate is not very convenient to work with, as it doesn't directly affect the CFTV operating curve. One can apply the development in Section 2.7 to compute the secondary mass flow as a function of the previously defined geometric variables (G, R, L) and the jet operating variables (M, T_0, J), based on the control pressure, P_B, used in the operating curve.

Upon setting these values, the iterative solution procedure can begin. The primary unknowns are α, γ, and R'. The attachment length, and equilibrium bubble pressure are directly calculated from these variables.

Section 3: Experimental Apparatus and Procedure

3.1 Experimental Apparatus

To verify the analytical jet attachment model, and study the operation of a CFTV system, an experimental jet facility was designed and constructed. The jet facility, illustrated in Figure 3.1, consists of a 7.5 hp regenerative blower, capable of exit plane velocities in excess of 180 m/s ($M \approx 0.5$). A two-way valve is mounted at the exit of the blower. By bleeding off high pressure air into the exhaust duct, the jet velocity can be varied. With the bypass valve fully opened, the exit plane velocity reduces to $M \approx 0.25$. To reduce the jet velocity further, a valve is installed at the pump inlet.

The air passing into the tunnel is first pumped through a water-cooled heat exchanger, fabricated from an automobile heater core. It then passes through a honeycomb mesh, that serves as a flow straightener, into a long plenum section fabricated out of 15.24 cm (6 in) inner-diameter acrylic tubing. Downstream of the 1.37 m (4.5-ft) plenum section, the flow passes into a cast epoxy nozzle, where it undergoes a 45:1 reduction in area culminating in a 4-cm x 1-cm rectangular jet. A total pressure probe, and a type-K thermocouple are mounted within the plenum, to monitor jet operating conditions.

A pair of symmetrical, circular-arc collars are installed symmetrically downstream of the nozzle, as shown in Figure 3.2. Collars of various radii, 2 cm, 3.5 cm, 5 cm, and 6 cm, were constructed. To expedite the switching of collars,

each collar pair is fitted into its own modular housing consisting of adjustable slider plates, to which the collar surfaces are mounted; and side-wall plates, to preserve the two-dimensionality of the flow. The collars are fabricated by sectioning arcs out of thick-wall acrylic tubing. The included angles of the arcs, in all cases, were in excess of 120°, to prevent any edge effects which may influence the point of attachment. Static pressure ports, 0.51 mm (0.020 in) in diameter, were drilled into the collar, with 2° circumferential resolution, to capture all the features of the flow.

Located upstream of the slider plates is a large plenum equipped with pressure ports. The pressure ports are blocked off in the non-counterflowing cases, and hooked up to a secondary flow system for studies including counterflow. Extreme care was taken in sealing this plenum, with silicon RTV, to insure against any leaks. The secondary flow system consists of a 5 hp regenerative blower which draws fluid through a 2.13 m (7 ft) long, 7.62 cm (3 in) inner-diameter PVC pipe. A laminar flowmeter is installed in the middle of the pipe so that the secondary mass flow rate can be accurately determined. The laminar flowmeter is calibrated by integrating velocity profiles taken using a combination pitot tube / temperature probe. This calibration is performed over a wide range of flowrates to insure the linearity and repeatability of the device; the resulting curve is shown in Figure 3.3. Each flowrate is corrected for temperature and pressure, using standards of 300K and 760 torr, respectively (very near actual operating conditions). This is necessary, owing to fluid viscosity changes which affect the calibration curve. A throttling valve assembly, similar to that used on

the primary pump, is used for the counterflowing pump allowing bypass air to be drawn in, and the flowrate of the secondary stream varied.

3.2 Data Acquisition Facilities

An illustrative schematic of the data acquisition system is shown in Figure 3.4. To allow multiple pressure port measurements, we have a 48-port Scanivalve which is indexed with a stepper motor. The stepper motor controller is operated remotely through an IEEE-488 parallel bus interface. The Scanivalve is used to channel individual pressure ports to one of four MKS Baratron capacitive pressure transducers of various ranges (1, 10, 100, and 1000 torr). The transducer is selected based on the estimated pressure being measured. Collar pressure is generally measured with a 100-torr head, whereas the pressure drop across the laminar flow meter is measured with a 1-torr head. Each transducer is calibrated at the factory to provide a linear voltage response curve, and is self-maintained at a constant temperature.

For flow measurements, a total pressure tube is used. A type-K thermocouple is mounted on the probe, and is referenced to an insulated ice bath. The temperature is calculated based on the thermocouple voltage, using conversion equations specified by the thermocouple manufacturer. The total pressure port is connected, via Tygon tubing, to one of the Baratron transducers; the 1000-torr head is usually the most appropriate for high speed flows. This probe is mounted to an automated two-axis traversing system. The stepper

motors, which position the probe, are connected to a controller so that the position of the probe can be remotely controlled and recorded.

Voltage output from the various transducers and thermocouples are fed, via coaxial cables, into one of two digital voltmeters. For high speed sampling, a programmable Keithley 194A, two channel, 16-bit, data acquisition box is used. For fixed sampling rate applications, such as thermocouple readings or laminar flowmeter measurements, the voltages are digitally converted using a Fluke 8502A. Both the Fluke and the Keithley are interfaced remotely, using an IEEE-488 interface, to an Everex-386 UNIX machine. Various data acquisition programs are written (in C language) to control the experiments. Commands to the voltmeters, and traversing equipment are sent out in a sequenced fashion, by this program. Digital signals, sent back to the computer (as ASCII string), were converted and stored in output files. These output files are downloaded to a Power Mac 7100 for processing, plotting, and presentation.

3.3 Operating Conditions

Because of high area ratio of the nozzle (45:1), the velocity in the plenum region is very low, even at maximum tunnel speed (M = 0.52). Thus, the pressure and temperature measurements within this region were taken as stagnation values. For an exit Mach number of 0.5 , the plenum pressure is within 0.001% of the computed isentropic stagnation pressure, which is well beyond the uncertainty limitations of our pressure measuring instruments. The jet Mach

number was measured by placing a total pressure probe immediately downstream of the nozzle exit.

The temperature of the jet is controlled by adjusting the temperature of the tap water entering the heat exchanger. The jet stagnation temperature is regulated to match the ambient temperature as closely as possible; usually within 1° C. In all cases, the jet is turned on and warmed up for at least 15 minutes prior to each experiment. Likewise, time is allotted between changes in jet Mach number, to allow the jet facility to reach steady state.

3.4 Free Jet Measurements

The experimental procedures used in data acquisition can be separated into two classes: free jet flow, or attached jet flow. "Free jet" refers to a flow that is not bounded by a wall. The "attached jet" studies refer to a flow condition where the jet is self attached to an adjacent collar surface. Numerous measurements were taken in the free jet to evaluate the potential core length, the vector angle of the jet, as well as the jet's mixing characteristics as a function of counterflow. All of these measurements involved traversing of the total pressure probe throughout the flow field.

3.4.1 Entrainment Data

To evaluate the non-dimensional core length, for non-counterflowing cases, entrainment data is taken. For these measurements, both collars and side plates are removed to allow free jet entrainment. A total pressure tube is mounted to the two-axis positioning equipment and traversed throughout the flow. Passes are taken in the transverse direction with very high resolution. Each pass begins at the centerline, and steps outward (in the +y - direction) until the velocity falls to within 5% of the centerline velocity. At this point, the probe is traversed back to the centerline, and stepped in the opposite direction. These passes are repeated for several axial positions, ranging from $X/H \approx 0$, to a downstream position of x/H=10. The velocity profiles are integrated numerically to obtain the flowrate at each axial position. Figure 3.5 shows the experimentally measured flowrate as a function of axial position. Using a linear curve fit, the slope is found. Equation (2.55) is then used to compute a potential core length of $c_L = 7.32$.

To evaluate the accuracy of our profile assumption, the experimentally measured velocity profiles are plotted against those predicted by equation (2.10) for two axial positions within the core region, see Figure 3.6. Although the match is not exact, the predicted profiles compare well enough with experiment to be used for this attachment model.

3.4.2 Vector Angle Data

Prior to measuring the vector angle, a visual estimate is made. The probe, which is mounted on a rotational stage, is rotated to nominally match the visual estimate. The probe is traversed back and forth, in a manner similar to that outlined above, to find the peak velocity (centerline velocity). This is repeated at several axial positions. The spatial coordinates of the local velocity maxima are plotted, and given a linear curve fit to obtain the vector angle. If the vector angle is not within five degrees of the probe angle, the data point is discarded, the probe angle is reset, and the experiment is run again with the updated probe angle.

3.4.3 Counterflow Measurements

Another aspect of the free jet which was studied, was the influence of counterflow on the jet's mixing characteristics. These studies were performed by installing a very short collar, R=2 cm, and applying suction to both sides of the jet. Figure 3.7 illustrates the experimental apparatus used. To prevent vectoring of the jet, counterflow must be applied identically on each side of the jet. Equal plenum pressure was attained by installing a cross-over tube between the two plenum chambers. The gap width was set very accurately, and checked at the top, middle, and bottom of the jet's span for each collar to insure straightness. The mixing characteristics were examined by taking velocity profiles axially along

the jet's centerline. To accomplish this, the total pressure tube was traversed axially downstream, stopping every 0.5 cm to measure the centerline velocity. Using this data, the length of the potential core length, defined by $u(x_C)/u_1 = 0.95$, was found as a function of counterflow*. The shear layer growth rate, which is linearly proportional to the core length, was computed as a function of counterflow, using equation (2.59).

3.5 Attached Jet

The second main category of measurements were made with the jet self-attached to the collar surface. Since one of the primary goals of this study was to evaluate and predict attachment location as a function of geometry, this category represents the largest volume of data taken.

To begin, the collars are installed symmetrically and the pressure taps are connected to the Scanivalve junction block; refer to Figure 3.2. The gap is accurately set using a small scale, which had been modified to fit between the collar surfaces. After setting the geometry, and tightening down the slider plates, sealant is inserted into the slider-plate/plenum-wall interface, to prevent any air leakage. The jet is then turned on, and the Mach number is set by adjusting the by-pass valves (in counterflowing cases, the secondary pump was switched on and the amount of secondary flow was set as well). Because jet attachment is a

* Since the core length is only being used here for purposes of comparison, how the core length is defined is not too critical, so long as we are consistent in applying this definition.

bistable process, the jet could attach to either collar, or in some cases exit straight. In any event, the jet is forced to attach to the instrumented collar by placing an object into the flow and physically pushing the jet over. If an equilibrium condition can be reached, the jet remains attached to the wall. If an equilibrium condition cannot be reached, the jet either exits straight or at an angle corresponding to a point on the CFTV operating curve, refer to Figure 1.2. After allowing sufficient warm-up time, the atmospheric conditions are recorded (manually) and the data acquisition program is started. The program measures the secondary mass flow rate, and jet Mach number, then scans through each of the pressure ports on the collar, taking 30,000 samples, at a rate of 1000 Hz, and averaging them. The Mach number, pressure tap location, and corresponding surface pressure, $P(\theta)$, is tabulated and placed in an output file for post processing.

In order to evaluate the attachment location, a flow visualization technique using oil and lamp-black dye is implemented. To accomplish this, a strip of paper is adhered to one of the collar surfaces. A solution of SAE 30-W oil and carbon powder, called lamp-black, is brushed onto the paper surface. The jet is then turned on, and attachment is induced, as outlined above. Flow impinging on the collar surface causes the dye solution to smear. Regions of high shear stress are indicated by a greater amount of smearing. The reverse flow present in the recirculation bubble smears the dye upstream. On the downstream side of the attachment point, the dye is smeared downstream. This leaves a distinct parting line at the point where the attaching streamline intersects the wall, i.e. where the

shear stress is zero. Visual measurements of this parting line location are made using a scale and protractor.

Section 4: Results and Discussion

4.1 Non-Counterflowing Cases

In total, collars of four different radii were fabricated: R=2 cm, 3.5 cm, 5 cm, 6 cm. The smallest of which was too short to cause attachment, except at exceedingly small gap widths, and therefore was not tested extensively for its attachment characteristics. However, the three larger collars were tested extensively over a wide range of gap widths. At each gap, the attachment location was found for several Mach numbers between 0.1 to 0.5.

4.1.1 Effects of Geometry on Attachment

Though the oil and lampblack visualization experiment was simple to perform, it was plagued with a relatively high uncertainty due to both accuracy and repeatability. For that reason, an alternative technique utilizing the static pressure distribution on the collar was employed. Using the high resolution pressure profiles that were obtained, the local maximum wall pressure could accurately and precisely be found. Over the wide range of geometry studied, the location of peak collar pressure correlated well with the visually located parting line, this comparison is illustrated in Figure 4.1. There was a tendency, though, for the point of maximum collar pressure to lie slightly downstream of the visually located parting line. This effect is caused by the compression of the high

velocity streamlines as they impact the wall. Due to the transport of momentum across the shear layer, flow along the stagnation streamline has a lower velocity, and hence a lower total pressure than the flow near the jet centerline. Yet it is these higher velocity streamlines that impinge on the collar slightly downstream of the stagnation streamline, and though they do not fully stagnate, they recover a good deal of their total pressure. The streamline compression slightly skews the pressure peak to the downstream side of the attachment point. However collar curvature diminishes this effect, and so for the three collars studied, dye visualization results matched pressure maxima well enough to justify using the pressure data to characterize the attachment point. Since the pressures could be time averaged, the repeatability of the experiments was vastly improved. Furthermore, since the locations of the pressure taps were precisely known, the accuracy was improved. Thus, it is advantageous to use the collar pressure profiles as the primary method of evaluating the attachment location.

A typical pressure profile for a full circular collar is shown in Figure 4.2. In the upstream half of the recirculation bubble, wall pressure is nearly constant. In the downstream half of the bubble, however, the flow begins to impinge on the collar. As a result, the pressure increases. It reaches a maximum value where the jet stagnates on the wall. This point will be denoted as the jet attachment point, since it is approximately congruent to the location of the parting line. The location of attachment is independent of Mach number throughout the range that was studied, which was to be expected, since there is no appreciable change in the behavior of shear layer until the convective Mach number exceeds 0.3 [17],

[19], which corresponds to M ≈ 0.6, for an unheated free jet. For high subsonic Mach numbers, and supersonic flows the shear layer dynamics change appreciably, therefore one would expect different collar pressure profiles (as a function of Mach number), and longer attachment distances. Due to the limitations of our facility, these cases were not investigated.

Presented in Figure 4.3 are experimental collar pressure profiles obtained by fixing geometry and varying Mach number. Upstream of the attachment point, the pressure scales with the exit momentum of the jet. Immediately downstream of the attachment location, the flow becomes wall bounded, and the collar pressure no longer scales perfectly with the momentum of the jet. This absence of scaling between pressure and momentum is expected, due to fact that viscosity plays an increasing role in the fluid mechanics after the flow becomes wall bounded. The flow remains attached to the wall for some distance, then separates when the boundary layer becomes too thick to continue into the adverse pressure gradient. Due to the jet's radial curvature, the pressure on the wall is sub-atmospheric until the separation point, where the pressure is equalized with the ambient. The higher momentum flows have higher wall Reynolds numbers. In other words, the viscous effects, which cause separation, are smaller compared to fluid inertial effects. As a consequence, high momentum flows are more resistant to separation, and they remain attached to the collar for a longer period of time. This can be seen in Figure 4.3 comparing the M = 0.52 profile with that of M = 0.18.

The goal of the experimental study is to qualify the validity of the model. In Figure 4.4, the angular attachment location is plotted as a function gap width for each of the three collars. Superimposed on this plot are the predictions of the model, as outlined in Section 2.

The angular attachment location is pushed progressively downstream, with increasing offset distance, until about 55°, corresponding to an attachment length of 0.82R. Beyond this point, attachment is not experimentally observed due to three dimensional effects. Boundary layers on the side plates begin to develop immediately downstream of the jet exit. Following the bubble region, the flow faces an adverse pressure gradient whose strength depends on P_B-P_∞. At some point, this adverse gradient will cause boundary layer separation on the side plates. The point where this occurs depends on strength of the pressure gradient (P_B-P_∞), which scales inversely with the collar curvature (1/R), and the local Reynolds number. When separation does occur, ambient fluid gets drawn into the bubble region via the boundary layers on the side plates, which extend to the outer edge of the collar, as shown in Figure 4.2. Due to this leakage, it becomes impossible for the jet to sustain the bubble pressure necessary to hold itself to the wall; thus it detaches. Leakage in the plenum chamber has a similar effect. This phenomenon is observed at attachment angles greater than 55°, which correspond to x/R = 0.96 and L/R = 0.82.

Figure 4.5 shows the average measured bubble pressure made dimensionless by the forward momentum flux of the jet and plotted vs. gap

width for each collar. Plotted on the same axes is the equilibrium bubble pressure predicted by the model. The pressure difference (P_B-P_∞) scales inversely with collar curvature, and is nominally independent of gap width. If this equilibrium pressure cannot be sustained by the jet, then the jet will not attach. Similarly, if the collar does not extend past the point of attachment, the attaching streamline will not seal against the wall, and the jet cannot attach, refer to Section 1.2 for a more detailed explanation.

In the actual implementation of a CFTV system, attachment must be avoided. This means that the pressure in the plenum must be kept from reaching the equilibrium pressure, or the collar length must be sufficiently shorter than the attachment length. If these conditions are met, jet attachment is not possible. From a design standpoint it is safer to prevent attachment by shortening the collar length, since pressure regulating devices are subject to a certain response time, and can fail. The model works well to predict this point, and therefore is a valuable tool in the CFTV design process.

The collar length plays a critical role in determining the overall performance characteristics of the system, as shown in equation (1.6) and Figure 1.2. It is therefore useful to characterize the attachment location as a length rather than an angular location. Plotted in Figure 4.6 is the attachment length, L/H, vs. nozzle offset distance, G/H, for all three collars tested. In addition, attachment length data for an adjacent flat plate (R=∞); from Bourque and Newman [9], and Rodrigue [18] is plotted. Observing how the data points collapse, it is apparent that the curvature of the collar plays a relatively minor

role in the attachment process. This can best explained by looking at the simplified equations of motion, given in Section 1.1. The equations of motion indicate that the radial pressure differential, required to turn the flow (i.e. P_B-P_∞), is inversely related to jet's radius curvature (i.e. 1/R'). For a given gap width, G, the jet's radius of curvature, R', for a curved wall (R/H = 5 for instance), has to be much smaller than it would be for a flat wall ($R \approx \infty$), if it is to attach at the same length, L_{att}. Therefore the pressure differential, in the case of the curved wall, must be much greater than with the flat wall case, in order to balance this additional curvature. Although, because of the geometry of the collar, the shear layer has a much longer exposure to the bubble region in the curved case. Because of this additional exposure, the jet is capable of sustaining a lower bubble pressure, thus enabling the jet to turn tighter and attach to the collar at nearly the same length. Plotted in Figure 4.7 is a least squares curve fit for all the data presented in Figure 4.6. To a good approximation, one can obtain a ball-park collar design length, based solely on gap width, using this curve. Mathematically, the maximum collar length in the absence of counterflow can be expressed as follows:

$$\frac{L}{H} = 1.92\,G/H + 1.9\left(1 - \exp(-2.1\,G/H)\right) \qquad (4.1)$$

4.1.2 Truncated Collar Surface

All of the data, shown in Figures 4.6 and 4.7, were taken such that the collar surface extended well beyond the point of attachment. This was purposely done to avoid any effects that flow separation, on the trailing edge of the collar, might have on the attachment location. This is consistent with the model, which assumes the jet attaches to an extended collar surface. However in a typical CFTV application, the collar will be truncated sharply. It was therefore necessary to investigate the possibility that the attachment location could be altered due to edge separation effects. To do this, the R=6 cm collar (R/H=6) was truncated in two stages: first to a length of 4 cm (included angle ≈ 42°), then to a length of 3 cm (included angle ≈ 30°). For both cases, the offset distance was varied, and collar pressure profiles were taken in the exact manner as with the full collar. Figure 4.8 depicts the collar pressure profile measured for G/H = 0.7, and L/H = 4. Above the plot is an illustration of average flow behavior as the jet attaches to the wall. The primary difference between the truncated collar and the full collar is that the pressure taps at the downstream edge show a significantly large negative pressure; contrasting the smooth transition to ambient pressure made by the jet on the full collar. This indicates that the jet is not separating on its own due to viscous effects, rather it separates on the trailing edge of the collar. So long as all of this occurs downstream of the attachment point, the relationship between attachment length and gap width for the truncated collars match that of the full collar very well, this is illustrated in Figure 4.9. Only as the attachment

length gets exceedingly close to the collar length do effects of the low pressure on the edge arise. However, in this study, all attachment data was within the experimental uncertainty of the model's predictions. In the case of the 4 cm collar, self attachment at gaps greater than 13 mm ($G/H \geq 1.3$) in the absence of counterflow, were not possible. Similarly, at the 3 cm length, attachment was not possible at gap widths greater than 7 mm ($G/H \geq 0.7$). Both these values are consistent with the predictions of our model, verifying its validity for truncated as well as extended surfaces.

4.2 Counterflowing Cases

In the design of a CFTV system, it is desirable to generate the control pressure, P_B, required to vector, without excessive amounts of counterflow. This is the case for two reasons. First, secondary mass flow requires energy input, which costs money. More importantly, increased secondary mass flow increases the susceptibility for attachment. Up to this point, our experiments have only addressed the influence that geometry has on attachment length. Two other factors that affect attachment location remain; the shear layer mixing rate and the amount of counterflow being drawn from the bubble region.

The mixing of the jet with the surrounding fluid can be characterized by the growth of its shear layers. By definition, the shear layer is the portion of the flow in which primary momentum is being transferred to the ambient. A growing shear layer signifies spatial entrainment of mass. The faster a shear

layer grows, spatially, the more rapidly fluid is entrained. A jet with highly active mixing attaches more readily, and requires less collar surface area to hold the itself to the wall, than a jet with poor mixing characteristics. The shear layer growth rate is affected by the velocity ratio, the density ratio, and the convective Mach number, according to equation (2.60).

The tests conducted in our facility were all done at convective Mach numbers sufficiently small to insure negligible variation in the mixing characteristics of the jet, i.e. $M_c \leq 0.4$ [18]. In addition, the jet's stagnation temperature was maintained at or near the ambient temperature; eliminating any appreciable density differences. The only external parameter that affected the mixing characteristics of the jet, in our experiments, was the presence of secondary flow. To quantify this effect, axial velocity measurements were taken along the centerline of the jet. The resulting profiles are shown in figure 4.10. Clearly, the core length decays with increasing counterflow ratio, signifying an increase in shear layer growth rate. To characterize this effect, let us define a measure of the potential core length, x_C, referring to these axial velocity profiles.

$$u(x_C) = 0.95u_1 \tag{4.2}$$

Values obtained using this definition are substituted into equation (2.59) to calculate an effective shear layer growth rate. Figure 4.11 shows this calculated quantity plotted against the velocity ratio. On the same axes is the

theoretical relationship given by equation (2.60). Both analyses show clearly that mixing is greatly enhanced by pulling counterflow.

The effect of secondary flow is to shorten the attachment length, however, not solely due to the enhanced mixing. The fact that flow is being drawn from the bubble region assists the jet in sustaining the equilibrium bubble pressure. As a result, the shear layer requires less contact with the bubble region to perform its pumping duties. Due to the additional flow leaving the control volume, the pressure inside the bubble region decreases. This allows the jet to turn with a tighter radius of curvature.

In the absence of counterflow, the attaching streamline originates from the edge of the nozzle. When counterflow is applied, there is a fraction of mass-flow pulled from the primary stream which exits the control volume as secondary flow. Hence the attaching streamline originates from a location above the edge. This effect, which is illustrated in Figure 4.12, reduces the magnitude of momentum leaving the control volume. Consequently, the bubble region is reduced in size which also results in a shorter attachment length.

To study the effect of counterflow on attachment distance, experiments were performed with the jet attached and the secondary flow system running. The geometry was left fixed, while the mass flow rate of the secondary flow stream was varied. Figure 4.13 shows the effect secondary mass flow ratio has on the collar pressure profile. The general shape of the profile remains the same. However flow is being drawn off the main jet against the will of the turbulent entrainment mechanisms within the jet; causing a reduction in bubble pressure,

and causing the jet to turn with a lower radius of curvature. Moreover, the reduced turning radius causes the intersection angle, between the attaching streamline and the wall, to increase. This results in higher pressure recovery at the stagnation point. Figure 4.12 illustrates this effect as well.

The effect of secondary mass flow on the attachment location is plotted in Figure 4.14 for two representative test geometries; G/H = 0.5, and G/H = 1.3, both utilize full circular collar surfaces of R/H=5. Superimposed on this plot are the predictions given by the model. The excellent correlation qualifies the model's ability to make predictions about jet attachment with counterflow.

Section 5: System Design

In Section 1, the advantages of implementing a thrust vectoring system were outlined. Indeed, there are disadvantages associated with thrust vectoring systems as well. First, there are costs required to modify the airframe, both structurally and in dimension. Regardless of the method chosen to steer the jet's thrust, there will be some additional weight and drag, as well as some sort of auxiliary power input required. Furthermore, the actual vectoring process can cause a significant loss in primary thrust, depending on how it's done. Of the three main methods discussed in Section 1 (moving the motor, installing turning vanes downstream of the jet exit, and fluidic control), counterflow thrust vectoring, "CFTV," fares comparatively well. Since the collar surfaces are the only additional hardware required, weight gain is kept to a minimum. Because the engines and the collars are stationary, the airframe need not be significantly modified. In addition, preliminary tests indicate that there is very little primary momentum loss due to fluidic vectoring, unlike deflection based methods [3]. This is because the jet is steering itself; there is no wall interaction. The counterflow will require additional power input, and the additional collar surfaces will cause drag; owing to the sub-atmospheric surface pressures. However in a carefully designed CFTV system, these penalties will be minimized.

In proposing a design for a CFTV system, the size of the engine–its dimensions and thrust output–will be specified. The external collar geometry

and the secondary flow system must be supplied by the designer. The secondary flow system is characterized by its pumping curve, which relates the potential mass flow rate with the pressure difference across the pump. The collar geometry is characterized by three independent geometric variables: the collar length, L, its radius of curvature, R, and the gap width, G. The system must be capable of vectoring continuously and rapidly to some specified maximum vector angle, $\delta_{v,max}$. Preliminary tests indicate that transient response is excellent, so continuous operation up to $\delta_{v,max}$ is the only quantifiable design output. The components of the CFTV system must be designed so as to minimize the penalties, i.e. thrust reduction, drag losses, and energy input, while maintaining this output.

5.1 Collar Design

It has already been established that the collar is critical to the performance of a CFTV system; because of its effect on the operating curve, as well as for attachment concerns. Therefore, designing the collar is the place to begin. There are three major criteria to consider when designing the collar. 1) It must be aerodynamically incorporated into the airframe. The farther the collar projects from the edge of the nozzle, the more drag it will incur on the aircraft. 2) It must facilitate vectoring with a minimal amount of energy input. The main benefit of fluidics is that, by taking advantage of the natural entrainment phenomena in the main jet, high momentum flows can be manipulated with low power flows. In

this sense, length plays a crucial role in the collar's "efficiency." 3) The operating curve must be smooth and continuous. This means avoiding jet attachment as well as any collar interference effects (which will be discussed in this section). This is the most formidable challenge in the design process.

5.1.1 Aerodynamic Drag

Aerodynamic drag can be expressed as a sum of the skin friction and the pressure drag. Assuming the collar can be incorporated into the engine in an aerodynamic manner, the drag due to skin friction will not be drastically increased. The majority of added drag will result from the sub-atmospheric pressure on the outward facing portions of the collar surface. Since the control pressure approximately prevails over the entire collar surface, the drag force per unit width can be written as the product of this pressure with the projected area.

$$\text{Drag} = (P_\infty - P_B)[G + R(1 - \cos\theta)] \tag{5.1}$$

Substituting in equation (1.6) for the operating curve:

$$\text{Drag} = \frac{J}{L}\sin\delta_v[G + R(1 - \cos\theta)] \tag{5.2}$$

$$\text{Drag} = J \sin\delta_v \left[\frac{G}{L} + \frac{R}{L}\left[1 - \cos\left(\sin^{-1}\left(\frac{L}{R} \right) \right) \right] \right] \qquad (5.3)$$

If minimizing drag were the only issue to consider, the collar surface would be flat (or with a large radius of curvature). In addition, the gap would be minimized. A design of this nature would make the best use of the collar's surface. The low pressure on the collar surface would be directed inwards; steering the jet, rather than outward; where it opposes the thrust force of the jet. The lack of collar curvature has virtually no effect on the jet attachment length, an important result of Section 4, nor does it affect the operating curve, see Section 1.1. However, slight curvature is necessary in order to achieve large vector angles. This is so the edge of the collar does not interfere with the jet.

5.1.2 Collar Interference

An example of wall interference is illustrated in Figure 5.1. For large vector angles and nearly flat collars, the wall physically impedes the flow, disallowing continuous CFTV operation beyond a certain angle. The jet does not necessarily reach an equilibrium attachment condition, yet the interference impedes the progression of the vector angle, and destroys the nature of the operating curve just the same. Fortunately, the condition under which jet interference (with the wall) occurs is easily computed in terms of the collar geometry, and the jet vector angle. Referring to Figure 5.1:

$$y_{collar} > y_{jet} \tag{5.4}$$

If the jet and collar are going to interfere with one another, without attachment, the limiting location is going to be the downstream edge of the collar. The position of the collar, with respect to the jet's axis, y_{collar}, can be expressed mathematically in terms of its geometric parameters.

$$y_{collar} = G + R\left(1 - \cos\left(\sin^{-1}\frac{L}{R}\right)\right) \tag{5.5}$$

The position of the jet boundary with respect to the axis can be separated into two components: the position of the centerline with respect to the axis, and the position of the shear layer with respect to the centerline. Assuming the jet arcs with a constant radius of curvature in the collar region, as suggested by equation (1.5), and exits straight thereafter, the location of the centerline is calculated as a function of vector angle.

$$y_{jet,1} = \frac{H}{2} + \frac{L}{\sin\delta_v}(1 - \cos\delta_v) \tag{5.6}$$

The outer boundary of the jet is defined as the edge of the shear layer. If we assume the shear layers grow linearly, at the same rate in which the potential

core decays, then the jet width is given by $x/2c_L$. Transforming this from streamwise (polar) coordinates into cartesian coordinates, we get:

$$y_{jet,2} = \frac{L\delta_v}{2c_L \sin\delta_v \cos\delta_v} \tag{5.7}$$

Summing these two parts, the jet position can be computed. It is most susceptible to interference with the collar, at the maximum vector angle, $\delta_{v,max}$.

$$y_{jet,max} = \frac{H}{2} + \frac{L}{\sin\delta_{v,max}}\left(1-\cos\delta_{v,max}\right) + \frac{L\delta_{v,max}}{2c_L \sin\delta_{v,max}} \frac{1}{\cos\delta_{v,max}} \tag{5.8}$$

Using equations (5.5) and (5.8), the inequality in (5.4) can be rewritten as a relationship between the collar length and the gap width, for a given $\delta_{v,max}$.

$$\frac{G_{min}}{H} \le \frac{L}{H\sin\delta_{v,max}}\left[1-\cos\delta_{v,max} + \frac{\delta_{v,max}}{2c_L\cos\delta_{v,max}}\right] - \frac{R}{H}\left(1-\cos\left(\sin^{-1}\frac{L}{R}\right)\right) \tag{5.9}$$

To prevent interference, this inequality must be maintained independently of any attachment considerations. This function is plotted in Figure 5.2 for a 15° vector angle, and collars of various curvature. For a collar with a small radius of curvature, the minimum gap requirement doesn't pose any design concern whatsoever, regardless of the collar length. However for flat collars of increasing

length, interference becomes a limiting factor in the design. Likewise, for large vector angles, interference becomes an important factor. Therefore, the design that would be ideal for drag reduction (flat collar with small gap width) becomes problematic when interference effects are considered.

5.1.3 Secondary Pump Power

To vector the jet, we need to sustain a sub-atmospheric pressure in the gap region. This requires the use of a secondary flow system. Technically, there is no prescribed amount of secondary flow needed to statically maintain a given vector angle; the vector angle is controlled solely by the pressure distribution on the collar surface. Practically, however, counterflow is needed to sustain the sub-atmospheric pressure distribution on the collar.

A simple analysis, brought forth in Section 2.7, is used to predict approximately how much secondary mass flow it will take to maintain a specific control pressure, P_B. In this analysis, the secondary flow passage is assumed to be analogous to flow through a turbulent pipe. The pressure at the inlet to the channel is atmospheric, while the pressure at the mouth of the channel is equal to the control pressure, P_B. The geometry of the channel, is characterized by the hydraulic diameter, D_H, and is dependent on the vector angle, and geometry of the collar, as given by equations (5.5) and (5.6). The resistance to the flow is characterized by a dimensionless friction factor, f. This factor was determined empirically. For the M=0.5 jet, f=0.1 gives the best overall fit to the data. By

making the friction factor proportional to the primary velocity, it is shown to be valid throughout a wide range, refer to Figure 2.9.

Counterflow requires energy input, which increases operating costs. Furthermore, it shortens the equilibrium attachment length, forcing the use of a shorter collar which reduces potential efficiency. Pumping power may be expressed mathematically as follows:

$$W_{pump} = \dot{m}_2 \frac{(P_\infty - P_B)}{\rho_2} \tag{5.10}$$

The secondary mass flow rate can be written in terms of the collar geometry, using equation (2.62). We can write the pump power in the following form:

$$W_{pump} = \dot{m}_2(G, R, L) \frac{u_1^2 H}{L} \sin\delta_v \tag{5.12}$$

It is clear that by making the collar long and the gap spacing as narrow as possible, the pumping power required to sustain a given vector angle will be minimized.

5.2 Optimization

The collar is the most vital component to the CFTV system. It channels the secondary fluid in parallel with the primary fluid, exciting the shear layer,

and initiating the vectoring process. The low pressure, which prevails on the collar surface, provides the force which ultimately steers the jet. A longer collar requires less surface pressure to achieve the same net surface force, thus less counterflow is needed to sustain a given vector angle. Optimizing the performance of our CFTV system begins by optimizing the collar geometry. The total penalty, χ, incurred by the addition of a collar is the sum of the power lost to drag and the power required to operate the pump.

$$\chi = \underbrace{\dot{m}_2 \frac{u_1^2 H}{L} \sin\delta_{v,max}}_{Pumping\_Power} + \underbrace{u_p \cdot J \sin\delta_{v,max}\left[\frac{G}{L} + \frac{R}{L}\left[1 - \cos\left(\sin^{-1}\left(\frac{L}{R}\right)\right)\right]\right]}_{Drag\_Power} \qquad (5.13)$$

Which can be rewritten as:

$$\chi = \frac{u_p \cdot J \sin\delta_{v,max}}{L/H}\left(\frac{\dot{m}_2}{\rho u_p H} + \frac{G}{H} + \frac{R}{H}\left[1 - \cos\left(\sin^{-1}\left(\frac{L}{R}\right)\right)\right]\right) \qquad (5.14)$$

The total penalty, expressed by the variable χ, is written here as a function of the collar geometry; G, R, and L; (collar offset distance, collar curvature, and collar length respectively) and the prescribed input variables. The minimization of χ, (with respect to these three geometric variables) will yield an optimal collar configuration.

First and foremost, it is necessary to maintain a smooth and continuous operating curve. This means no jet attachment or collar interference. To safely avoid jet attachment, the collar length must be shorter than the attachment length, L_{att}. To guard against collar interference, the gap width must be greater than the value given by equation (5.8). These criteria restrict the domain of the geometry, however the minimization problem still has three degrees of freedom (DOF), and therefore will be difficult to perform.

The DOF may be reduced by implicitly prescribing up to two variables. For example, if the flow system is only capable of supplying a certain pressure drop, then the DOF would reduce to two. In addition, if the secondary flowrate was limited to a certain quantity, the DOF would reduce to unity, and the minimization of χ could be readily performed. However, generally, the design process of a CFTV system includes selection of a secondary pump, and thus no information about the pumping curve would be known beforehand. In this case it is still possible to reduce the optimization to one DOF, but using an alternative approach.

To avoid attachment, the collar length must be less than the attachment length, L_{att}, which is a function of G, R, and the known input parameters. The restriction imposed on the collar length will be $L \leq L_{att}$. However, it is fairly clear that the best efficiency will be achieved at a collar length equal to that of the attachment length, $L = L_{att}$. This intuitive selection effectively reduces the minimization to two DOF.

To avoid jet-collar interference, the gap must be greater than some minimum value; $G \geq G_{min}$, as given by equation (5.8). Once again, it is fairly obvious that a small gap can reduce drag as well as secondary mass flow rate, and therefore reduce χ. Therefore, we can force $G = G_{min}$ and simplify the minimization to a single DOF problem, which is readily solvable. This solution technique is to applied to the present jet facility, and the results are discussed in Section 5.4.

5.3 Secondary Flow System Design

The results of the geometric optimization of the collar can be used to compute the amount of control pressure necessary for sustaining the desired vector angle, and the corresponding mass flow rate of the secondary stream. Hence, we have determined a critical point on the pumping curve. Through the use of throttling valves, the control pressure, and the vector angle may be varied. Closing the valves altogether, would shut off all counterflow causing the jet to exit straight. The remaining issue is how to generate this secondary flow.

The incorporation of the collar design and counterflow system onto an existing jet engine is a challenging task. Due to cost, weight, and space limitations, it is advantageous to utilize some auxiliary power from the engine for pumping, rather than installing a separate vacuum pump. On a jet engine, there are numerous places to draw high pressure, high velocity air, however we

require low pressure source to provide counterflow. A convenient way to convert high velocity air into a low pressure source is to use an ejector pump.

An ejector pump is a device which employs principles similar to that of an attaching jet. Due to viscosity and turbulent transport mechanisms inherent in the shear layer, a jet entrains fluid. In a sense, a jet is a pump. It can be effectively harnessed by restricting its natural entrainment. This is essentially what is happening with a jet attaching to an adjacent surface. The jet is pumping itself right to the wall, and remaining there due to its own entrainment mechanism. Recall that, under equilibrium conditions, there is a region of sub-atmospheric air recirculating near the wall. An ejector pump merely takes advantage of this vacuum region to pump secondary fluid, see Figure 5.3. Ejector pumps are good at providing small amounts of mass flow at high pressure drops. They don't function well in high flowrate applications, however this seems to meet our requirements quite nicely.

The use of an ejector pump has numerous advantages over a conventional secondary pump. 1) It eliminates any moving parts, which reduces both initial costs as well as long term maintenance costs. 2) It weighs much less than a rotating pump, and can be incorporated into the existing engine very elegantly. 3) It makes use of existing high pressure air. The actual details of its implementation are dependent on the specifications of the engine and the collar design, but the basic physical idea is the same.

5.4 Optimization Results

The optimization technique described above was applied, through the use of a computer program. The model was solved iteratively using a commercially available software package, EES; the worksheet is listed in Appendix B2. The model consists of three parts. One to calculate attachment length, another to find the interference limited gap width, and a third block to calculate pumping power losses, and drag on the collar surface. Input variables are the same as with the attachment model, with the addition of vector angle. Geometric parameters are set to initial guess values. To begin, the minimum gap, at which interference occurs, is computed. If the initial guess value of gap with is less than the minimum value, $G < G_{min}$, then it is updated to: $G = G_{min}$. Next, attachment length is calculated. If the collar length is greater than the attachment length, $L > L_{att}$, then: $L = L_{att}$. For this current geometric configuration, the secondary flowrate requirements, and the drag can be estimated. They are summed to obtain χ. The computer program iterates, varying collar geometry, until the total penalty is minimized.

This procedure was applied for conditions corresponding to our present experimental jet facility, described in Section 3 (4 cm x 1 cm rectangular jet). The operating conditions were: $M = 0.5$, and $T_0 = 298$ K. The maximum desired vector angle was 17°. Since the secondary flow system in the laboratory had sufficient capacity, there were no restrictions placed on it; rather the collar length was set to equal the attachment length, and the gap width was set to its

minimum (interference limited) value. Tabulated in Table 5.1 are the dimensionless geometric parameters which describe this optimal design. A scaled drawing of this nozzle geometry is pictured in Figure 5.4.

G/H	0.18
L/H	1.15
R/H	2.6
m_2/m_1	3.5%
ΔP_B	65 torr

Table 5.1: Results of geometric optimization for present jet facility

To confirm that a collar of this geometry would perform as designed, one of similar geometric dimension was fabricated. An existing collar of R/H = 6, was truncated to L/H = 1.15; the gap was set to G/H = 0.2. The collar was installed, and the level of counterflow was varied throughout the pump's range. The vector angle was measured for each level of suction by traversing a pitot probe throughout the velocity field (this is outlined in Section 3).

Figure 5.5 shows the experimentally determined operating curve, along with the predicted operating curve given by equation (1.6). Figure 5.6 shows the counterflow requirements compared with the model predictions. It is impossible to say, for sure, whether or not this geometric configuration truly represents the optimum without testing the whole geometric regime. However, the system was

capable of smooth and continuous operation up to (and slightly past) 17°, with relatively low amounts of counterflow, as shown in Figure 5.4 and 5.5, therefore, it is operating "as designed."

Section 6: Conclusion

6.1 Summary

The ability to redirect the thrust of a aircraft engine, offers several advantages. It provides a vertical component of thrust which may be used, especially at low speeds, to augment the lift force generated by the wings. This allows the aircraft to take off in a shorter distance, and climb at a faster rate. In flight, maneuverability will be enhanced and the aircraft will be able to fly under post-stall conditions. During landing, approach speeds may be reduced without increasing the rate of descent. Thus the runway can be approached at a slower speed, reducing required landing distance.

There are various methods to vector the exhaust thrust of a jet engine; possibly the most promising method is counterflow thrust vectoring (CFTV). With CFTV, no moving parts are directly required to steer the jet. Consequently, reliability is greatly enhanced. In addition, there are no surfaces in direct contact with the high temperature, high velocity exhaust gases. This eliminates the need for expensive materials or exotic cooling schemes. Furthermore, because the jet is steering itself, and there is no contact by any external surfaces, a much greater percentage of the thrust is recovered, thereby increasing aircraft performance. Finally, the CFTV system may be retrofitted into an existing aircraft's engine without significant alteration of the airframe. The result is a reliable, robust system with a relatively low initial cost, and minimized maintenance costs.

CFTV works by pulling small amounts of secondary flow in parallel with the primary flow of the jet. When this is done, the turbulent mixing characteristics of the shear layer are markedly improved. When this is done asymmetrically, that is, only on one side of the planar jet, there is a transverse pressure gradient formed. The addition of a collar amplifies this effect in two ways. First, it channels the secondary flow, effectively creating a countercurrent mixing layer over the entire length of the collar. Second, it restricts the natural entrainment of the jet, which intensifies the cross stream pressure gradient. A longer collar has more surface area for the pressure forces to act on. Thus, a smaller pressure differential will impart an equal transverse force on the jet. Hence, the same vector angle is achievable with a smaller amount of vacuum from the secondary flow system. The net effect is an increase in system efficiency. The functional operating curve is given by equation (1.6), which is rewritten here:

$$\delta_v = \sin^{-1}\left(\frac{(P_\infty - P_B)L}{J}\right) \qquad (1.6)$$

Where:

δ_v = the exit vector angle

J = the forward momentum of the jet

L = the collar length

P_B = the control pressure

P_∞ = the local ambient pressure

While the collar is vital to the efficiency of the CFTV system, it poses potential bistability problems which can disrupt the continuity of the operating surface. Fortunately, the collar; whose geometry can be characterized by its length, L, radius of curvature, R, and the gap width, G; can be designed to prevent this situation from occurring. The primary focus of this study was the prevention of jet attachment, often referred to as the Coanda effect. This is where the jet reaches a stable equilibrium on the wall. Upon attaching to the collar, the jet's vector angle makes a discontinuous jump, making implementation impossible. To avoid jet attachment, the conditions necessary for attachment equilibrium on the wall must be avoided.

A model is developed herein to predict the steady state, equilibrium attachment conditions. This model employs a control volume approach, which is similar to previous modeling studies [7]-[16], see Section 1.2. The boundary conditions are based on physical arguments or simplified analyses. By conserving the flow of mass and momentum into the control volume, the equilibrium attachment conditions can be computed for various collar geometries and jet operating conditions. To test the validity of the model, over a wide range of operating conditions, an experimental facility was fabricated. Full circular arc collars, of three different radii of curvature, were tested extensively at various offset distances, various jet Mach numbers ranging from 0.15 to 0.50, and various levels of counterflow. The attachment locations, predicted by the model correlate remarkably well with data obtained via experiment, for the full collar as

well as truncated collar surfaces, and with varying levels of counterflow. An important observation is that the attachment length, measured from the exit plane of the jet to the attachment point, is nominally independent of collar curvature. In addition, the equilibrium bubble pressure scales inversely with collar curvature, and was nominally independent of gap width.

The design of the collar geometry should incorporate three qualities. It must be aerodynamic, vector efficiently and operate continuously up to the maximum desired vector angle. To preserve continuity of the operating curve, the jet cannot be allowed to attach to the collar surface. Moreover, the collar cannot interfere with the jet at any time during its operation. The efficiency refers to the amount of power required to operate the secondary pump, as compared with the power of the primary stream. Aerodynamics are characterized by the amount of power needed to overcome the additional drag caused by the collar. The sum of the power spent on operating the secondary pump, and overcoming drag effects reflect the total "penalty" inflicted by the collar. By minimizing this penalty, we arrive at an optimal geometric configuration. The use of the model, shown in Appendix B2, allows the penalty to be written in terms of the collar geometry (G, R, and L) and the known input variables ($\delta_{v,max}$, J, H, $T_{0,JET}$, and M), so that the optimization can be quantified. In essence, we have a tool that aids our CFTV system design. This optimization was carried out for the jet facility described in Section 3 (namely an unheated, M = 0.5 jet, exiting through a 1 cm x 4 cm rectangular nozzle); the results are shown in table 5.1. Tests conducted using this geometry indicate rapid and continuous

vectoring, up to the designed $\delta_{v,max}$ of 17°, while using less than 5% counterflow (compared to primary flow); performance nearly identical to that which is predicted.

6.2 Current and Future Work

Current research on CFTV is focusing on supersonic axisymmetric vectoring using both a circular nozzle with an annular collar, and a diamond shaped nozzle and collar. For both cases, the nozzles are designed for M = 2 operation, with a variety of flow conditions being studied: including over, under, and ideally expanded flow; with and without heating of the primary flow. At present, no optimization procedure, such as the one presented herein has been developed for axisymmetric nozzles. It is not clear how the performance characteristics of the CFTV system will change with the circular, and diamond shaped, nozzle geometries. Similarly, it is not clear, as no attachment data has been taken in a supersonic jet, whether the attachment model developed in Section 2 will accurately extend to supersonic flow. To adequately design an axisymmetric CFTV system, these issues need to be addressed. The first step to such a design procedure would be to look at the operating curve for each of the axisymmetric facilities. It will then be necessary to accurately predict, either analytically, or empirically, the jet attachment characteristics of each nozzle-collar configuration. Once this background is in place, a design procedure may be proposed.

Appendix A1: Velocity Profile Beyond the Potential Core

Generally, it is desirable to have a CFTV system that is compact in size; for aerodynamic purposes. This precludes the use of long collars, or collars with large gap widths. As a consequence, the potential core region is the region of interest for our modeling study. However, there is no reason why the velocity profile assumption can't be altered to accommodate the region downstream of the potential core.

As a planar jet exits into the ambient, turbulent and viscous transport mechanisms cause a transfer of momentum from the high speed jet to the ambient. As the fluid travels in the downstream, the shear layers grow, and eventually merge. Upon merging, the centerline velocity, u_{max}, begins to decay, though axial momentum is still conserved. Assuming that the profile given by Görtler [10] remains applicable (which is reasonable since it was originally developed for this regime) the momentum of the jet is written as follows:

$$\frac{\rho u_1^2 H}{2} = \int_0^\infty \rho u_{max}^2 \operatorname{sech}^4\left(\frac{4c_L y}{3x}\right) dy \qquad \text{(A1.1)}$$

Since ρu_{max}^2 is not a function of y, it can be taken out of the integral. Thus evaluating the integral, we get:

$$\frac{u_1^2 H}{2} = \frac{3x}{4c_L}\left(\frac{2}{3}\right)u_{max}^2 \qquad \text{(A1.2)}$$

Simplifying we get:

$$u_{max} = u_1\sqrt{\frac{c_L H}{x}} \qquad \text{(A1.3)}$$

We now have a mathematical expression for the velocity field outside the core region in terms of the potential core length, c_L, and the initial jet conditions.

$$u(x,y) = u_1\sqrt{\frac{c_L H}{x}}\,\text{sech}^2\left(\frac{4c_L y}{3x}\right) \qquad \text{(A1.4)}$$

Appendix A2: Supersonic Jet Attachment

Since pressure signals travel at the speed of sound, there is no upstream feedback of pressure information in a supersonic flow. Therefore, there will be no skewing of the velocity profile. Instead, there will be a pressure discontinuity at the exit plane of the jet. Axial momentum, however, must be conserved across the exit plane, even in the case of a shock. It is therefore convenient to express the pressure forces, per unit depth, acting on the control volume, F_{jet}, in terms of the flow conditions immediately prior to leaving the nozzle exit, since they are dependent only on the nozzle design conditions, and the nozzle pressure ratio, i.e. upstream conditions. The pressure acts uniformly across the exit plane, thus the pressure forces, minus the ambient pressure, can be written as:

$$F_{jet} = (P_{exit} - P_{\infty})H \qquad (A2.1)$$

The momentum cross the exit plane can be written as:

$$J_{in} = \gamma P_{exit} M^2 H \qquad (A2.2)$$

Both of these quantities acting on the control volume are dependent on the pressure in the exit plane, P_{exit}, which can be found by assuming isentropic flow within the nozzle.

$$P_{exit} = NPR \cdot P_{\infty}\left(1+\frac{\gamma-1}{2}M^2\right)^{\frac{\gamma-1}{\gamma}} \qquad \text{(A2.3)}$$

Where NPR is the nozzle pressure ratio. Combining (A2.3) with (A2.1) we get an expression for the pressure forces acting on the control volume.

$$F_{jet} = P_{\infty}H\left[NPR\cdot\left(1+\frac{\gamma-1}{2}M^2\right)^{\frac{\gamma-1}{\gamma}} - 1\right] \qquad \text{(A2.4)}$$

Combining (A2.3) with (A2.2), we get an expression for the momentum inflow to the control volume.

$$J_{in} = \gamma M^2 P_{\infty}H\cdot NPR\left(1+\frac{\gamma-1}{2}M^2\right)^{\frac{\gamma-1}{\gamma}} \qquad \text{(A2.5)}$$

Along with the inherent change in the shear layer dynamics brought about by the increased convective Mach number, which is discussed in detail in section 2.5, these are the only modifications necessary to extend the model into the supersonic jet regime. It should be noted, however, that due to facility limitations, no experimental data is available for this range of flow conditions, therefore validation of the model is not available.

Appendix B1: Attachment Model

This worksheet is written to calculate the attachment location and various other peripheral variables, using the methodology set forth in Section 2. The input variables are listed at the top of the worksheet. They include all geometric configuration of the collar, characterized by G, R, and L; the jet operating conditions, and the amount of counterflow being drawn from the bubble. The operating conditions of the jet are used to evaluate the mixing characteristics, i.e. potential core length, c_L. Essentially the program conserves mass and momentum inflow to the control volume. The force variables and momentum fluxes are summed and the unknowns are computed iteratively. The output variables are written at the very bottom of the worksheet. They include the attachment length, bubble pressure, and the dimensionless variables used for presentation.

```
{Set Ambient Conditions}
Tinf=300                    {ambient temperature}
Pinf=101325*(743/760)       {ambient pressure}
rhoinf=Pinf/287/Tinf        {ambient density}

{Set Flow Conditions}
wc=.0       {counterflow ratio}
phi=1.3     {empirical constant describing exit angle}
M=0.5       {primary stream Mach number}
NPR_ideal=(1+.2*M^2)^3.5    {ideal nozzle pressure ratio}
NPR=NPR_ideal               {actual nozzle pressure ratio}
T0jet=300                   {jet stagnation temperature}

{Set Geometry }
Gap=5   {gap in mm}
R=.05   {5 cm radius collar}
H=.01   {1 cm nozzle height}
G=.06   {accounting for 1 mm thick nozzle wall}

{Shear Layer Mechanics}
Pstag=NPR*Pinf
Pstag=NPR_ideal*Pexit
Texit=T0jet/(1+.2*M^2)
rhojet=Pexit/287/Texit
dens_ratio=rhoinf/rhojet
vel_ratio=wc*H/(G-.001)
ddeltadx=.3*.067*(1+dens_ratio^.5)*(1-vel_ratio)/(1+vel_ratio*dens_ratio^.5)
cl=.9743/ddeltadx
sigma=4/3*cl

{Continuity}
Y=max((H/2-.5*x/cl),0)+y'   {equation for attaching streamline}
t=2/3-4*cl*H*wc/3/x         {streamfunction}
y'=.75*x/cl*arctanh(t)
vel=(1/cosh(sigma*y'/x))^4  {velocity on attaching streamline}

{Momentum Variables}
Jout=(1+.75*x/H/cl*(t-t^3/3-2/3))   {outflow normalized by J}
Jc=wc^2*H/(G-.001)                  {counterflow normalized by J}

{Control Volume Forces which include momentum terms in them}
Fgap=Jc-G/R'
{Fjet=1+1/(1.4*M^2)*(1-((1+.2*M^2)^3.5)/NPR)} {used for supersonic flow}
Fjet=1+H/2/R'                                 {used for subsonic flow}
Fcx=-R/R'*(1-cos(alpha))+R/2/H*vel*(2/alpha*(sin(alpha)-sin(alpha/2))-cos(alpha))
Fcy=-R/R'*(sin(alpha))+R/2/H*vel*(2/alpha*(cos(alpha)-cos(alpha/2))+sin(alpha))

{Force Balance}
```

num=-Fcy
denom=Fjet+Fgap+Fcx
ratio=num/denom
tan(exit)=ratio
exit=phi*alpha+(1-phi)*gamma

{*geometric variable relationships*}
R***sin**(alpha)=**sin**(gamma)*(x/gamma-Y)
R+G+H/2-x/gamma+(x/gamma-Y)***cos**(gamma)=R***cos**(alpha)
R'=x/gamma {*jet centerline radius of curvature*}

{*Angular variable converted to degrees*}
gam=gamma*180/**pi**
angle=alpha*180/**pi**

{*Output Variables*}
Lmax=R***sin**(alpha) {*attachment length*}
LmaxbyH=Lmax/H
GbyH=G/H
xbyH=x/H
deltaPb=(1.4*Pinf*M^2*H/R')/133.322 {*bubble pressure converted to torr*}
deltaPI=deltaPb-vel*133.322 {*stagnation pressure on collar*}

Appendix B2: Optimization Model

This worksheet is written to minimize the penalty due to drag and secondary flow power, created by the addition of a collar surface. The input variables are listed at the top of the page. They include the operating conditions of the jet, the ambient conditions, and the imposed design parameters such as maximum vector angle, or any restrictions on the independent variables. The second part consists of simple flow variables computed based on the jet operating conditions. These variables are then used to evaluate the mixing characteristics of the jet. The main body of the program contains the attachment model, the interference model, and the model to predict secondary mass flowrate in terms of bubble pressure. The output is characterized by geometric variables, G, R, and L; and the secondary flow requirements.

```
{Design Specifications Input by User}
H=.01                          {nozzle height, m}
M=0.5                          {primary jet Mach number}
T0=300                         {primary jet stagnation temperature}
Tinf=300                       {Ambient temperature, K}
Pinf=101325                    {ambient pressure in Pa}
dvmax=10*pi/180                {maximum desired vector angle, rad}
R=5*H                          {Collar radius, m}
G=0.3*H                        {gap width, m}
L=Latt                         {Collar Length, m}
wc=0.00                        {secondary mass flow ratio}
{dv'=0.000}                    {jet vector angle in degrees}
{delta_P=750}                  {control pressure in torr}

{Simple Relationships Based on User Inputs}
NPR_ideal=(1+.2*M^2)^3.5       {ideal pressure ratio}
NPR_ideal=P0/Pexit
NPR=NPR_ideal                  {real pressure ratio}
NPR=P0/Pinf
Texit=T0/(1+.2*M^2)            {jet exit plane temperature}
rhojet=Pexit/287/Texit         {primary jet density (in exit plane)}
rhoinf=Pinf/287/Tinf           {ambient density}
u0=M*(401.8*Texit)^.5          {primary flow velocity}
us=u0*wc*H/G/dens_ratio        {secondary flow velocity}
Q=rhojet*H*u0
J=1.4*M^2*Pexit*H
jetpower=J/2*u0
wc=Qc/Q

{Shear Layer dynamics}
dens_ratio=rhoinf/rhojet                                    {density ratio}
Mconv=(u0+us)/((401.8*Texit)^.5+(401.8*Tinf)^.5)            {convective Mach number}
const=if(Mconv,.45,1,1,max(.43,1-1.14*(Mconv-.45)))        {constant affecting mixing}
vel_ratio=-(us/u0)                                          {velocity ratio}
ddeltadx=.067*const*(1+dens_ratio^.5)*(1-vel_ratio)/(1+vel_ratio*dens_ratio^.5)
cl=.9743/ddeltadx                                           {potential core length}

{----------Jet Attachment Model----------}
sigma=4/3*cl

{Continuity}
Y=max((H/2-.5*x/cl),0)+y'      {equation for attaching streamline}
t=2/3-4*cl*H*wc/3/x            {streamfunction}
y'=.75*x/cl*arctanh(t)
vel=(1/cosh(sigma*y'/x))^4     {velocity pressure along attaching streamline}

{Momentum Variables, non dimensionalized by J}
Jout=(1+.75*x/H/cl*(t-t^3/3-2/3))
```

```
Jc=wc^2*H/G/dens_ratio

{Control Volume Forces, All non dimensionalized by J and simplified}
Fgap=Jc-Jout*G/R
Fjet=if (M,1,1+Jout*H/R/2,1+Jout*H/R/2,1+(Pexit-Pinf)*H/J)
Fcx=-Jout*(1-cos(alpha))+R/2/H*vel*(2/alpha*(sin(alpha)-sin(alpha/2))-cos(alpha))
Fcy=-Jout*(sin(alpha))+R/2/H*vel*(2/alpha*(cos(alpha)-cos(alpha/2))+sin(alpha))

{Force Balance}
num=-Fcy
denom=Fjet+Fgap+Fcx
ratio=num/denom
tan(exit)=ratio
exit=1.3*alpha-.3*gamma          {control volume exit angle}

{geometry}
R*sin(alpha)=sin(gamma)*(x/gamma-Y)
R+G+H/2-x/gamma+(x/gamma-Y)*cos(gamma)=R*cos(alpha)
angle=alpha*180/pi
R'=x/gamma

Latt=R*sin(alpha)                    {attachment length}
{equilibrium bubble pressure for attached jet, psig (matches experiment best)}
dPbubble=J/((R'+R)/2)*14.7/101325
{-------------------------------------------------------------------------}

{Interference Criterion}
Fdv=dvmax/(2*cl*sin(dvmax))+(1-cos(dvmax))/sin(dvmax)
Gint=L*Fdv-R*(1-cos(theta))          {minimum gap width}

{Operating Surface}
dv=dv'*pi/180
sin(dv)=dP*L/J
delta_P=dP/133.322

{Drag}
Dragloss=sin(dvmax)*(GbyL+(1-cos(theta))/LbyR)          {drag force / thrust force}

{Secondary mass flow rate}
f=(.1/170)*u0                    {friction factor for secondary flow prediction}
Abar=G+R*(1-cos(dv/2))-L/dv*(1-cos(dv/2)+dv/4/cl/cos(dv/2))*cos(dv/2)
D=4*H*Abar/2/(Abar+4*H)
dP=4*f*L*dv/sin(dv)/D*.5*rhoinf*us^2     {control pressure}
Pumploss=(Qc/rhoinf*dP)/jetpower         {pumping power / jet power}

{Geometric relationships}
LbyR=L/R
theta=arcsin(LbyR)
GbyL=G/L
```

LbyH=L/H
GbyH=G/H
RbyH=R/H

{*Total Losses*}
loss=Dragloss+Pumploss

References:

[1] Henderson, W. P., "Propulsion Systems Integration in High Performance Aircraft," **Aerospace Engineering**, vol 10, #2, p21, 1990

[2] Van der Veer, M. R., Counterflow Thrust Vectoring of a Subsonic Rectangular Jet, Master's Thesis, University of Minnesota, Minneapolis, MN, 1995.

[3] Strykowski, P. J., Krothapalli, A. and Forliti, D.J. "Counterflow Thrust Vectoring of Supersonic Jets", AIAA 96-0115, 34th Aerospace Sciences Meeting & Exhibit, Reno, NV, Jan 15-18, 1996.

[4] Strykowski, P. J. and Niccum, D. L., "The Influence of Velocity and Density Ratio on the Dynamics of Spatially Developing Mixing Layers", **Physics Today**, Vol 4, #4, pp 770-781, 1992.

[5] Strykowski, P. J. and Khemakhem, A. S. D., "The Influence of Counterflowing Velocity Ratio on the Dynamics of the Planar Mixing Layer", To be Published, 1996.

[6] Belsterling, C. A., Fluidic Systems Design, Wiley Interscience, 1971.

[7] Kirshner, J. M., Fluid Amplifiers, McGraw Hill Book Co., 1966, pp.125-134.

[8] Foster. K and Parker, G.A. , Fluidics Components and Circuits, John Wiley & Sons Ltd, New York, 1970.

[9] Bourque, C. and Newman, B. G., "Reattachment of a two-dimensional, incompressible jet to an adjacent flat plate," **Aeronautical Quarterly**, v11, p201, 1959.

[10] Schlichting, H., Boundary Layer Theory, Permagon Press, Any Èdition.

[11] Newman, B. G., "The delexion of plane jets by adjacent boundaries–Coanda effect," Boundary Layer and Flow Control, its Principles and Application, Permagon Press, pp. 232-264, 1961

[12] Perry, C. C., "Two dimensional jet attachment," Symposium on Fluid Jet Control Devices, ASME, pp. 205-217, 1962.

[13] Sawyer, R. A., Two-dimensional reattaching jet flows including the effects of curvature on entrainment," **Journal of Fluid Mechanics,** vol. 17, pp. 481-498, 1963.

[14] McRee, D. I., and Moses, H. L., "The effect of aspect ratio and offset on nozzle flow and jet reattachment," Symposium on Fluid Jet Control Devices, ASME, pp. 142-161, 1962.

[15] Mueller, T.J., "An experimental investigation of the reattachment of compressible two-dimensional jets," ASME Paper 64-FE-18, 1964.

[16] Olson, R. E., "Reattachment of a two-dimensional compressible jet to an adjacent plate," Symposium on Fluid Jet Control Devices, ASME, 1962.

[17] Papamoschou, D. and Roshko, A., "The compressible turbulent shear layer: an experimental study," **Journal of Fluid Mechanics**, vol. 197, pp. 453-477, 1988.

[18] Strykowski, P. J., Krothapalli, A., and Jendoubi, S., "The effect of counterflow on the development of comressible shear layers," **Journal of Fluid Mechanics**, vol. 308, pp. 63-96, 1996.

[19] Rodrigue, G., "Recollement d'un jet incompressible à une paroi adjacente avec injection dans la bulle de séparation." Thesis submitted at Laval University, September, 1966.

Additional References:

Jendoubi, S., Strykowski, P. J., "The Effect of Curvature on the Stability of Axisymmetric Jets," Bull. American Physical Society, Vol. 37, 1992.

Krothapalli, A., Baganoff, D., and Karamcheti, K., "On the mixing of a rectangular jet," **Journal of Fluid Mechanics**, Vol. 107, pp 201-220, 1981.

Shih, C., Krothapalli, A., and Gogineni, S., "Experimental Observations of Instability Modes in a Rectangular Jet," **AIAA Journal**, Vol. 30, No. 10, pp. 2388-2394, 1992

Strykowski, P. J., and Krothapalli, A., "The Countercurrent Mixing Layer: Strategies for Shear-Layer Control," AIAA 93-3260, AIAA Shear Flow Conference, Orlando, FL, July 6-9, 1993.

Strykowski, P. J., and Wilcoxon, R. K., "Mixing Enhancement Due to Global Oscillations in Jets with Annular Counterflow," **AIAA Journal**, Vol. 31, No. 3, 1993.

Strykowski, P. J., Krothapalli, A., Alvi, F., and King, C. J., "Mixing Characteristics of Countercurrent Compressible Turbulent Shear Layers," Proc. From 7th ONR Propulsion Conference, Buffalo, NY, Aug. 29-31, 1994.

Strykowski, P. J., Krothapalli, A., and Wishart, D., "Enhancement of Mixing in High-Speed Heated Jets Using a Counterflowing Nozzle," **AIAA Journal**, Vol. 31, No. 11, 1993.

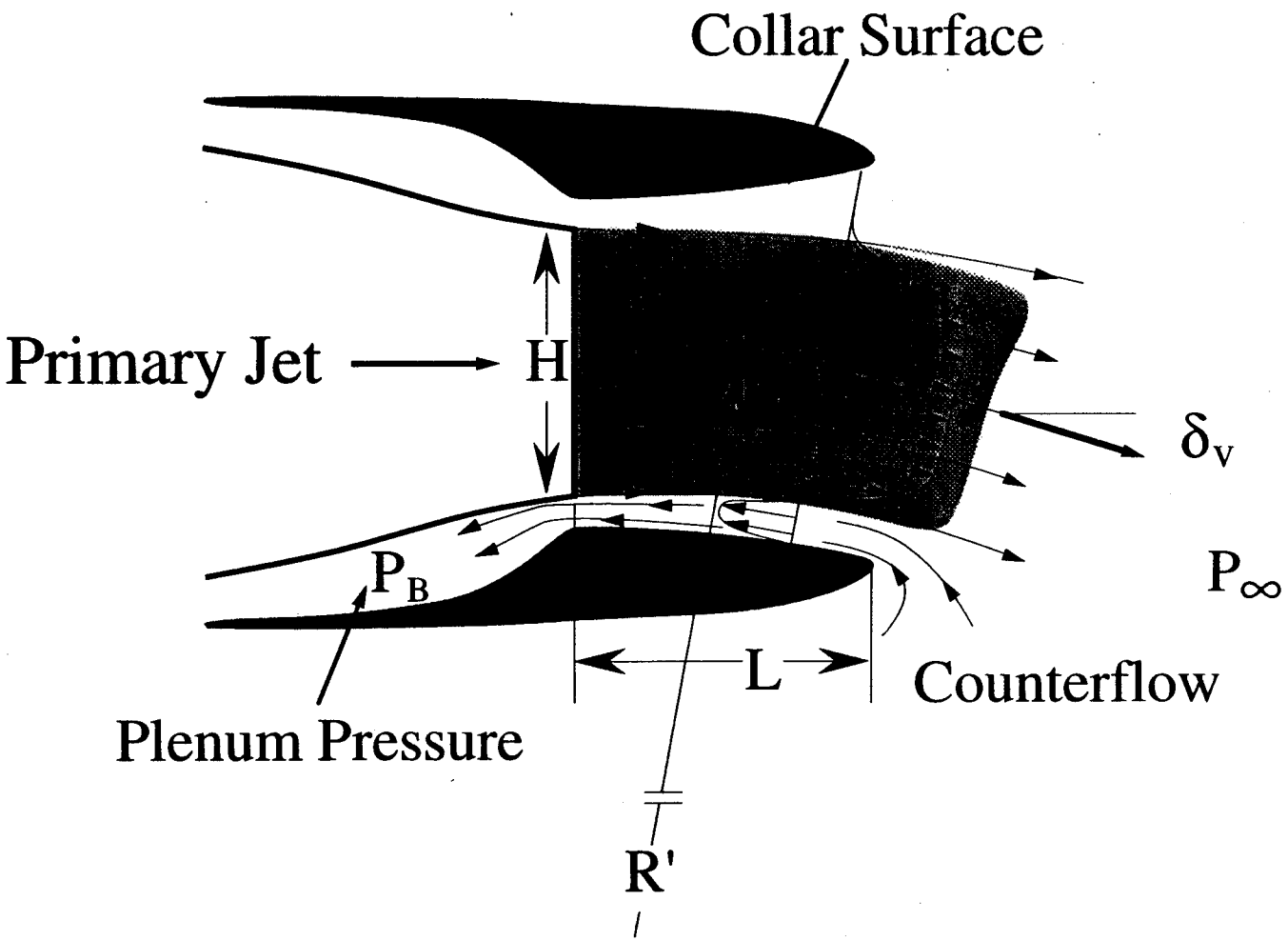

Figure 1.1 Schematic of typical counterflow thrust vectoring (CFTV) system showing primary jet being vectored by secondary flow stream.

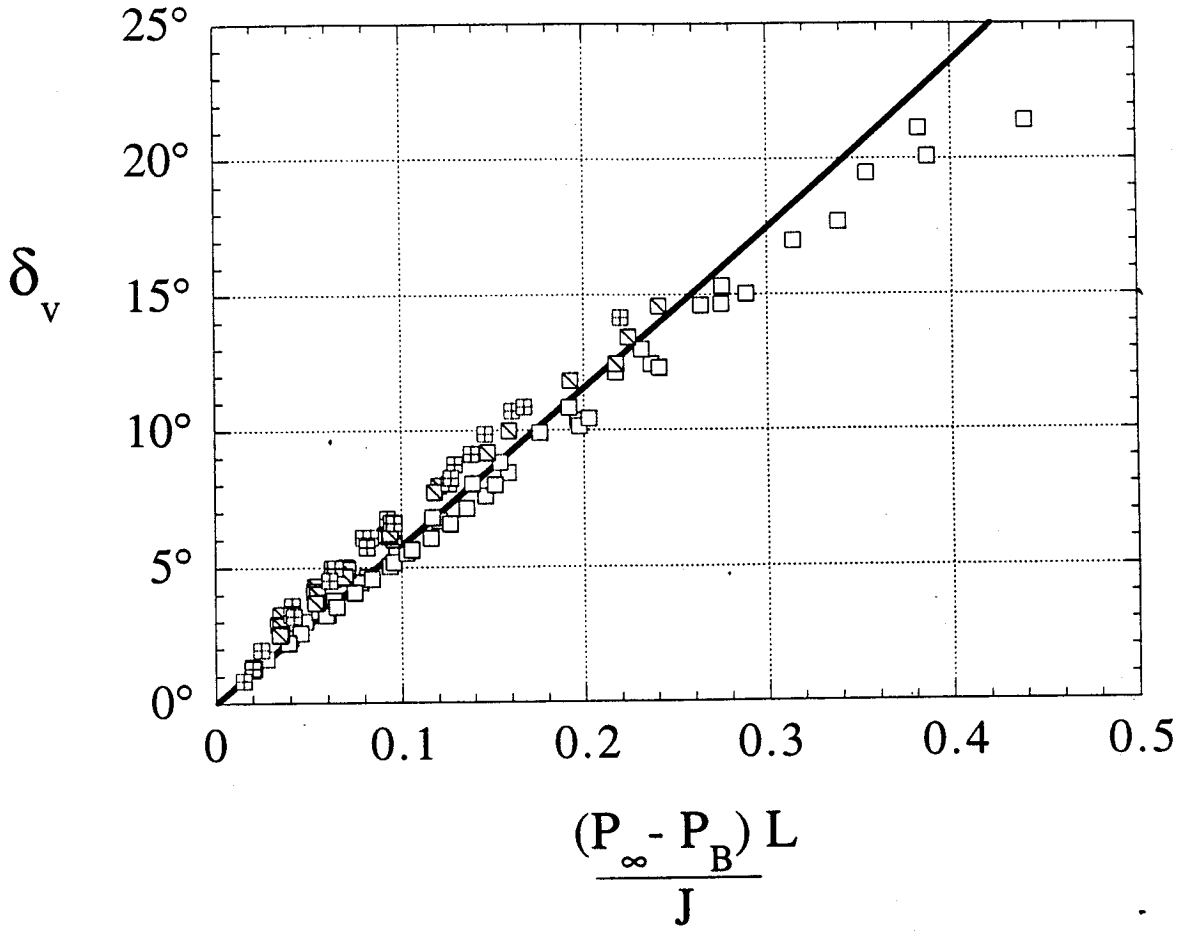

Figure 1.2 Exit vector angle plotted vs. dimensionless control parameter. Data points represent experimental work by Van der Veer [1], and Strykowski, Krothepalli, and Forliti [2], at Mach numbers ranging from 0.2 to 2.0, using collars of various lengths, and radii of curvature. Solid line represents analytical prediction set forth by equation (1.6).

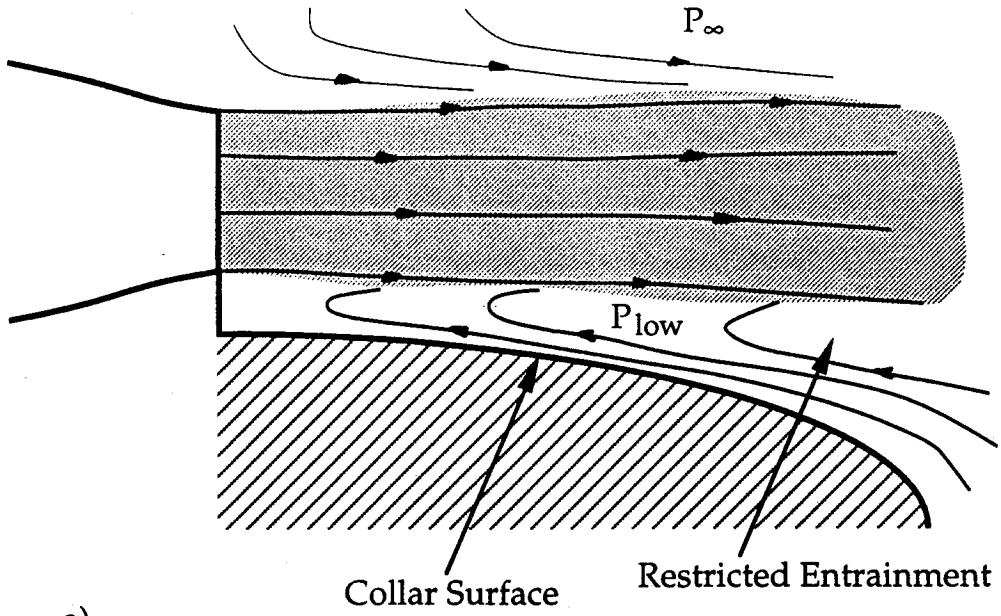

a)

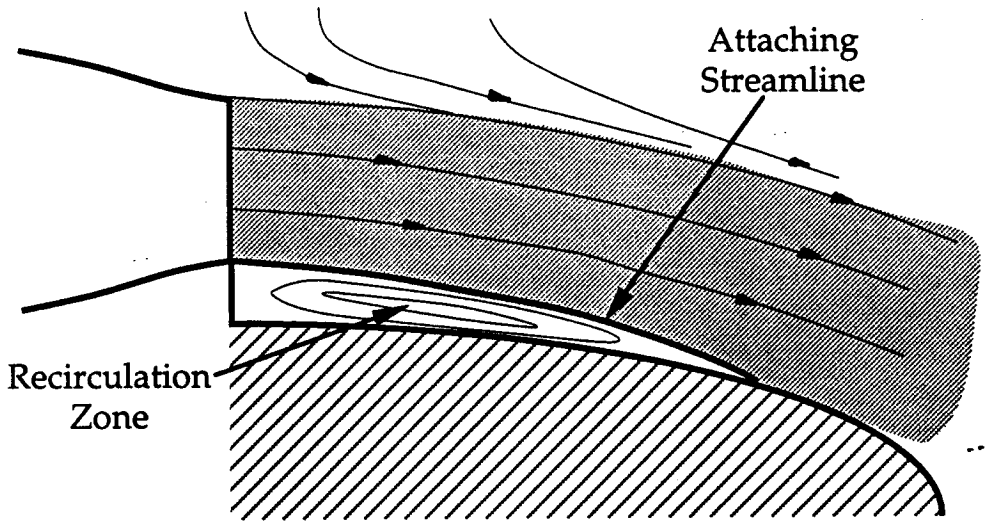

b)

Figure 1.3 Illustration of mechanism responsible for jet attachment. (a) Jet entrainment is restricted by presence of collar surface, which gives rise to cross-jet pressure gradient. (b) Jet reaches stable equilibrium attached to the collar which creates a low pressure recirculation zone.

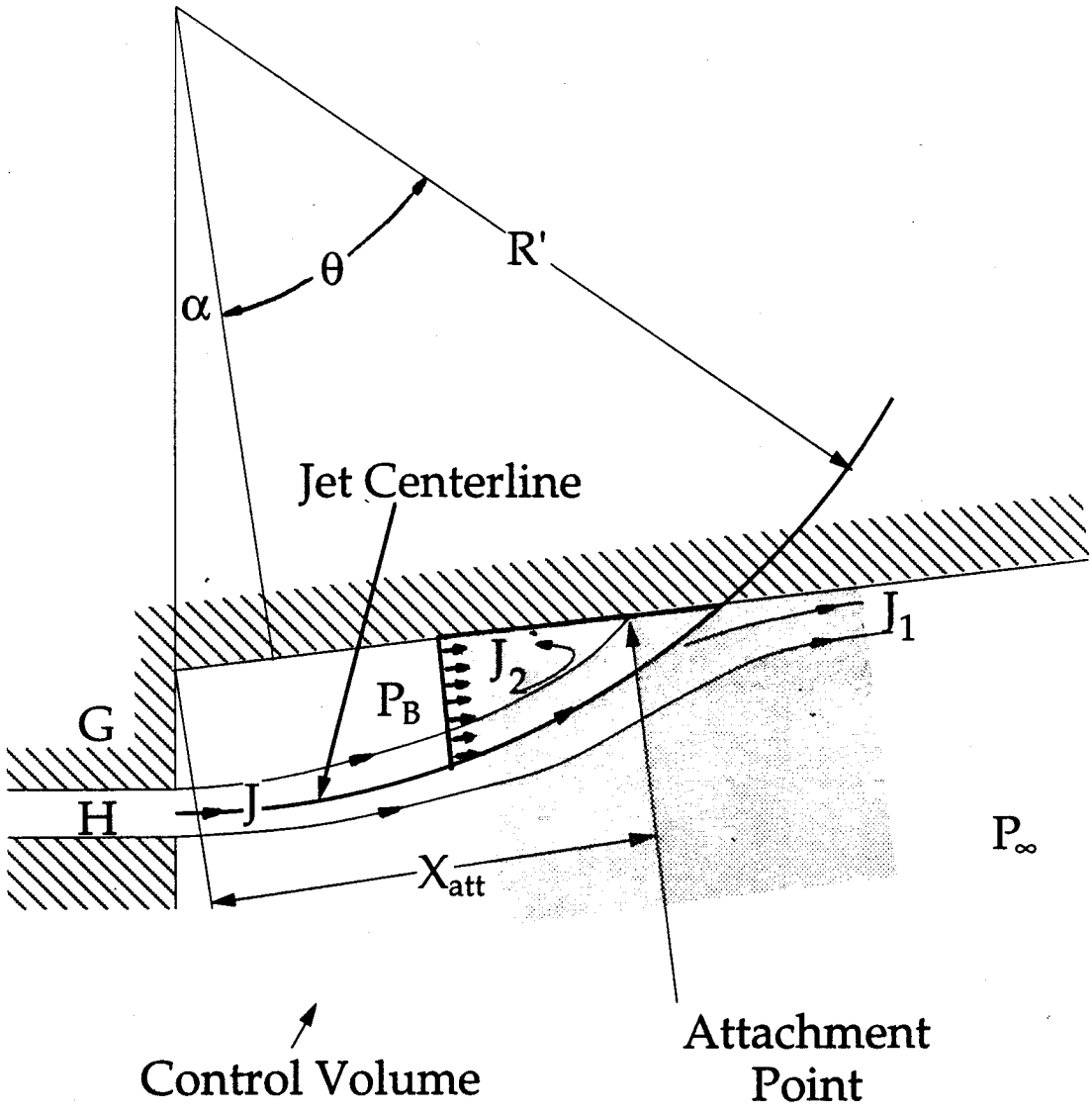

Figure 1.4 Schematic of control volume employed by Bourque and Newman [9], to analytically model a jet attachment to an adjacent flat plate. Attachment location x_{att} is computed by applying mass and momentum conservation equations.

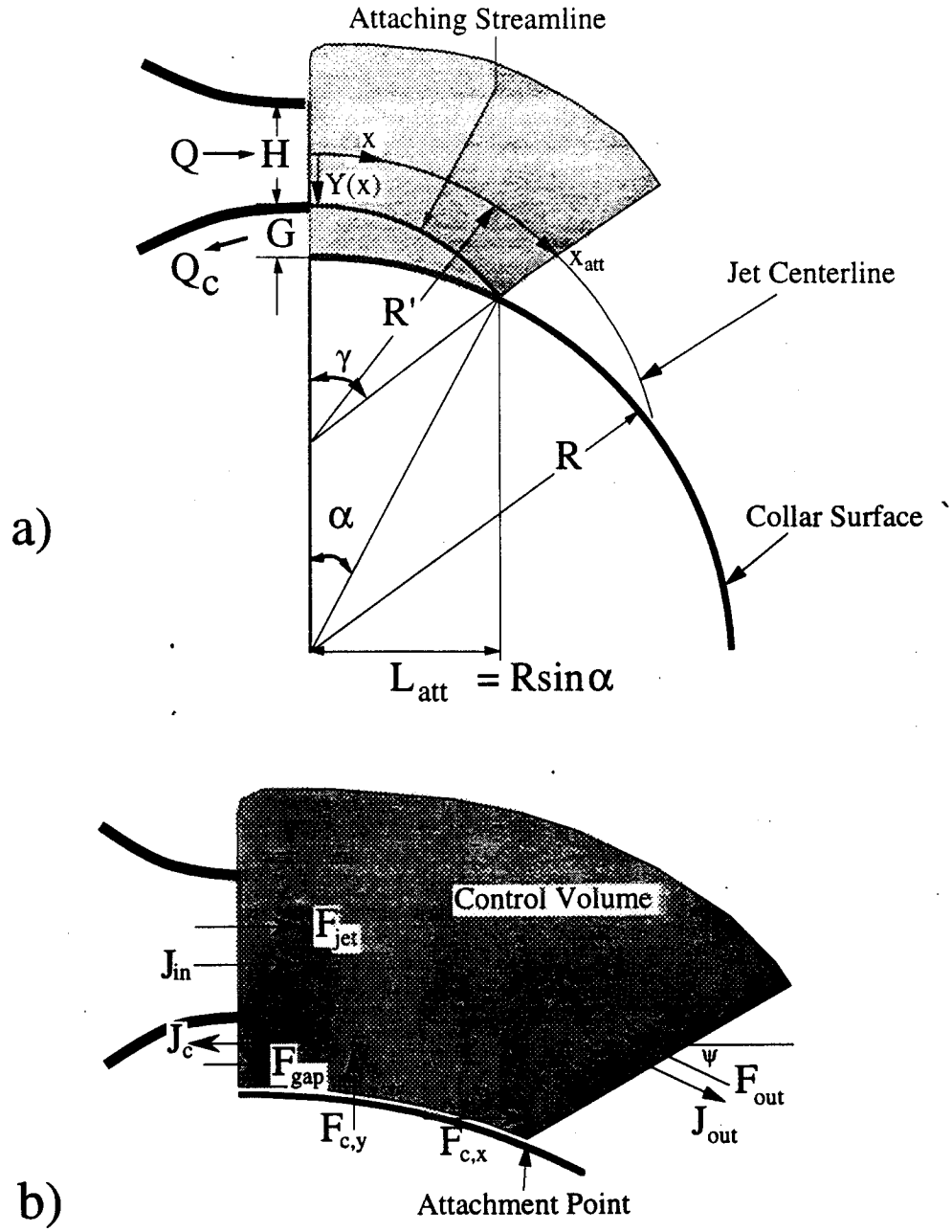

Figure 2.1 Schematic of control volume employed in this study. Part (a) shows the relevant notation used in describing the geometry. Part (b) details the pressure forces and momentum fluxes which act on the control volume. By applying mass and momentum conservation, the attachment length L_{att}, and the associated variable may be found.

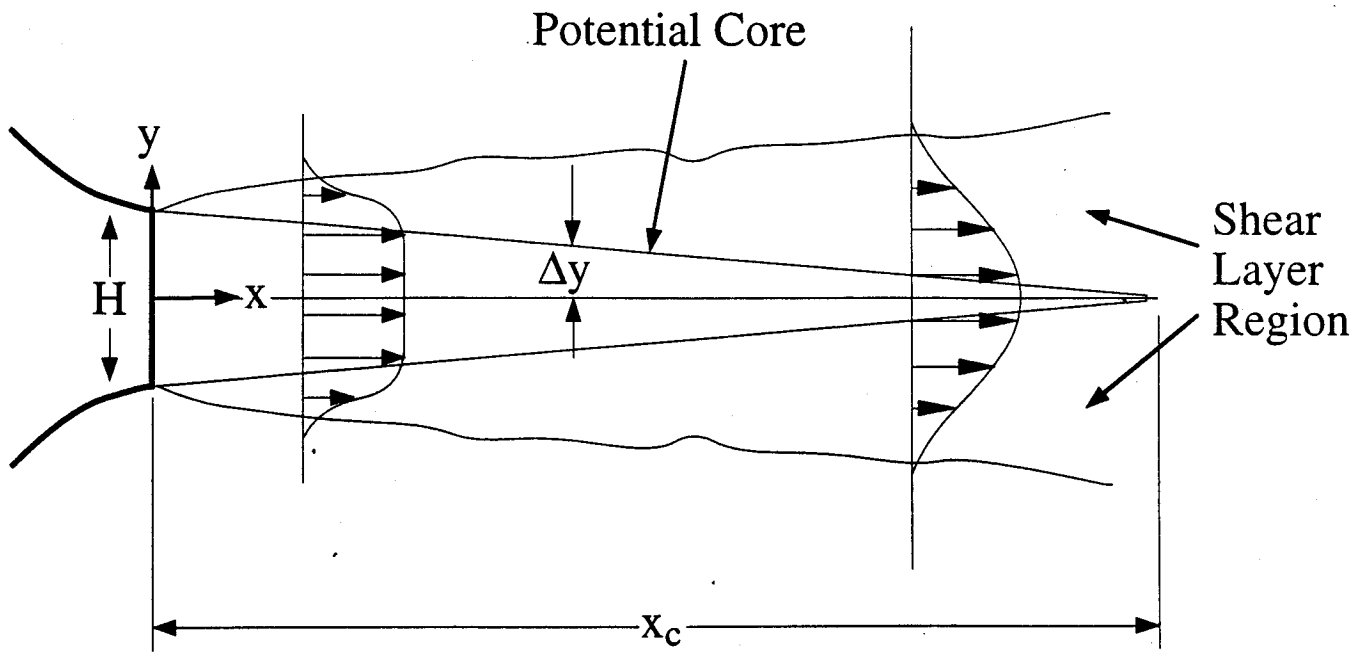

Figure 2.2 Illustration of the potential (or inviscid) core of a planar jet. Due to linear growth of the turbulent shear layers, the potential core region decays linearly with axial postion. The shear layers merge at x_c, which typically occurs 6H to 8H downstream of nozzle exit, depending on initial conditions.

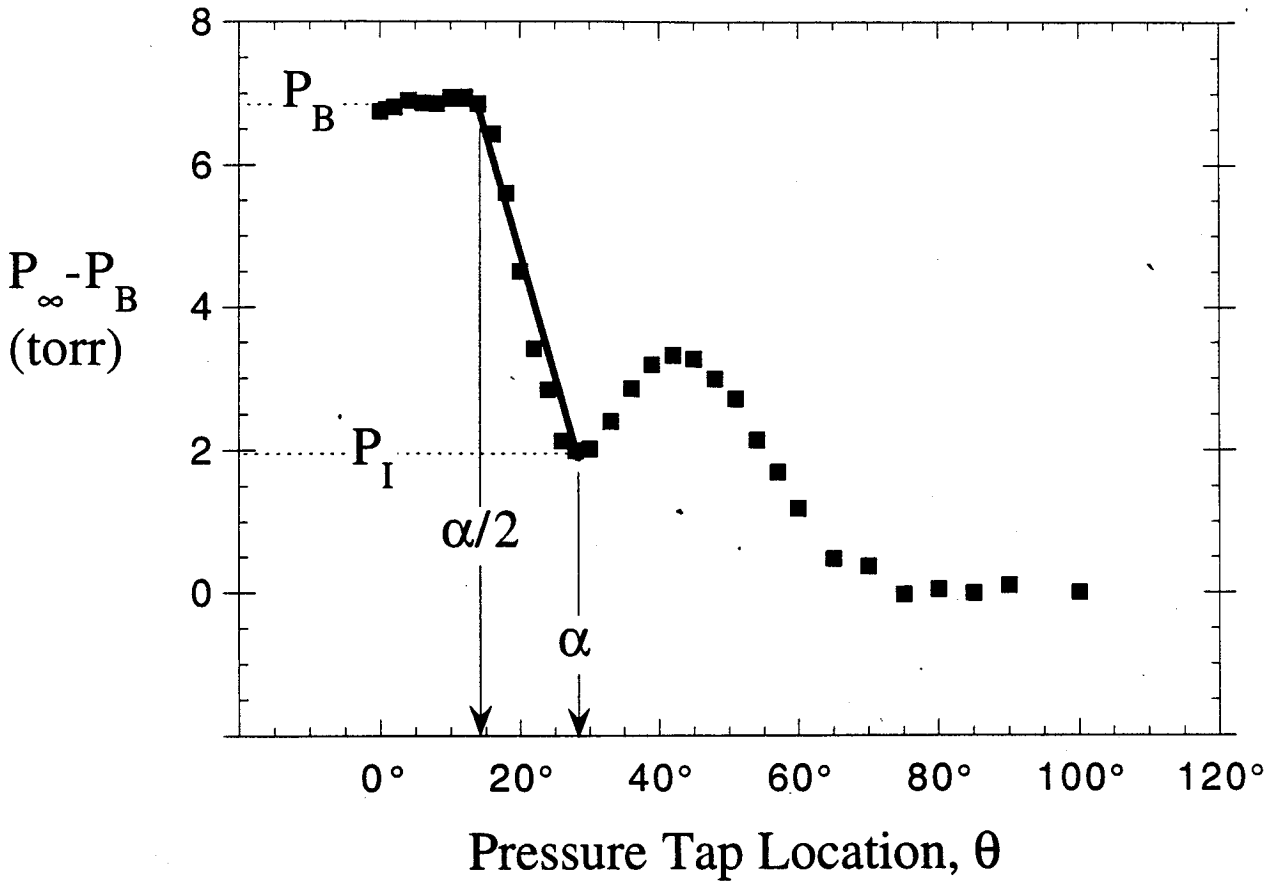

Figure 2.3 Typical collar pressure profile, showing the collar pressure remains constant in the first half of the bubble region, then increases to a pressure PI at the stagnation point. This increase is assumed to be linear.

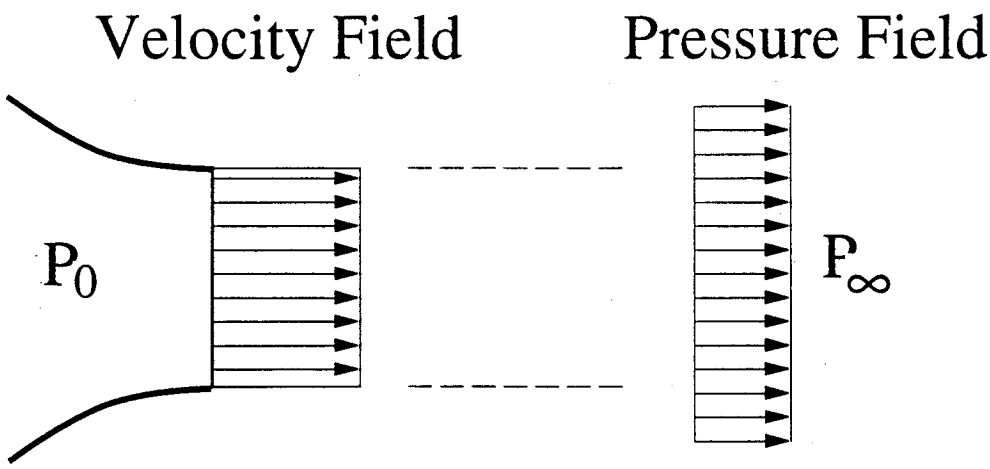

A: Uniform Pressure Field: Uniform Velocity Profile

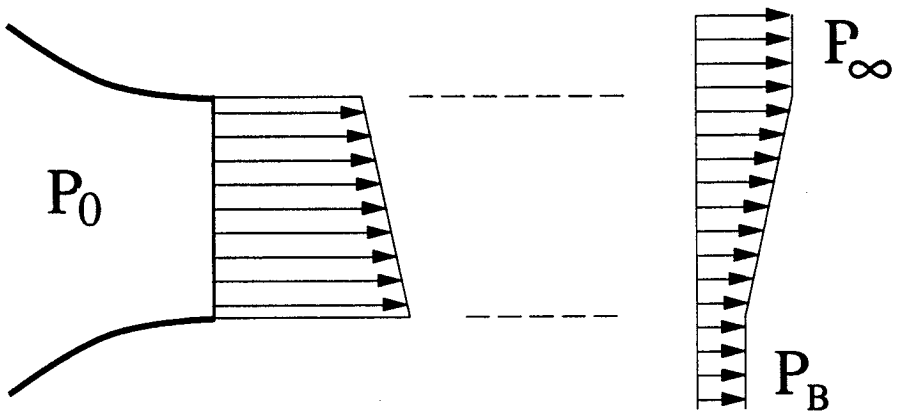

B: Non-Uniform Pressure Field: Skewed Velocity Profile

Figure 2.4 Schematic of velocity skewing effect, which is caused by the transverse pressure gradient in the jet exit plane. Part (a) represents free jet conditions, part (b) represents conditions during attachment. This skewing of the velocity distribution significantly augments the momentum inflow to the control volume.

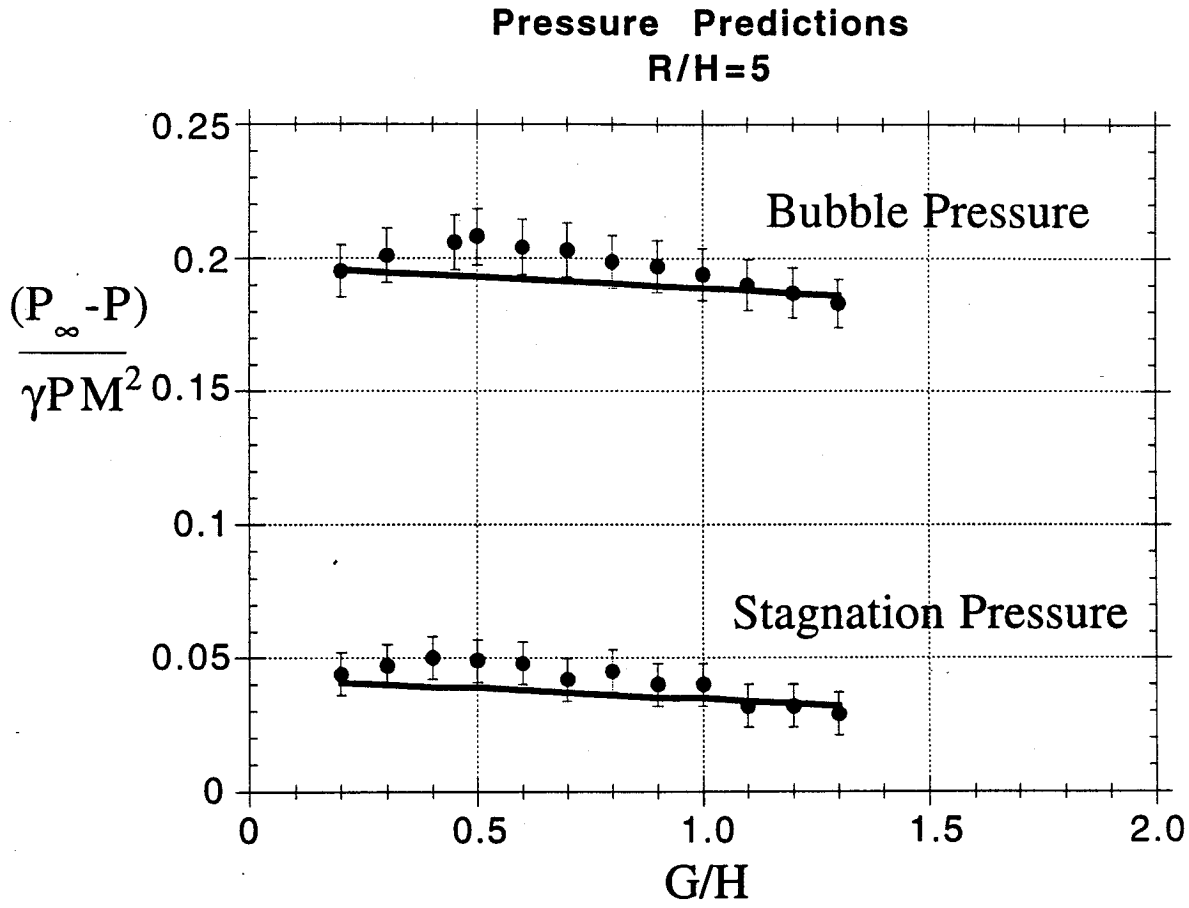

Figure 2.5 Experimentally measured, bubble pressure, P_B, and collar stagnation pressure, P_I, averaged over a range of Mach numbers from 0.15 to 0.52, and plotted vs. gap width, G/H, for a R/H = 5 collar. Plotted using solid lines are the predictions given by the model.

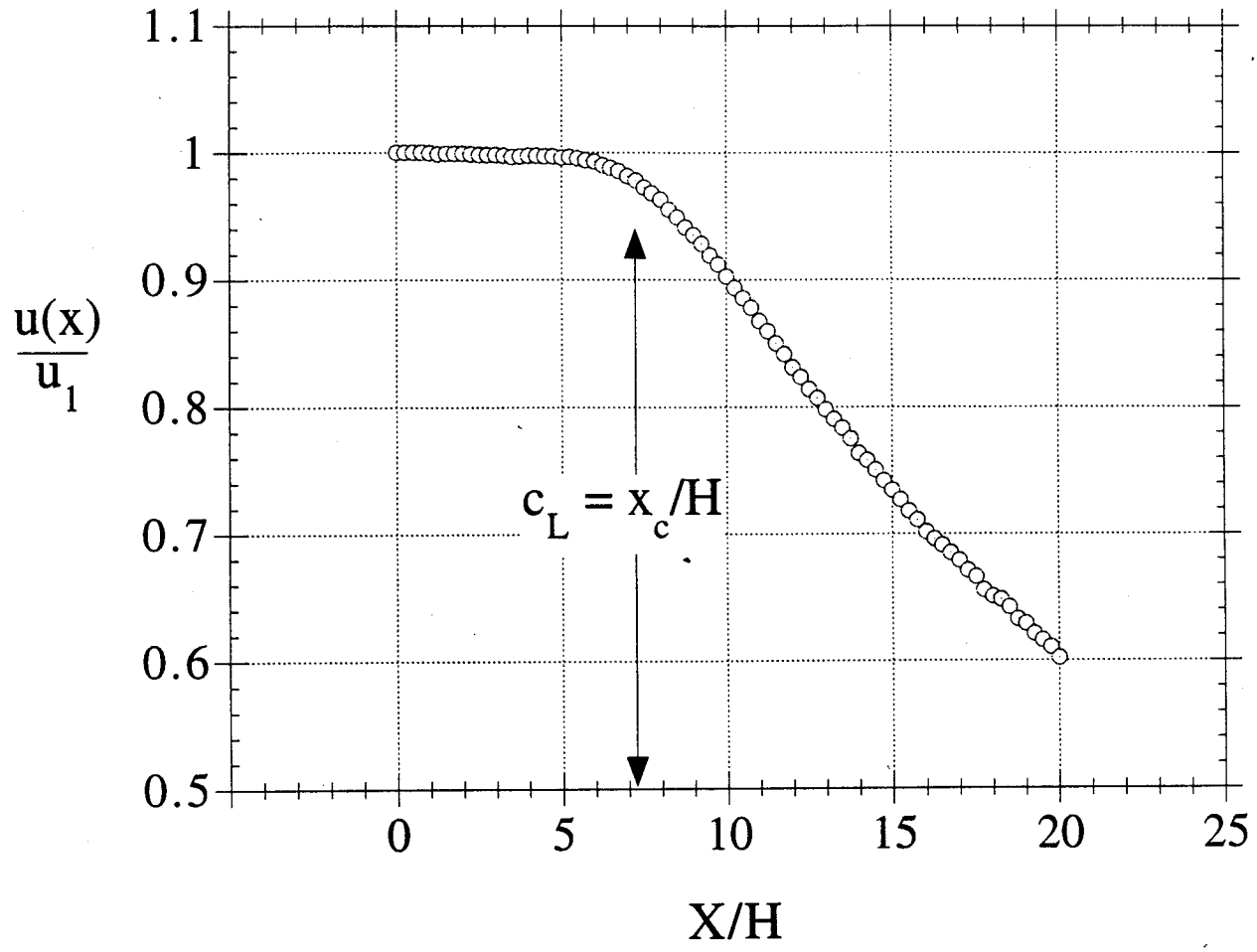

Figure 2.6 Experimentally measured axial velocity distribution for unvectored jet M=0.5 jet. Velocity measurements were taken along the centerline of the jet using a pitot tube. It is difficult to obtain precise values of c_L, using this plot, due to ambiguities about the definition. Subsequent measurements using entrainment data give $c_L = 7.3$.

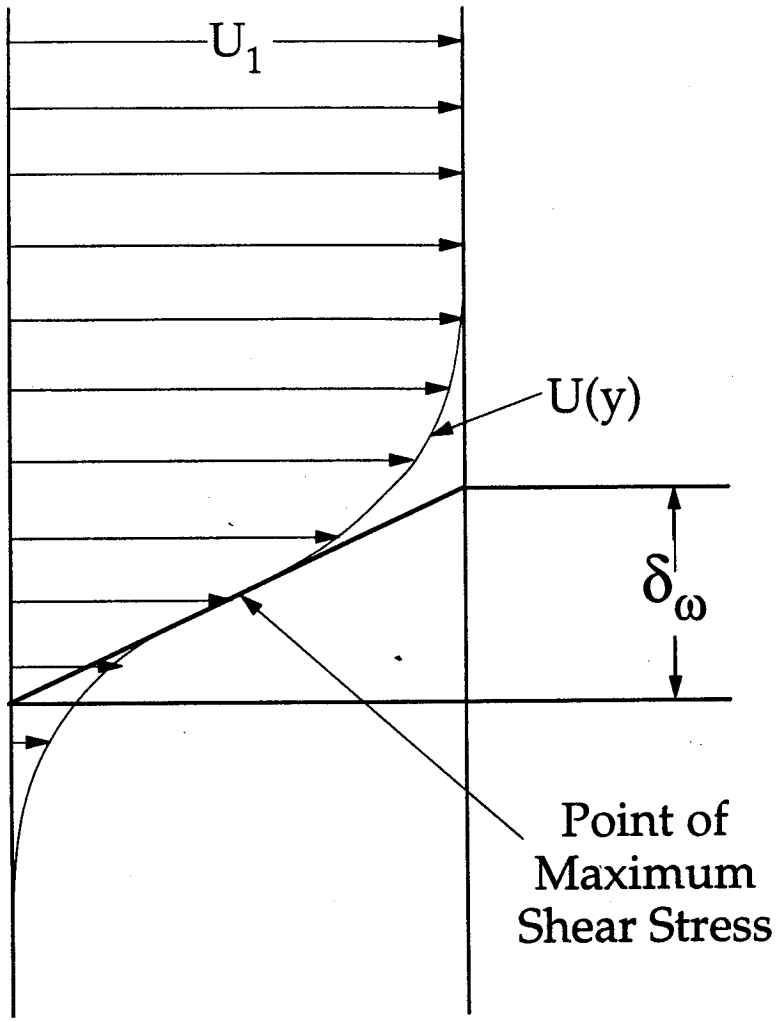

Figure 2.7 Diagram illustrating the definition of vorticity based shear layer thickness δ_ω, which is the thickness an equivalent layer would be if it had a uniform shear stress equal in magnitude to the shear layer in question.

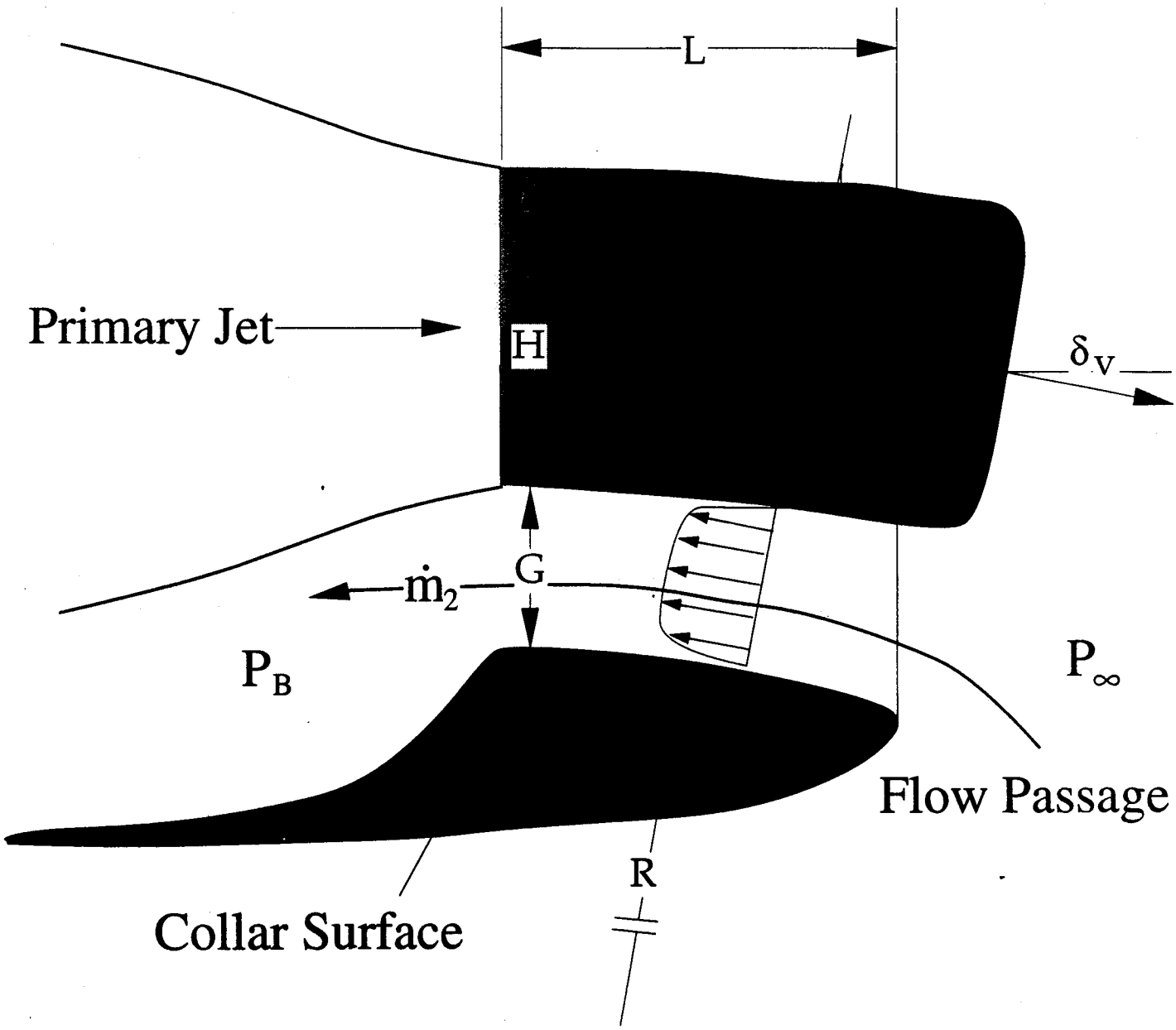

Figure 2.8 Schematic of the secondary flow passage. To compute the level of counterflow, the flow is treated as a turbulent channel flow. Pipe geometry is a function of the geometry of the collar and the exit vector angle. An empirically determined friction factor, f, is used to characterize the shear stress imparted on the flow by its surroundings.

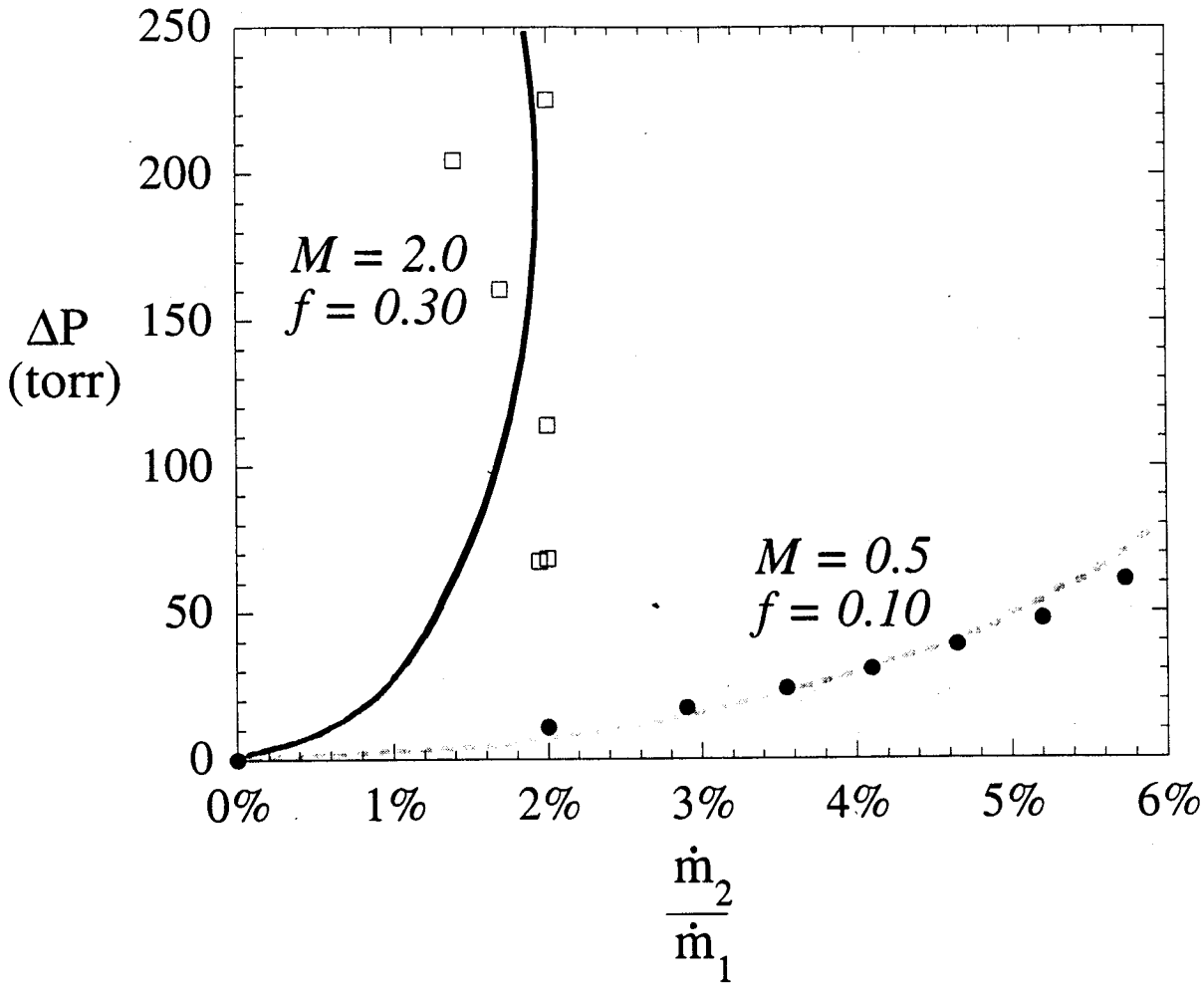

Figure 2.9 Experimental data relating the secondary mass flowrate, normalized by the primary mass flowrate, to the plenum pressure, P_B. Data for M = 2.0 flow was taken from Strykowski et. al. [2]. Collar geomerty: L/H=6.9, R/H=15, G/H=0.385. For M=0.5 flow, collar geometry: L/H=1.15, R/H=6, G/H=0.2. The M=0.5 data is best matched using f=0.1; M=2.0 data is best matched using f=0.3.

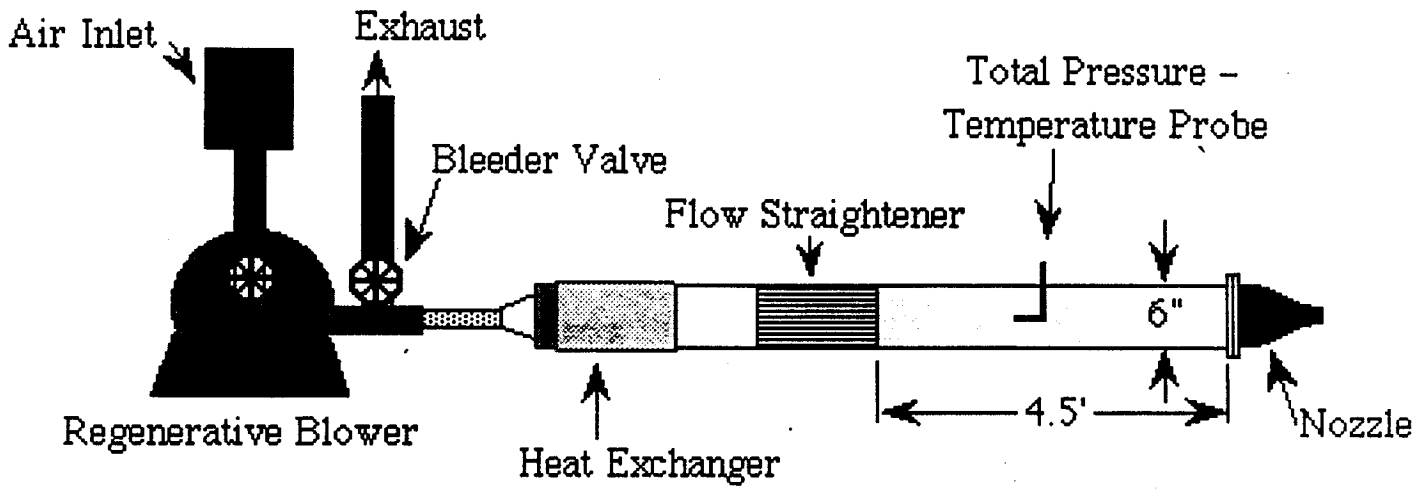

Figure 3.1 Approximately scaled diagram of experimental jet facility used in this study. Include 7.5 hp blower, 45:1 area reduction nozzle culminating with 4 cm x 1 cm rectangular nozzle.

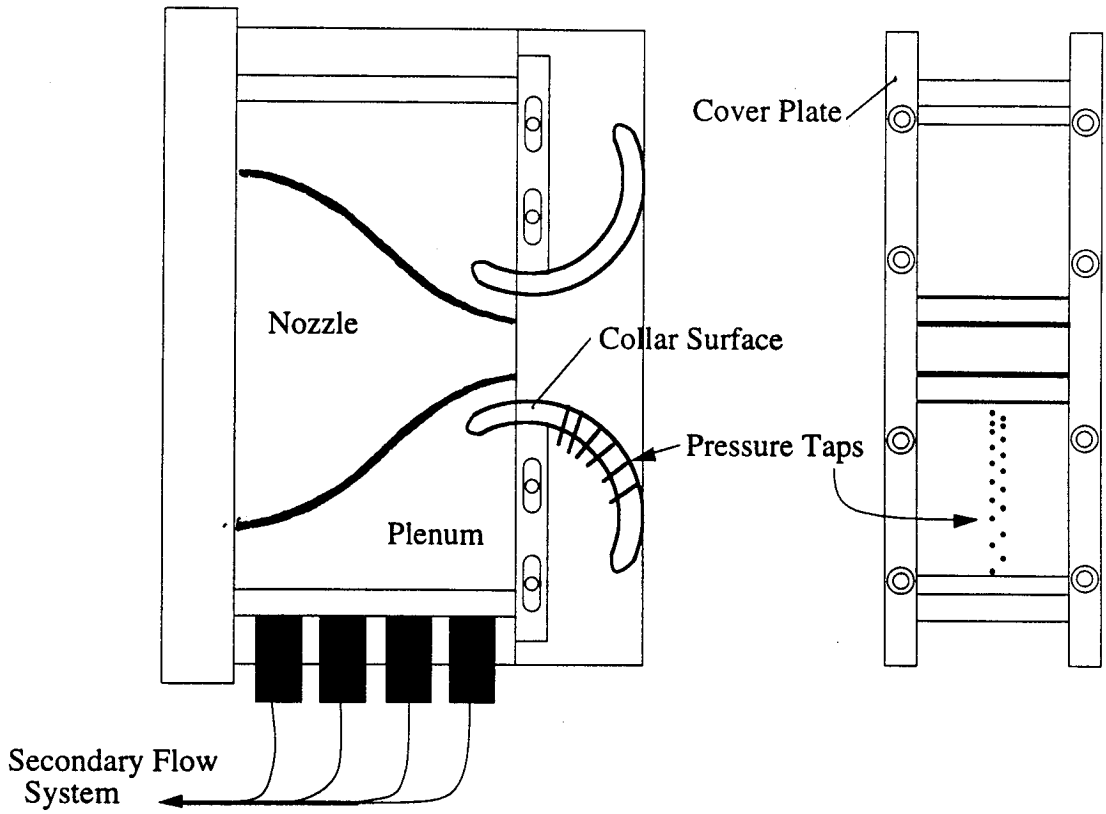

Figure 3.2 Scaled diagram of collar set-up used for experimental jet attachment studies. Circular arc collars of various sizes were tested at various gap widths.

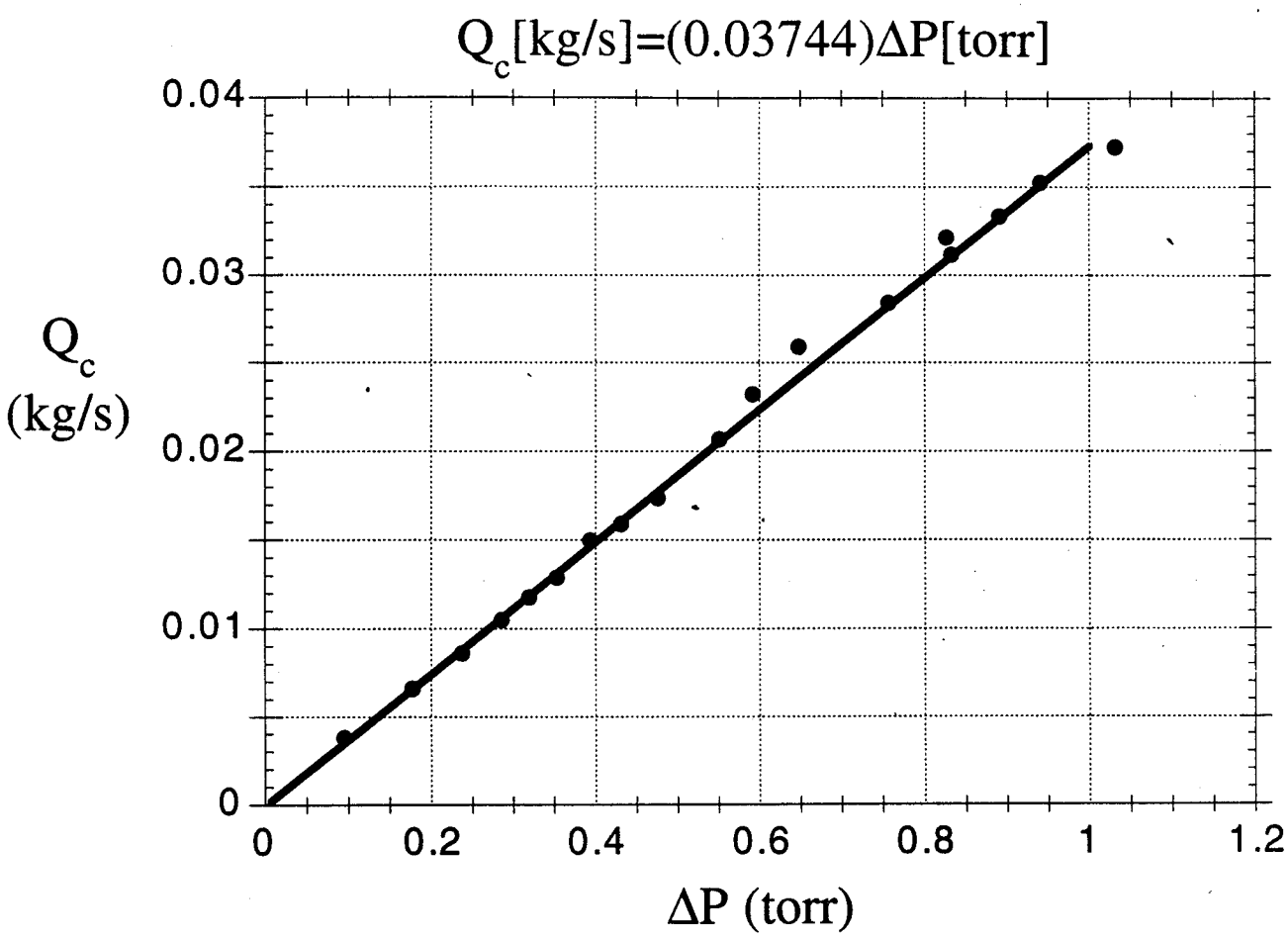

Figure 3.3 Calibration curve for laminar flow meter used for secondary flow measurement. Applies for secondary stream temperature ≈ 300K at a pressure of 1 atm, which was standard operating conditions for this study.

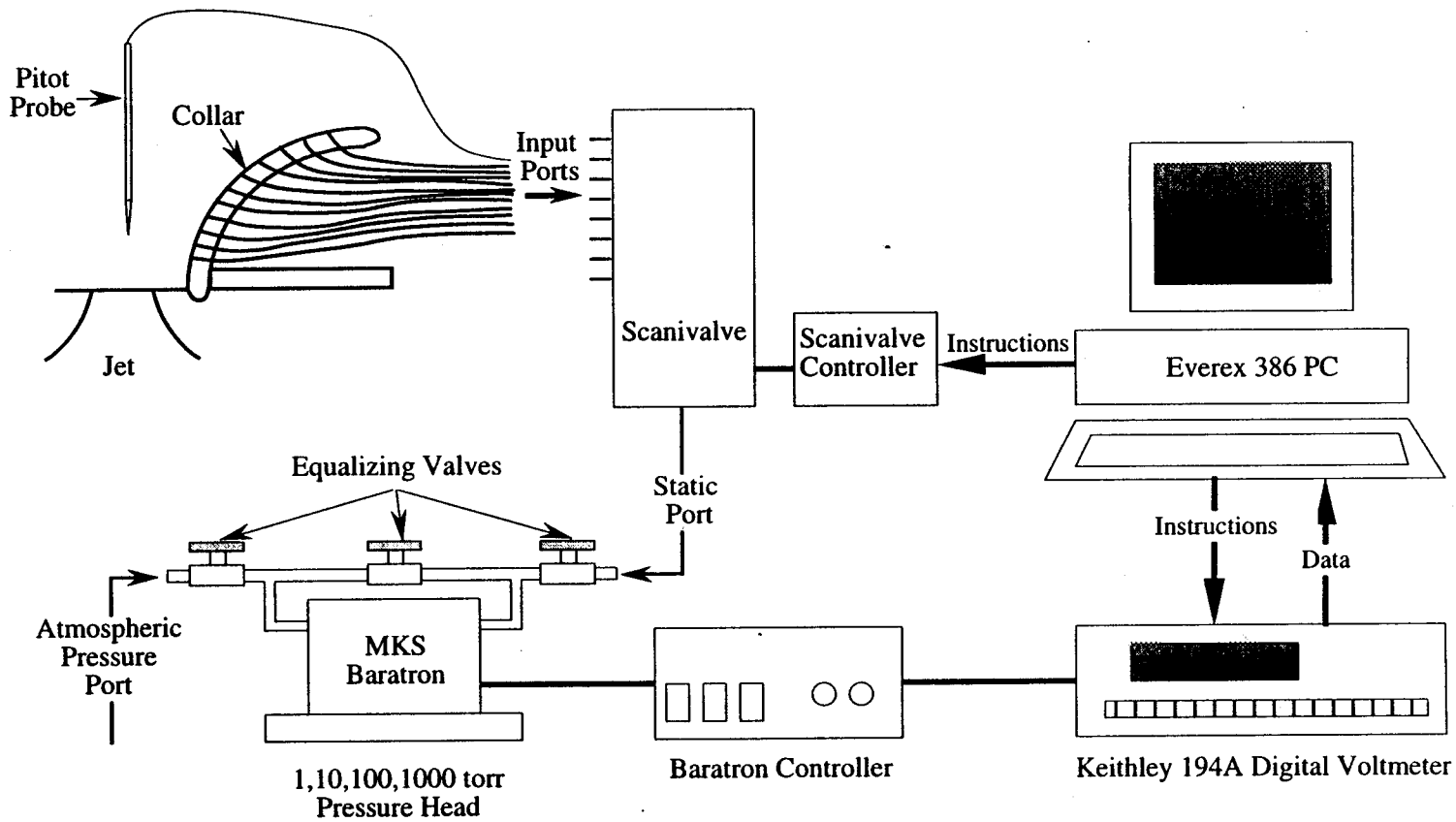

Figure 3.4 Schematic of data acquisition system used to take pressure measurements of all types. Computer uses IEEE-488 parallel bus connections to communicate with all devices. Digital voltage signals are sent back to computer for post processing.

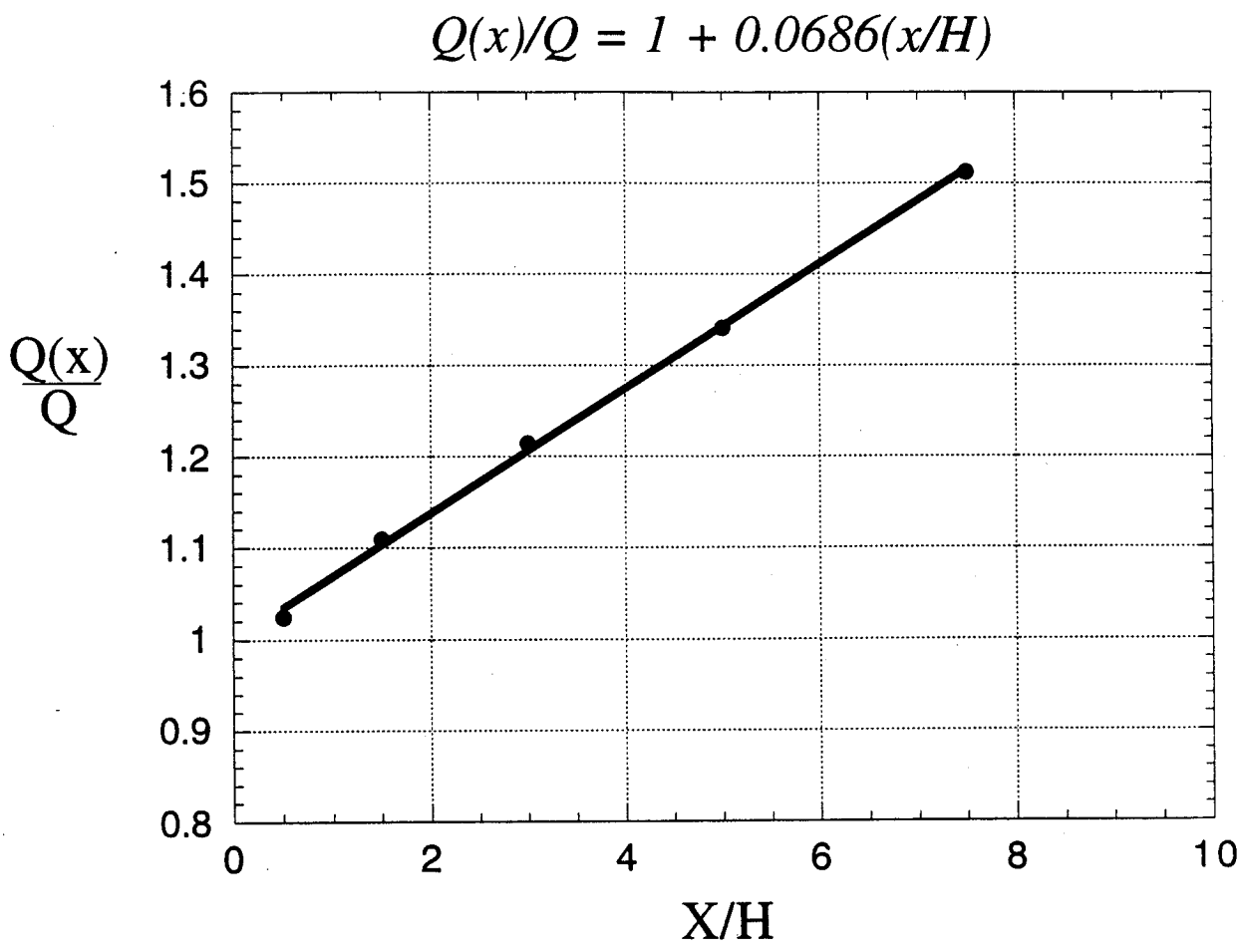

Figure 3.5 Experimentally measured mass flowrate, normalized by exit plane flowrate, plotted vs. axial position for M=0.5 jet, T_0=300K. Linear curve fit is used to compute a c_L = 7.3.

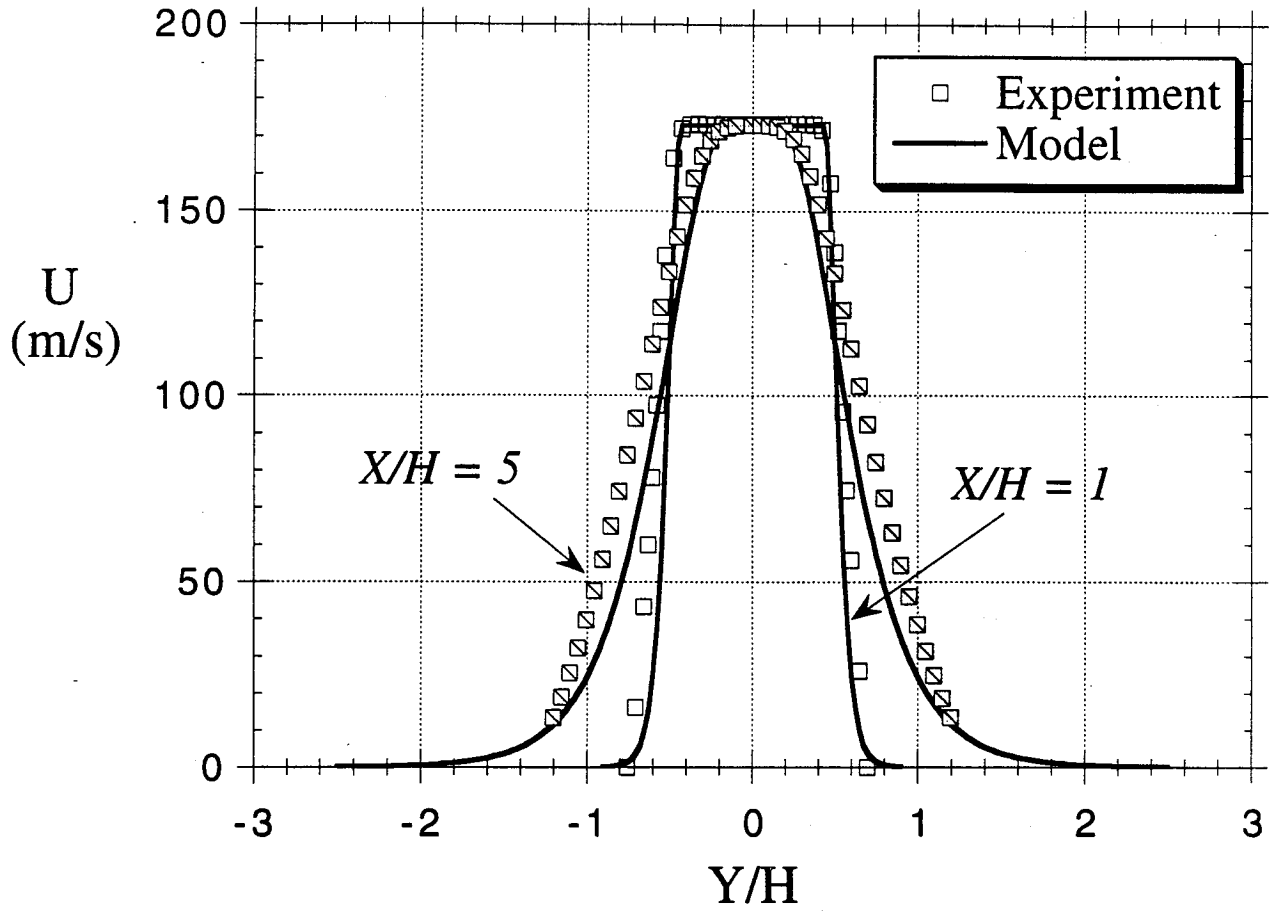

Figure 3.6 Measured velocity profile, for M=0.5, T_0=300K flow at X/H=1 and X/H=5, compared against velocity profile assumption used in model; for cL = 7.3, as determined by entrainment rate data.

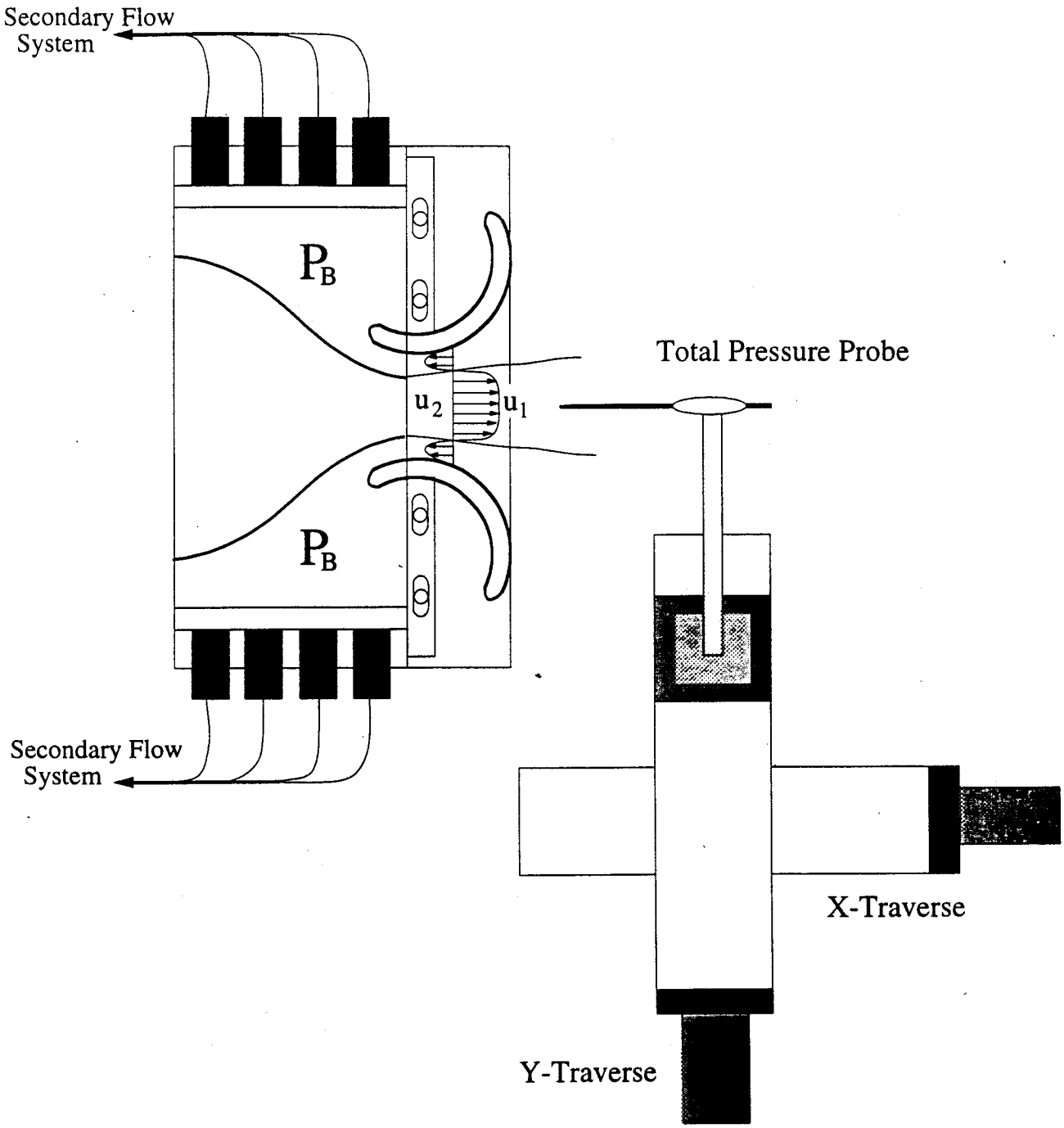

Figure 3.7 Schematic of apparatus used to experimentally obtain free jet velocity measurements taken throughout the course of this study.

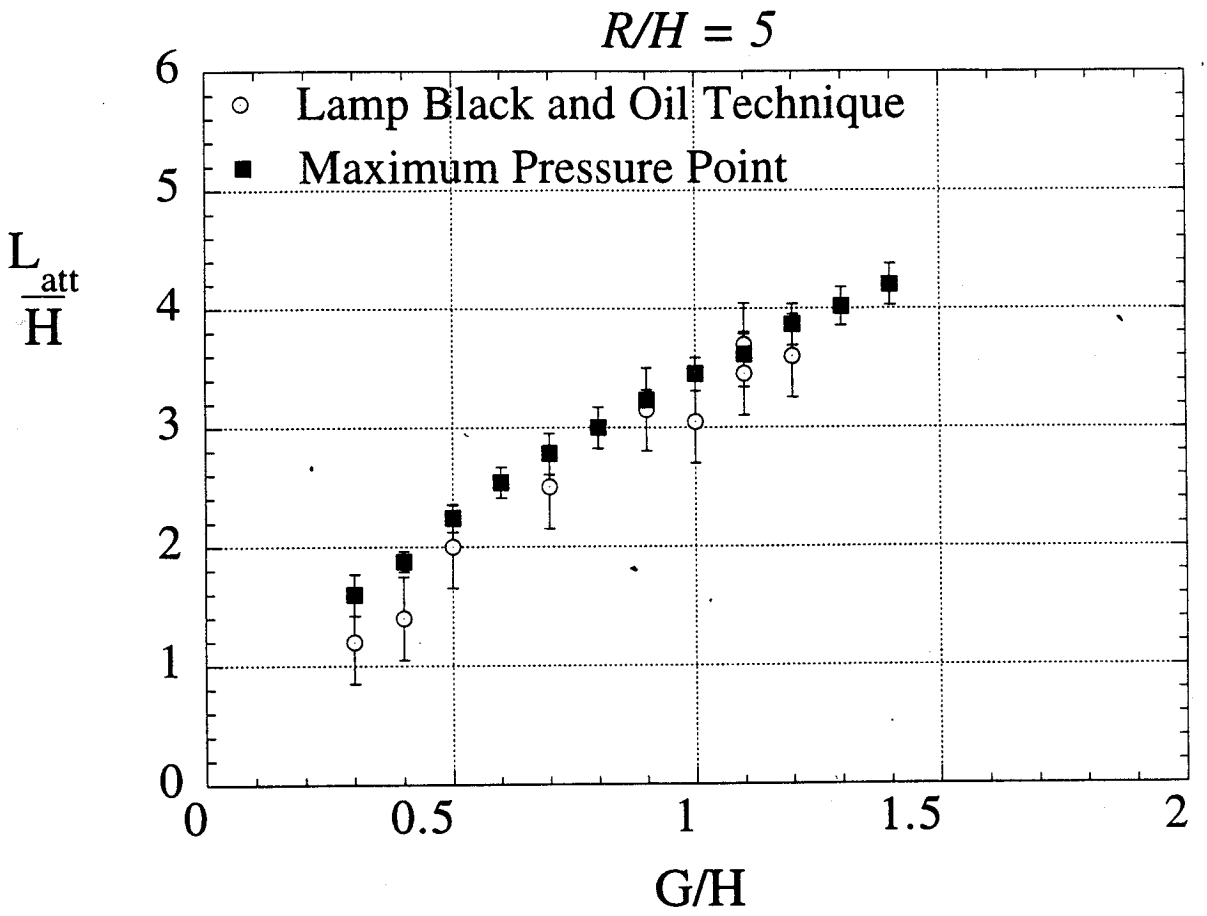

Figure 4.1 Plot showing the correlation between attachment location, determined using oil-lampblack flow visualization technique, and the location of peak collar pressure as experimentally measured for R/H=5.

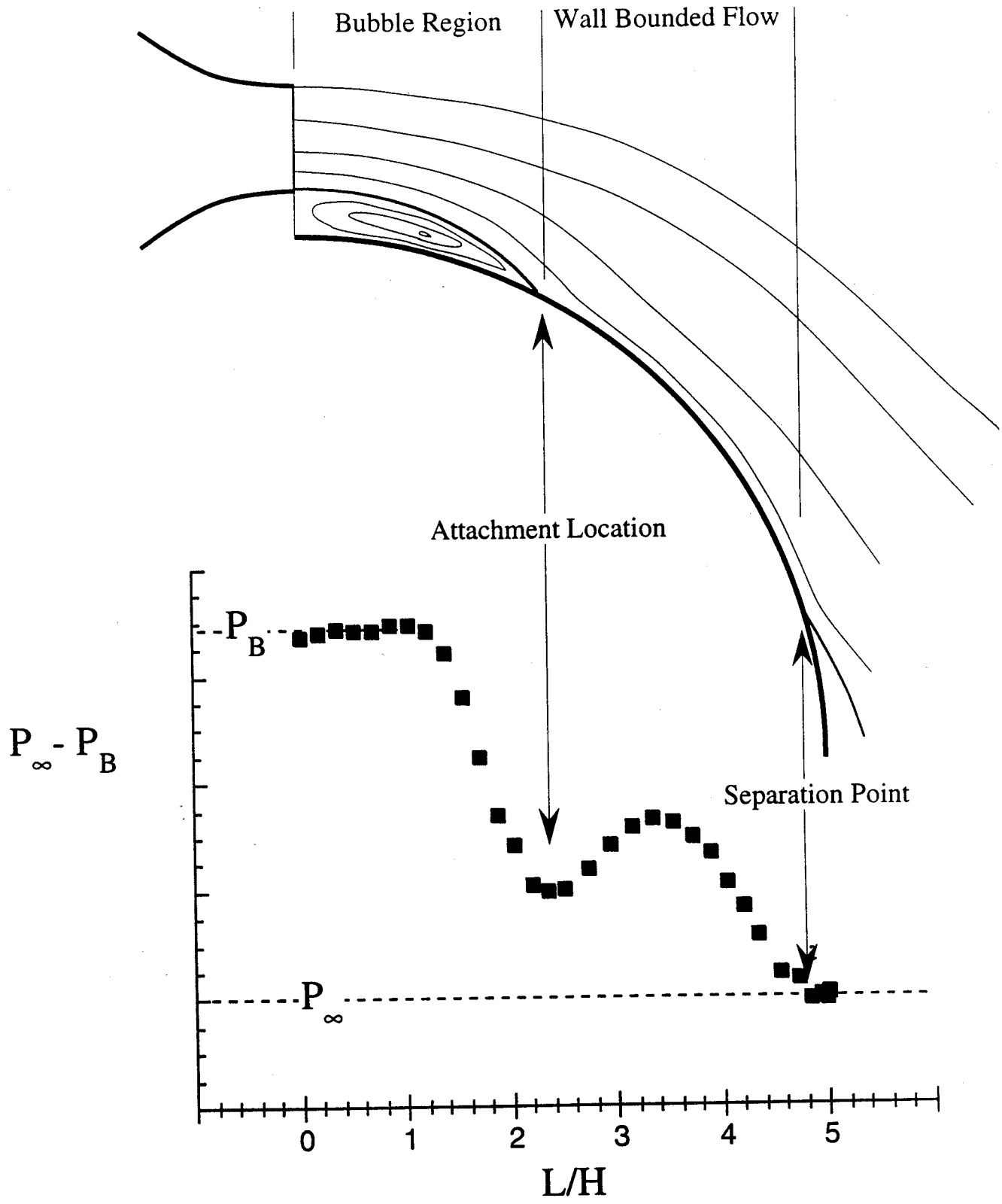

Figure 4.2 Diagram comparing features of a typical collar pressure profile with averaged flow phenomenon occurring in the vicinity of the collar surface. Purpose is to illustrate attachment and separation points.

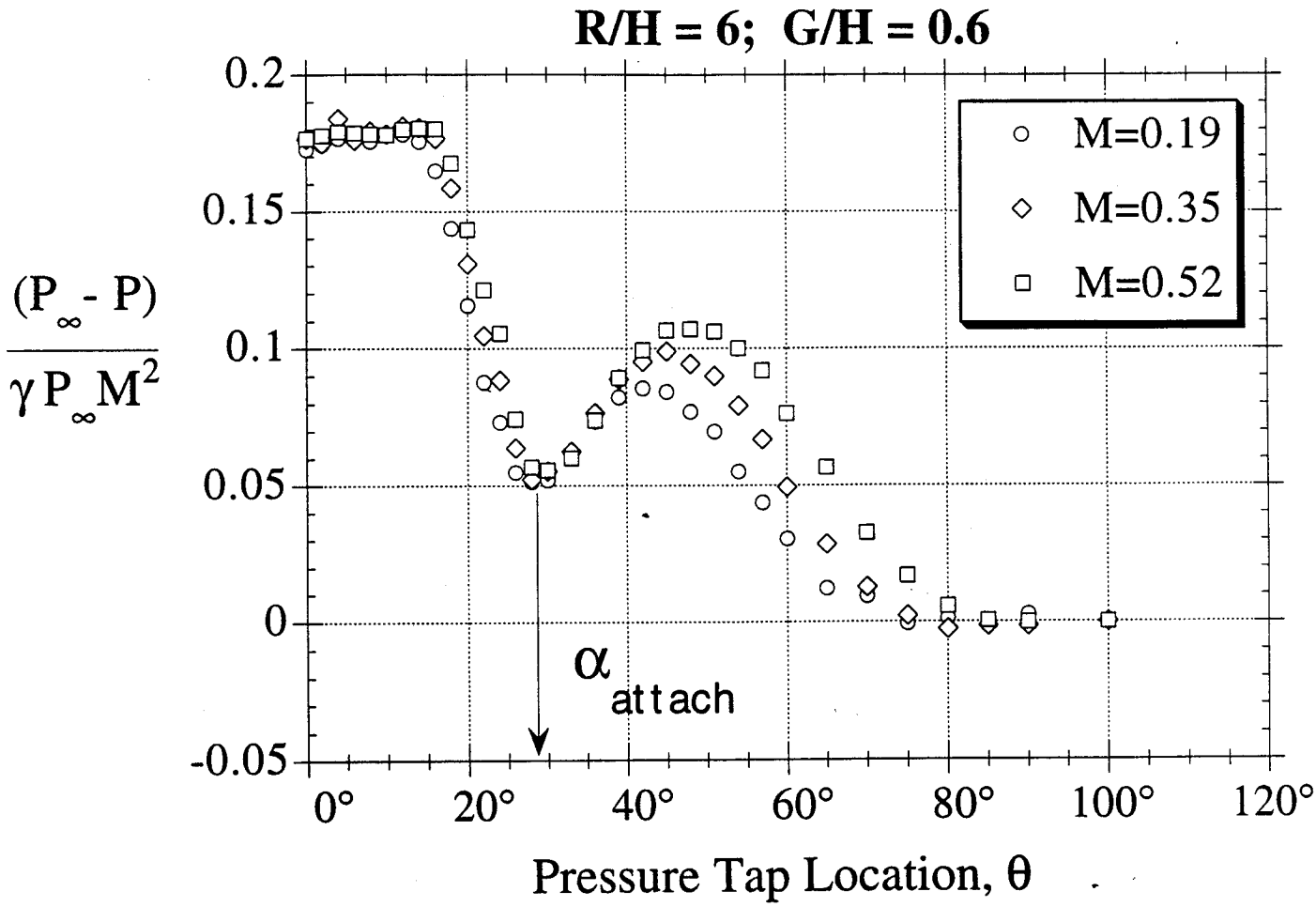

Figure 4.3 Experimentally measured collar pressure profile for attached jet. Collar geometry: R/H=6; G/H=0.6. M=0.19, 0.35, and 0.52.

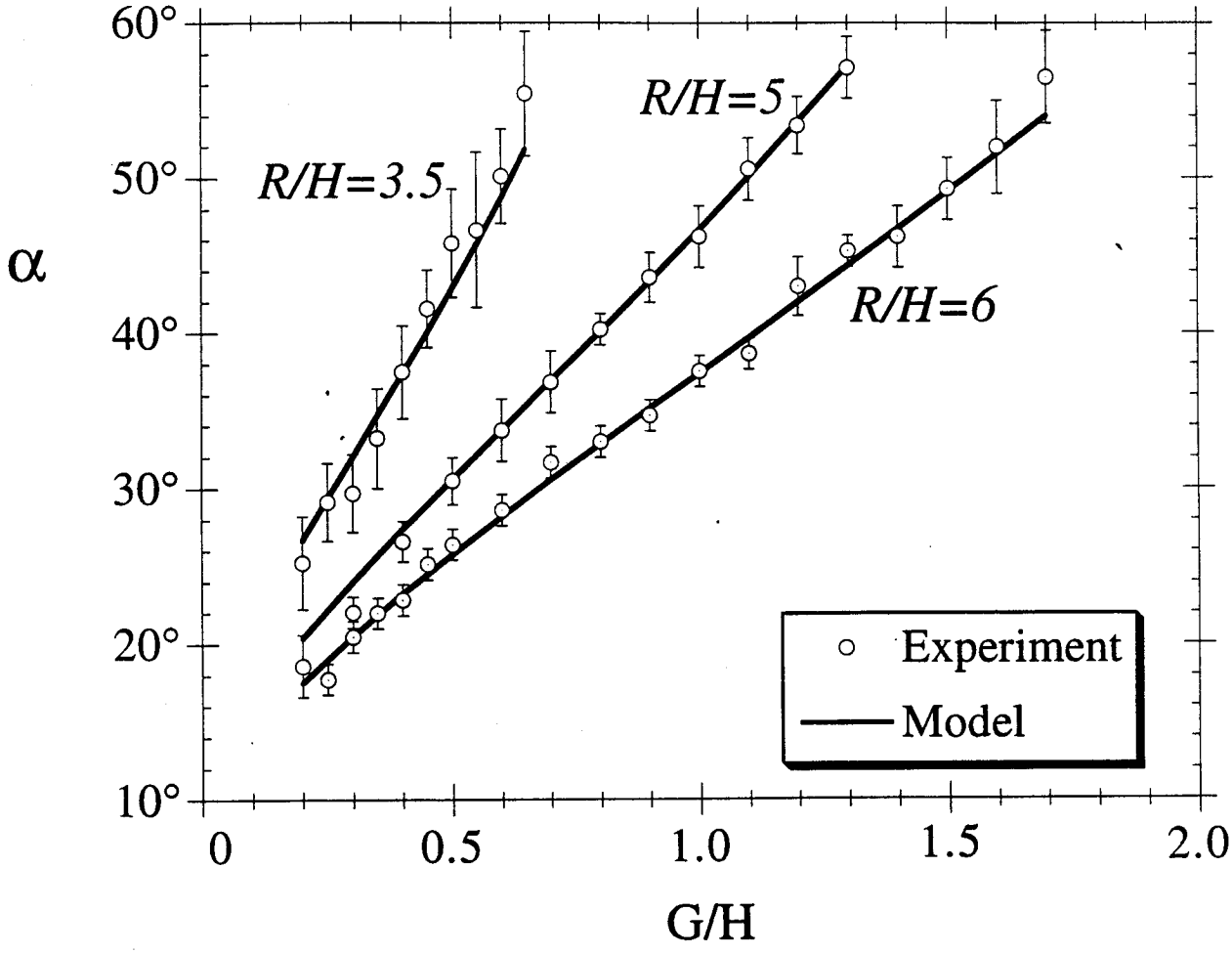

Figure 4.4 Experimentally measured attachment location, α, vs. gap width for collars of: R/H = 3.5, 5, and 6. Each point represents average over wide Mach number range. For all cases, no counterflow was applied, w_c=0. Solid lines represent predictions using model with ϕ=1.3.

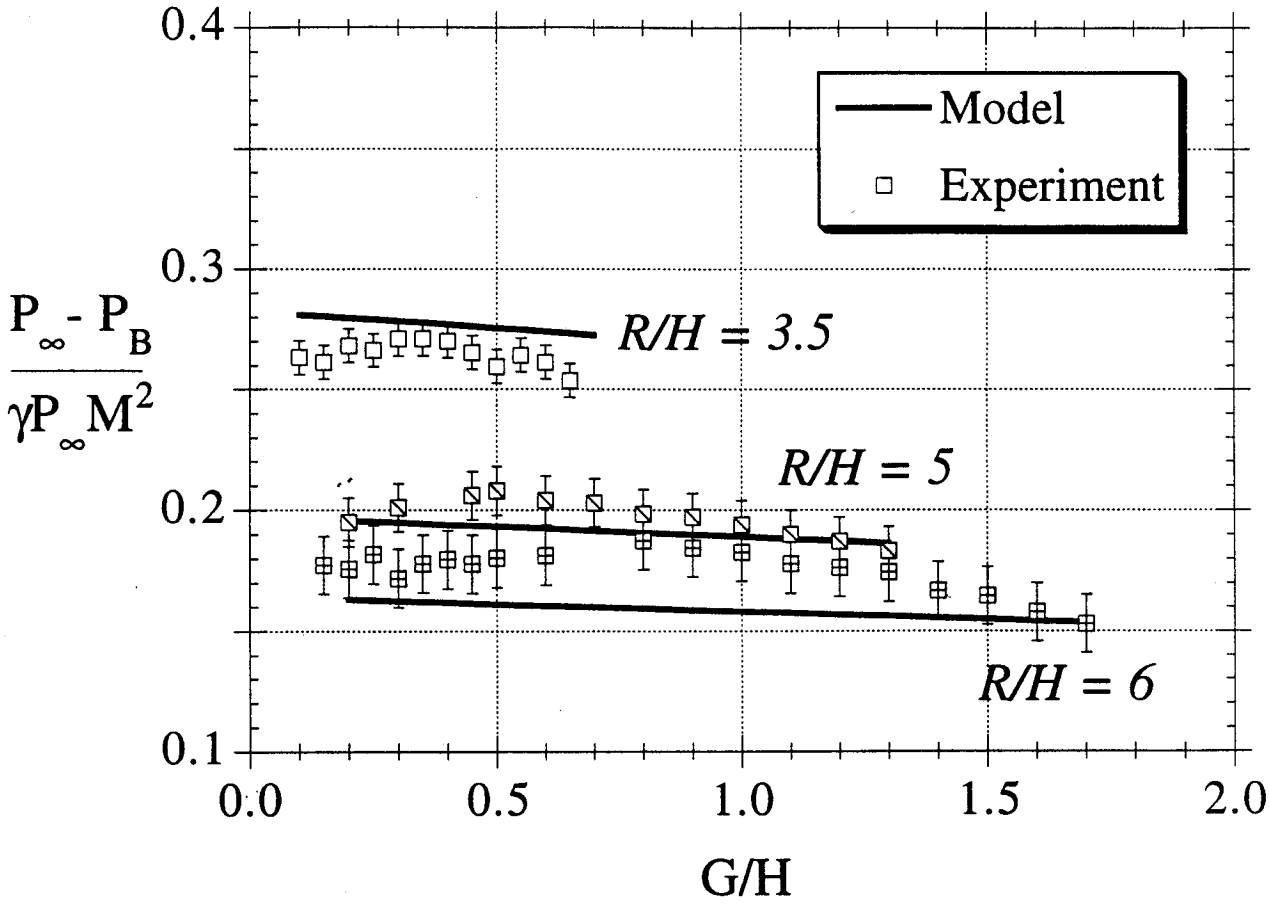

Figure 4.5 Average bubble pressure, P_B, for attached jet cases, plotted vs. gap width, G/H for R/H=3.5, 5, and 6. Each data point represents an average P_B over a wide range of Mach numbers. Solid line represents equilibrium bubble pressure predicted by model with ϕ=1.3.

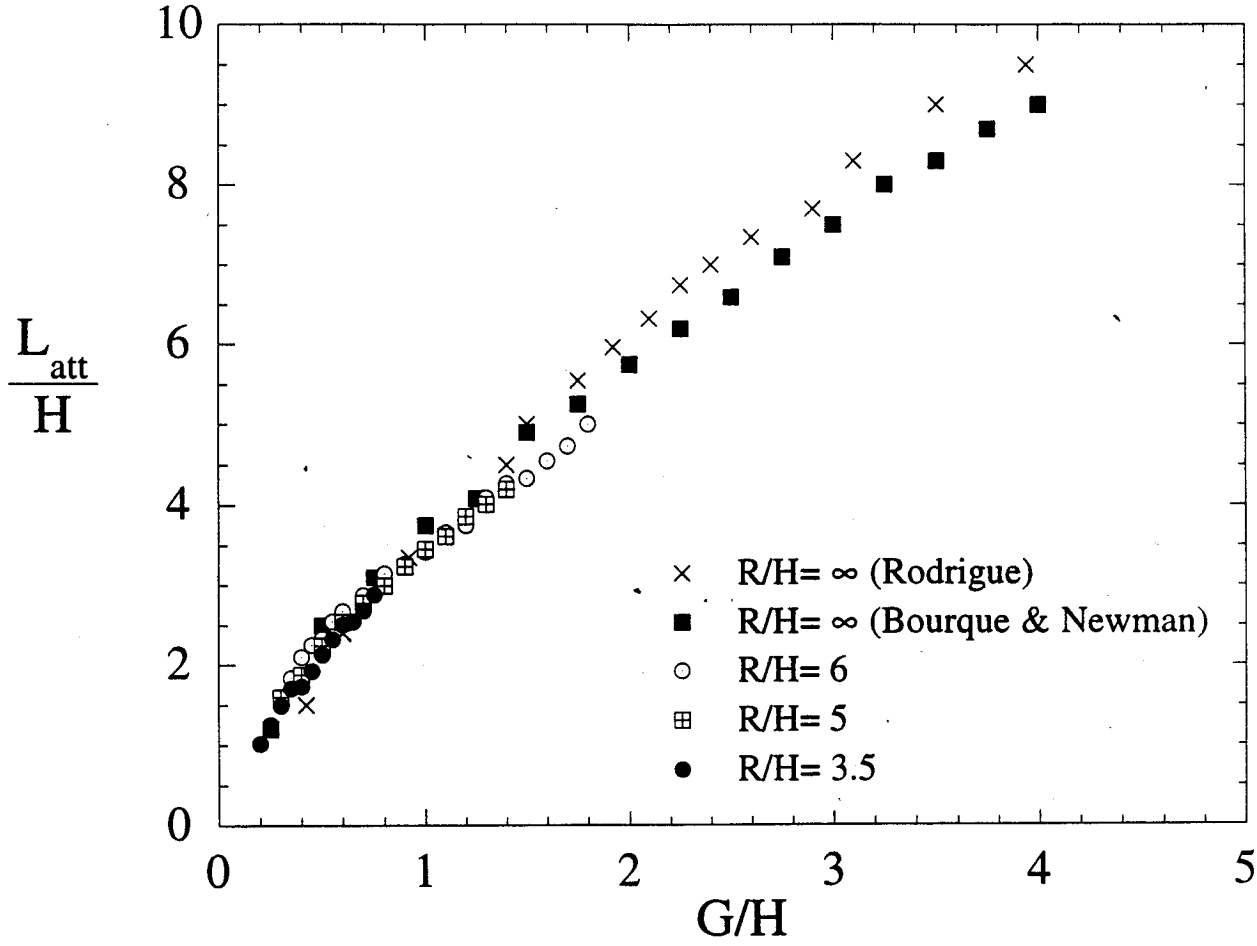

Figure 4.6 Experimentally determined attachment length plotted vs. gap width for R/H=3.5, 5, 6, and flat plate (R/H=∞). Flat plate data was taken from Rodrigue [19], and Bourque and Newman [9], and replotted.

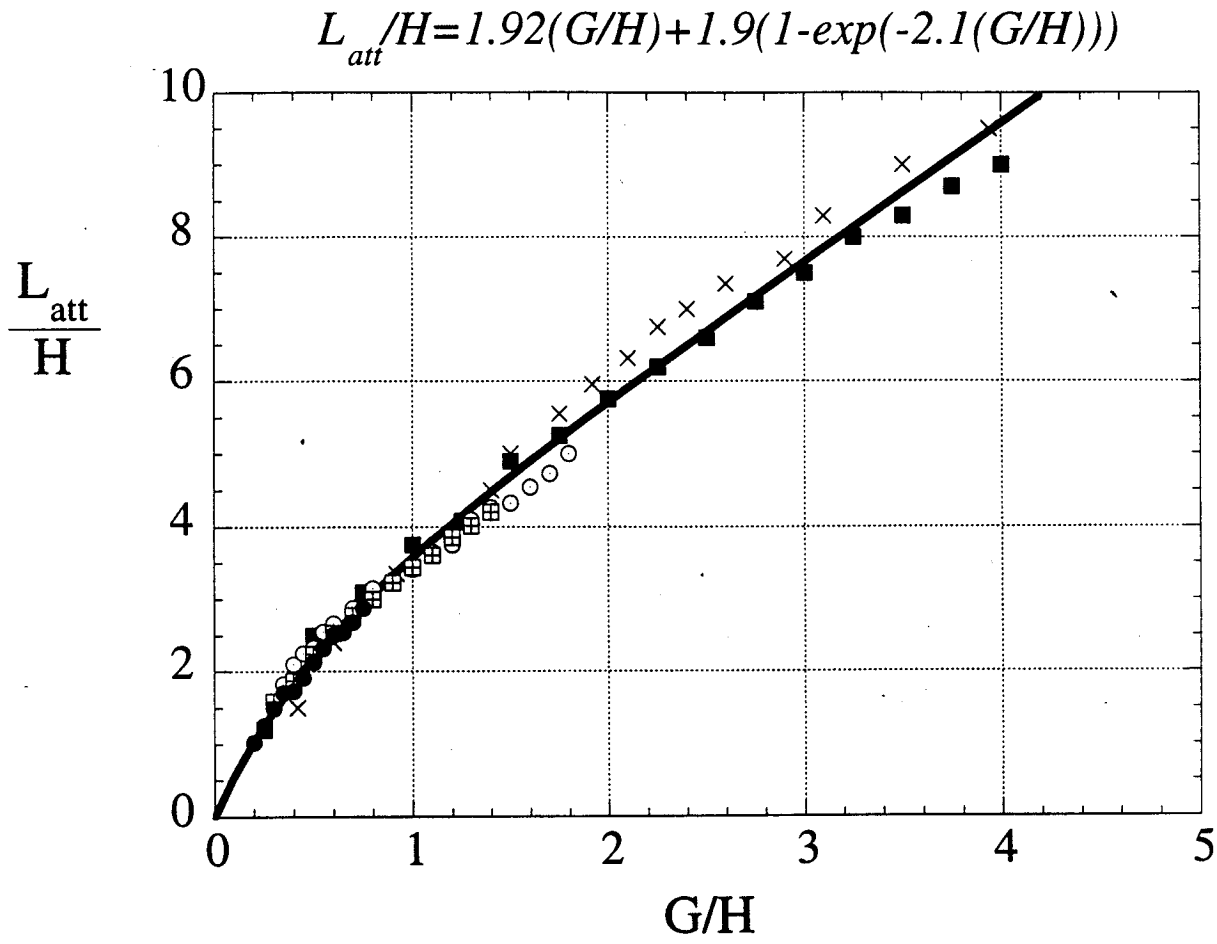

Figure 4.7 Experimental attachment length data presented in Figure 4.6, is replotted and curve fit vs. gap width using all R/H=3.5, 5, 6, and flat plate (R/H=∞) data.

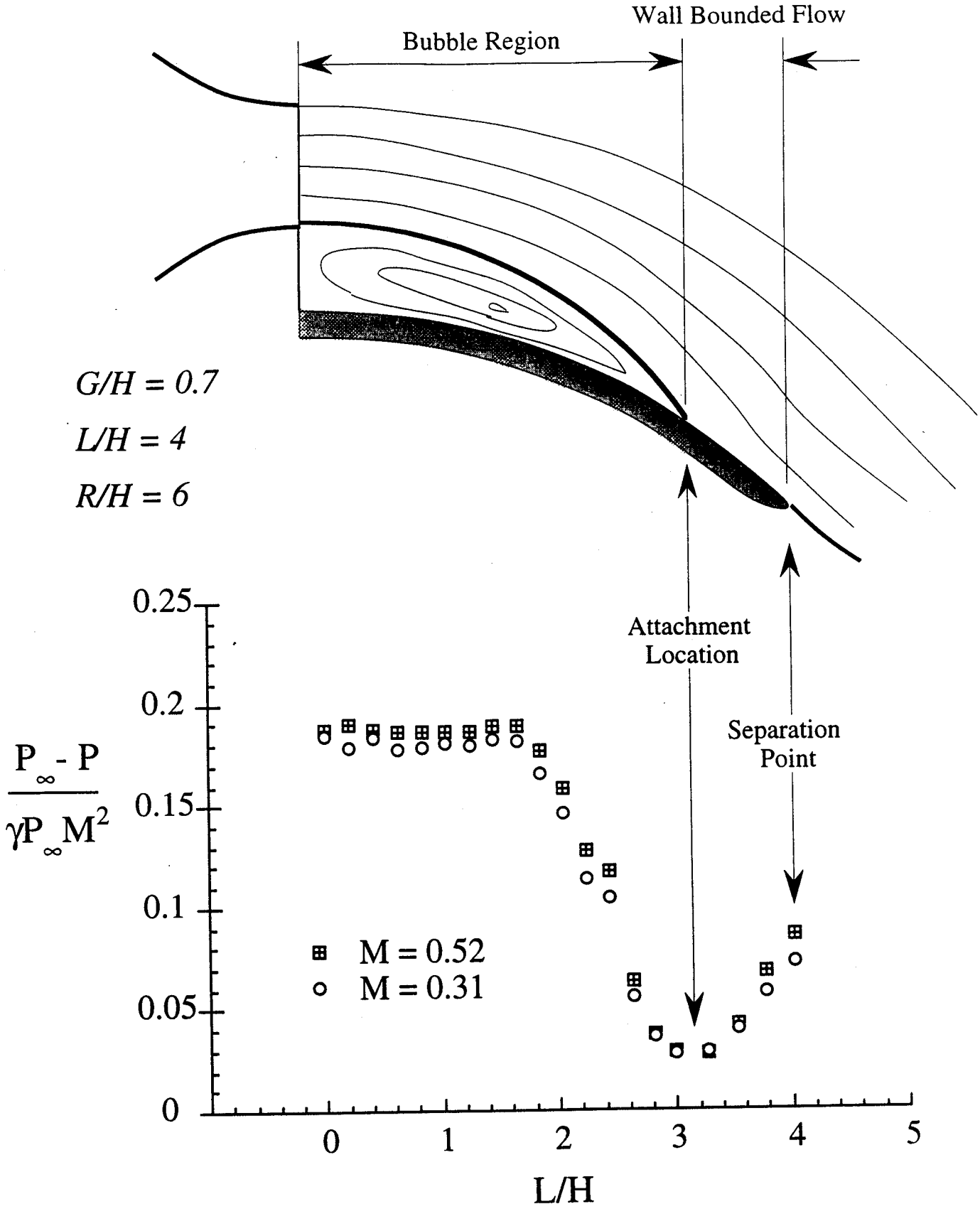

Figure 4.8 Scaled diagram comparing features of the pressure profile for jet of M=0.31 and 0.52 attached to truncated collar surface; having G/H=0.7, L/H=4, R/H=6; with averaged flow phenomenon in the vicinity of the truncated collar surface.

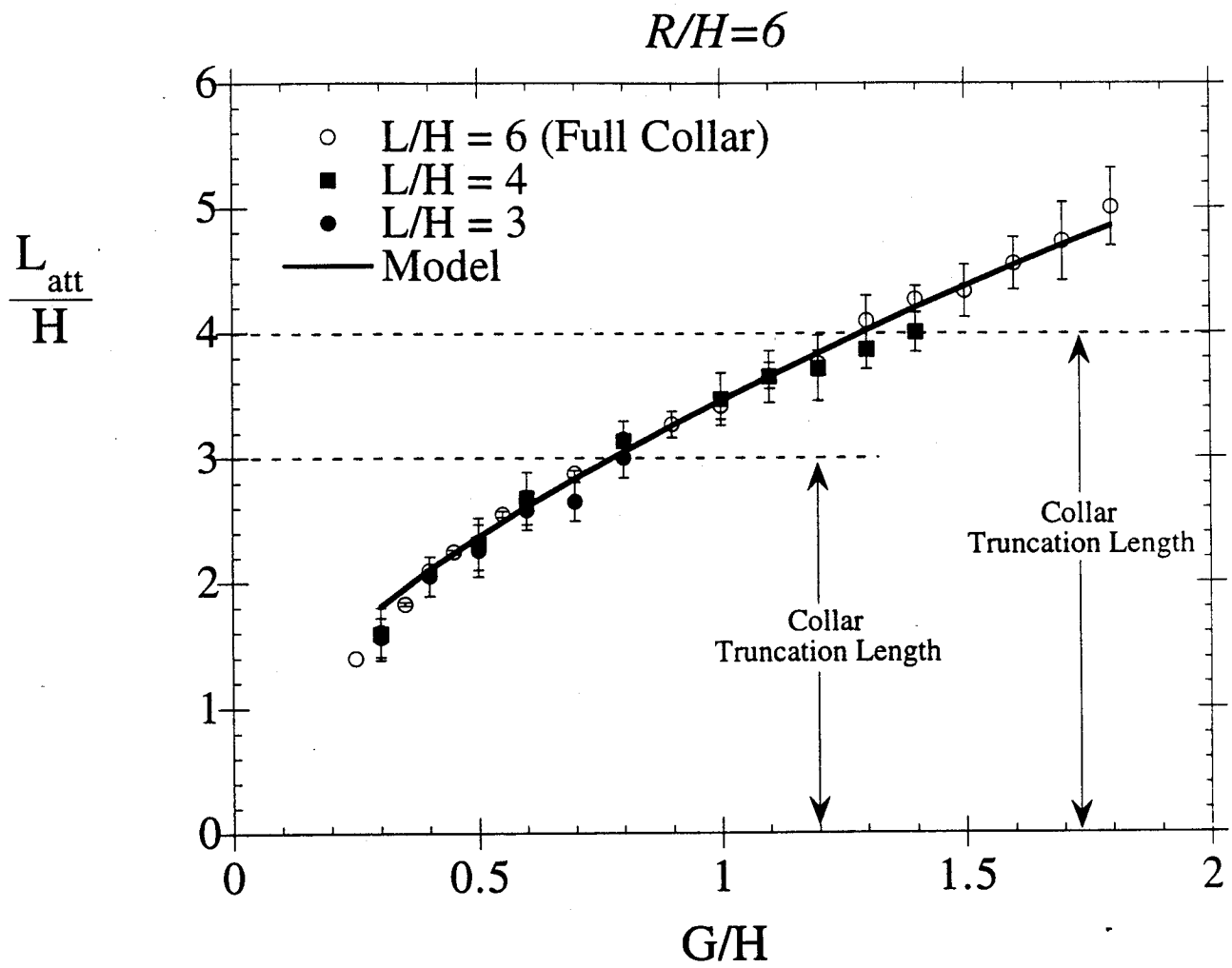

Figure 4.9 Experimentally measured attachment length plotted vs. gap width for two truncated collar surfaces; L/H=4, and L/H=3; as well as the full collar. For all cases: R/H=6. Solid line represent the predictions of the model using ϕ=1.3.

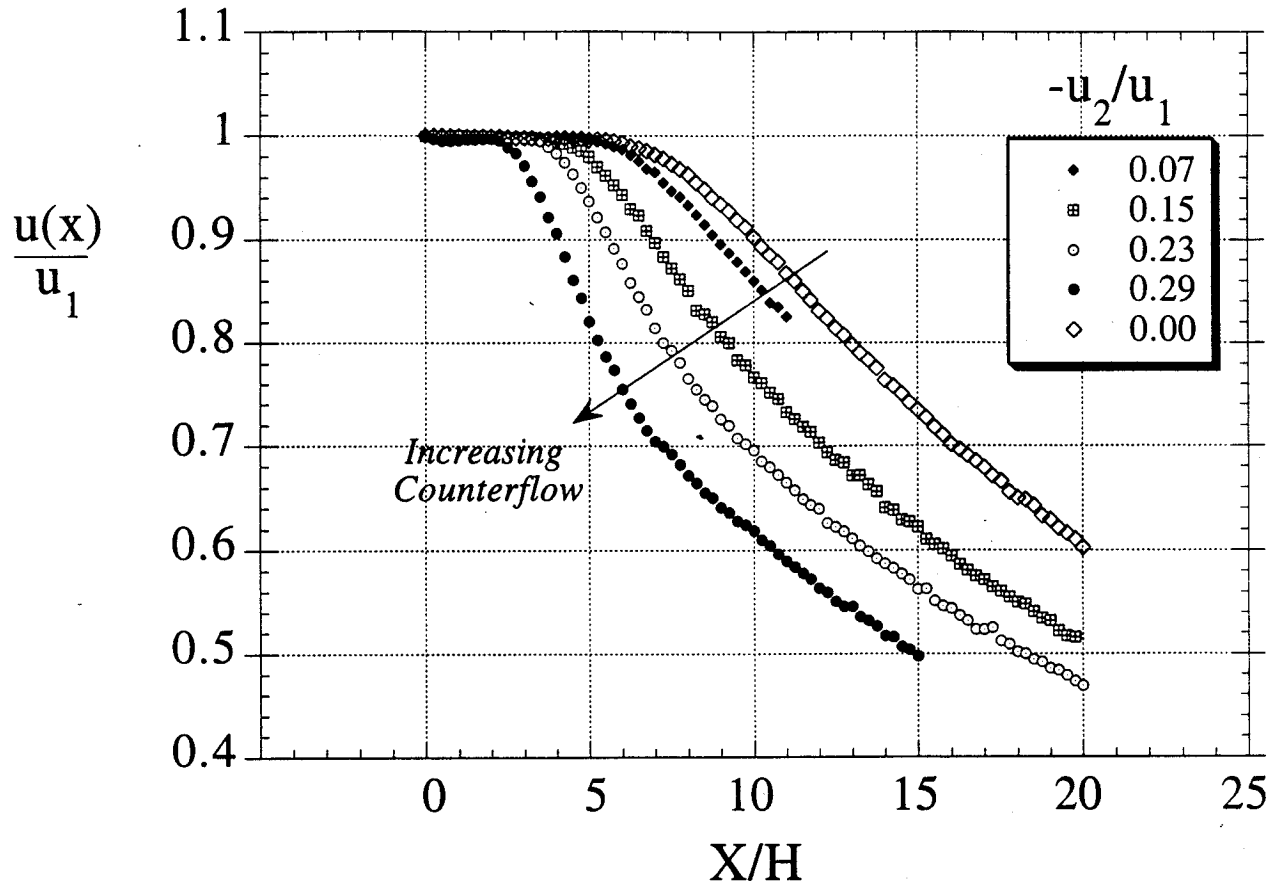

Figure 4.10 Axial velocity distribution along the centerline of the jet, with M=0.5. Plotted for various levels of counterflow, applied uniformly to both sides of the jet.

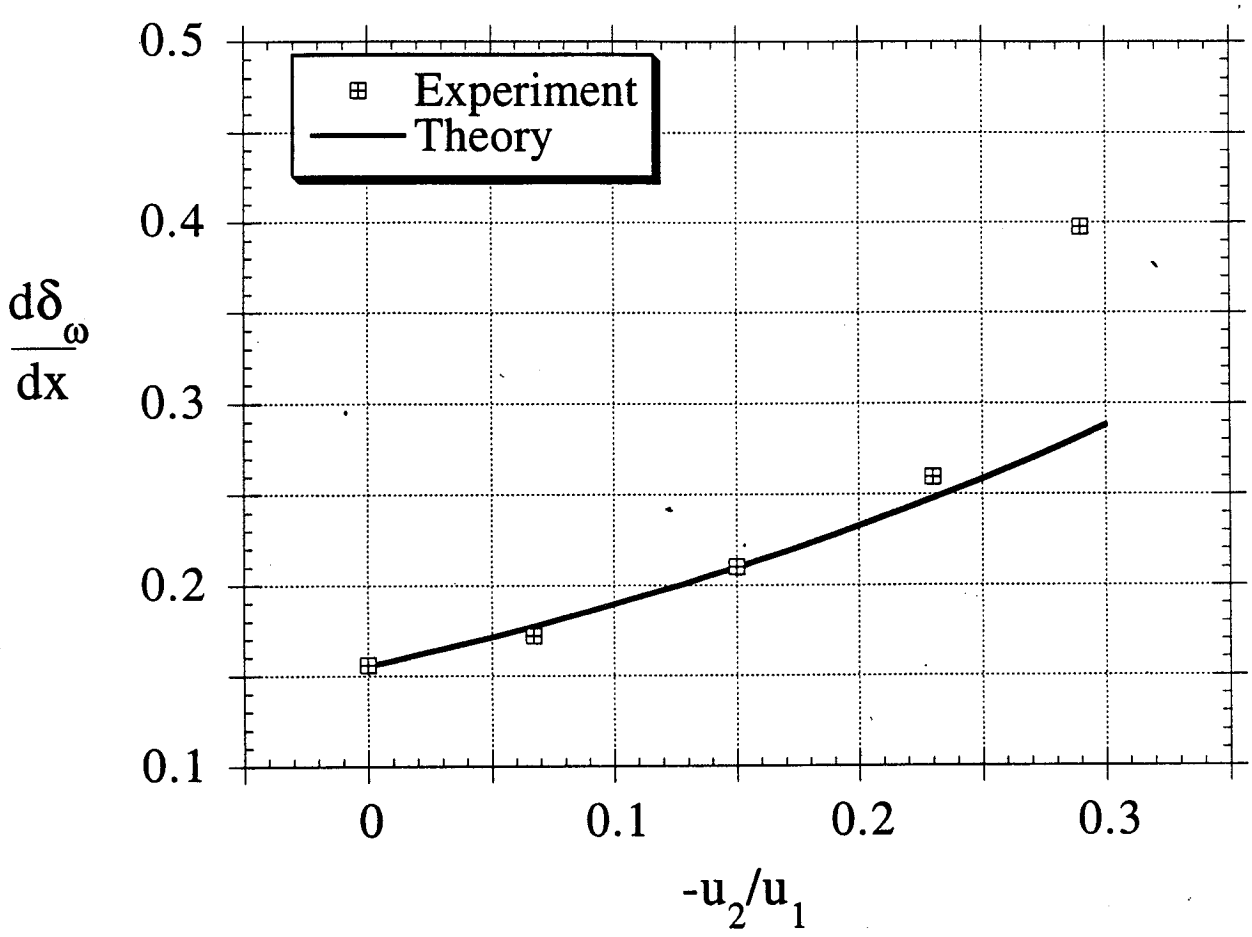

Figure 4.11 Shear layer growth rate, calculated based on potential core length using equation (2.59), vs. velocity ratio. Experimental data uses M=0.5, T_0=300K jet. Solid line represents theoretical prediction set forth by Popamoshou, in equation (2.60).

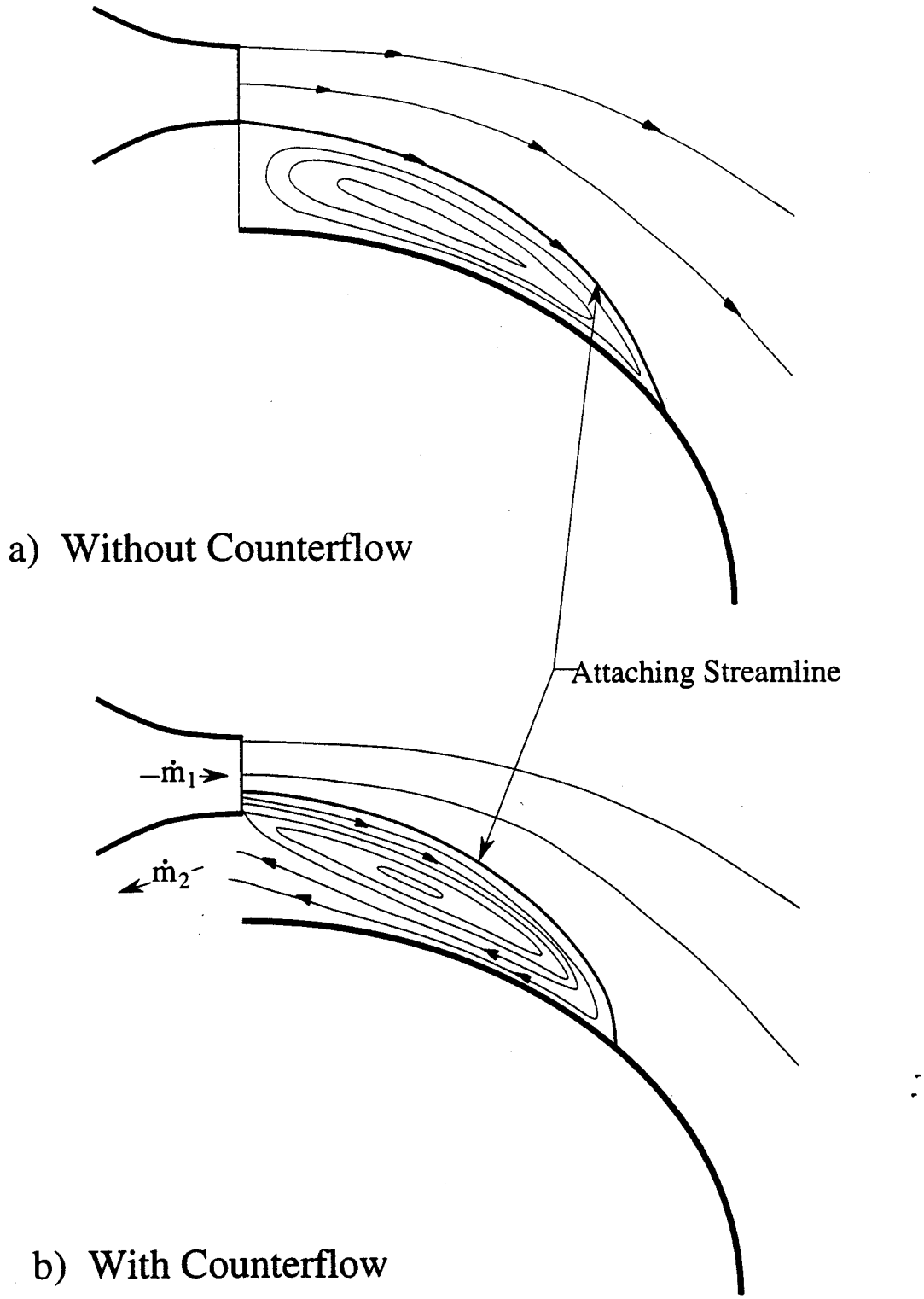

Figure 4.12 Schematic illustrating differences in the nature of the attaching streamline, and surrounding mean flow behavior for counterflowing and non-counterflowing cases

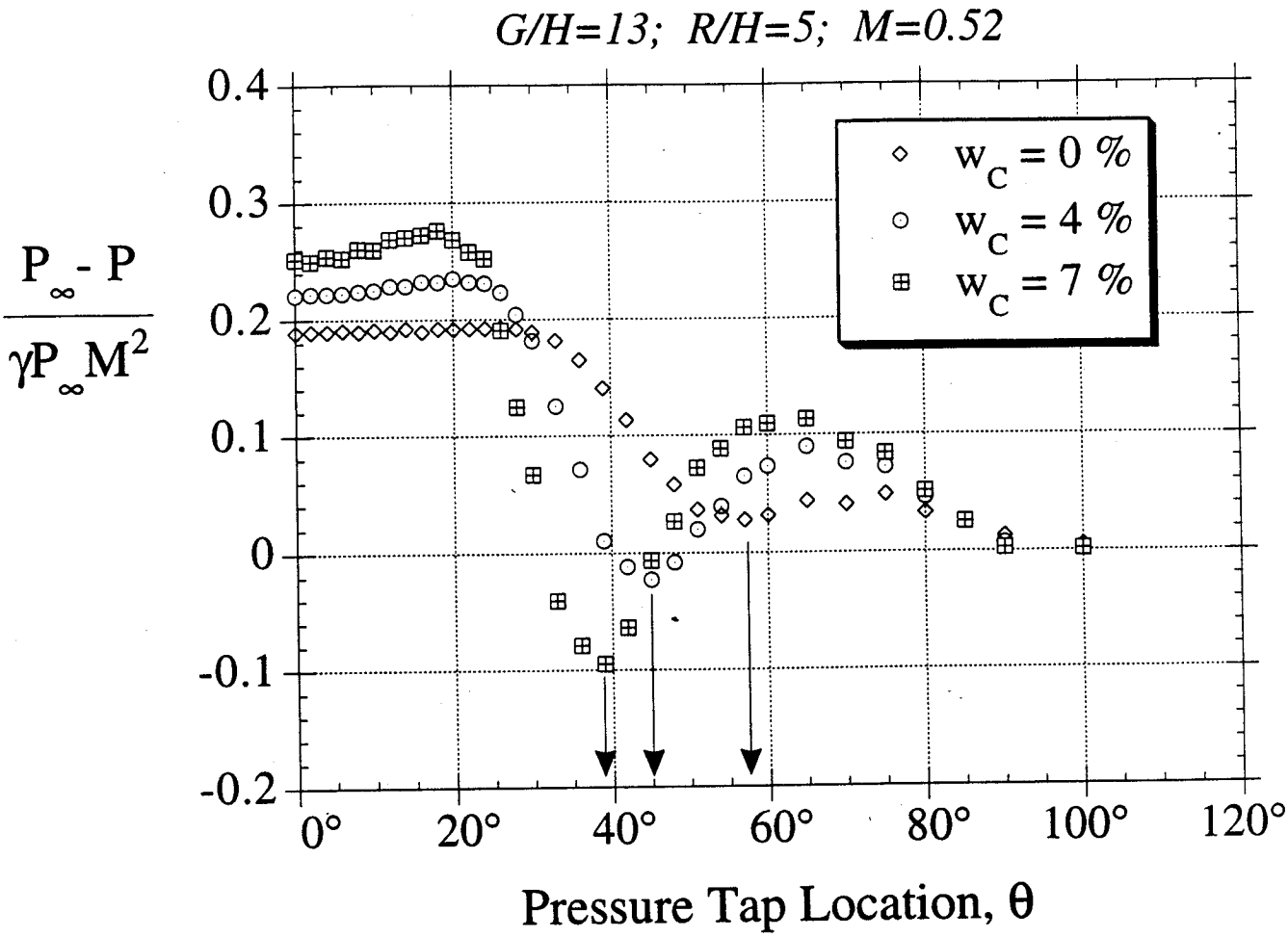

Figure 4.13 Experimentally measure collar pressure profiles for attached jet case with various levels of counterflow. Collar geometry: R/H=5; G/H=1.3; M=0.52;

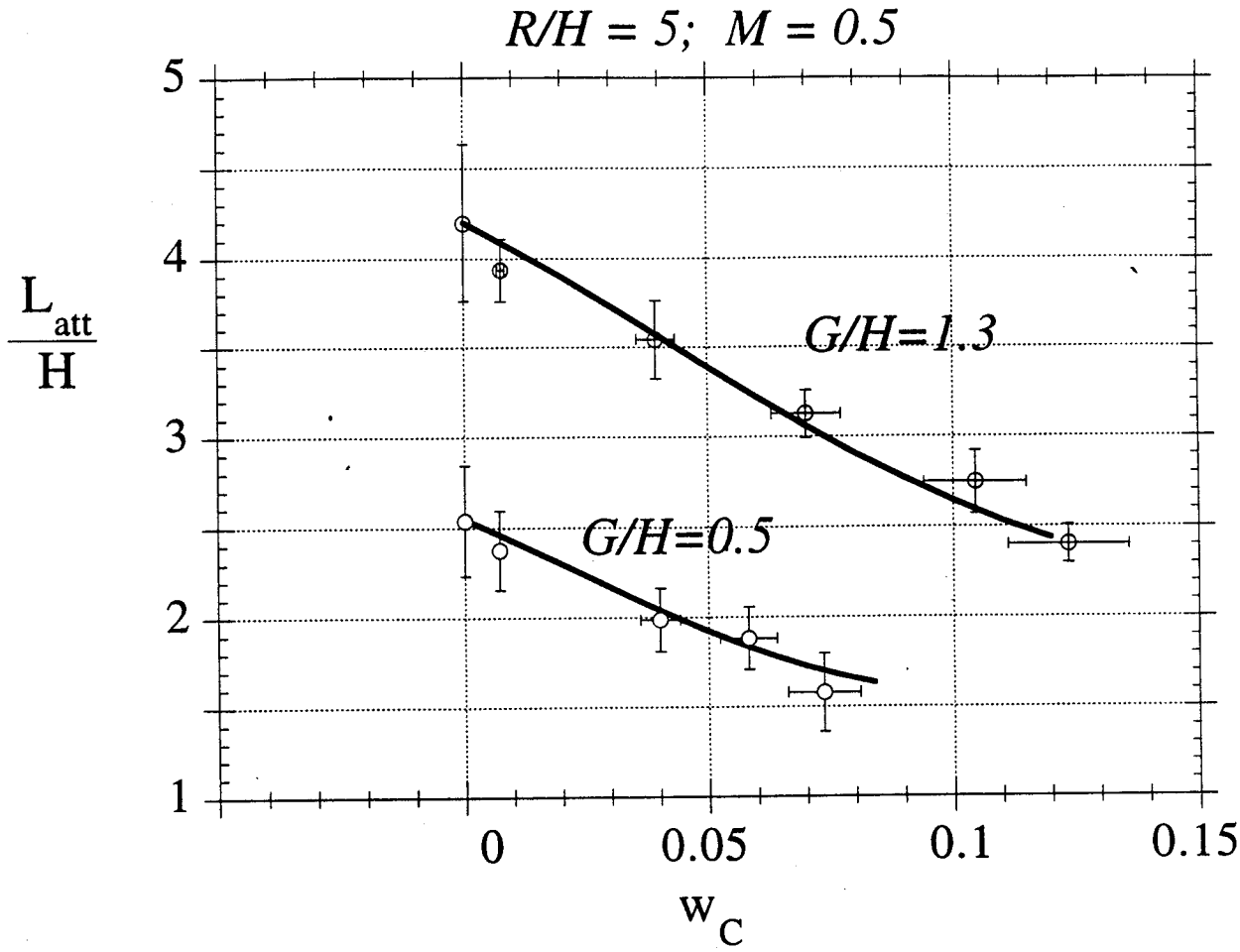

Figure 4.14 Experimentally determined attachment length plotted vs. counterflow ratio for G/H=0.5 and G/H=1.3. For both cases, R/H=5 and M=0.52. Solid lines represent predictions given by the model using ϕ=1.3.

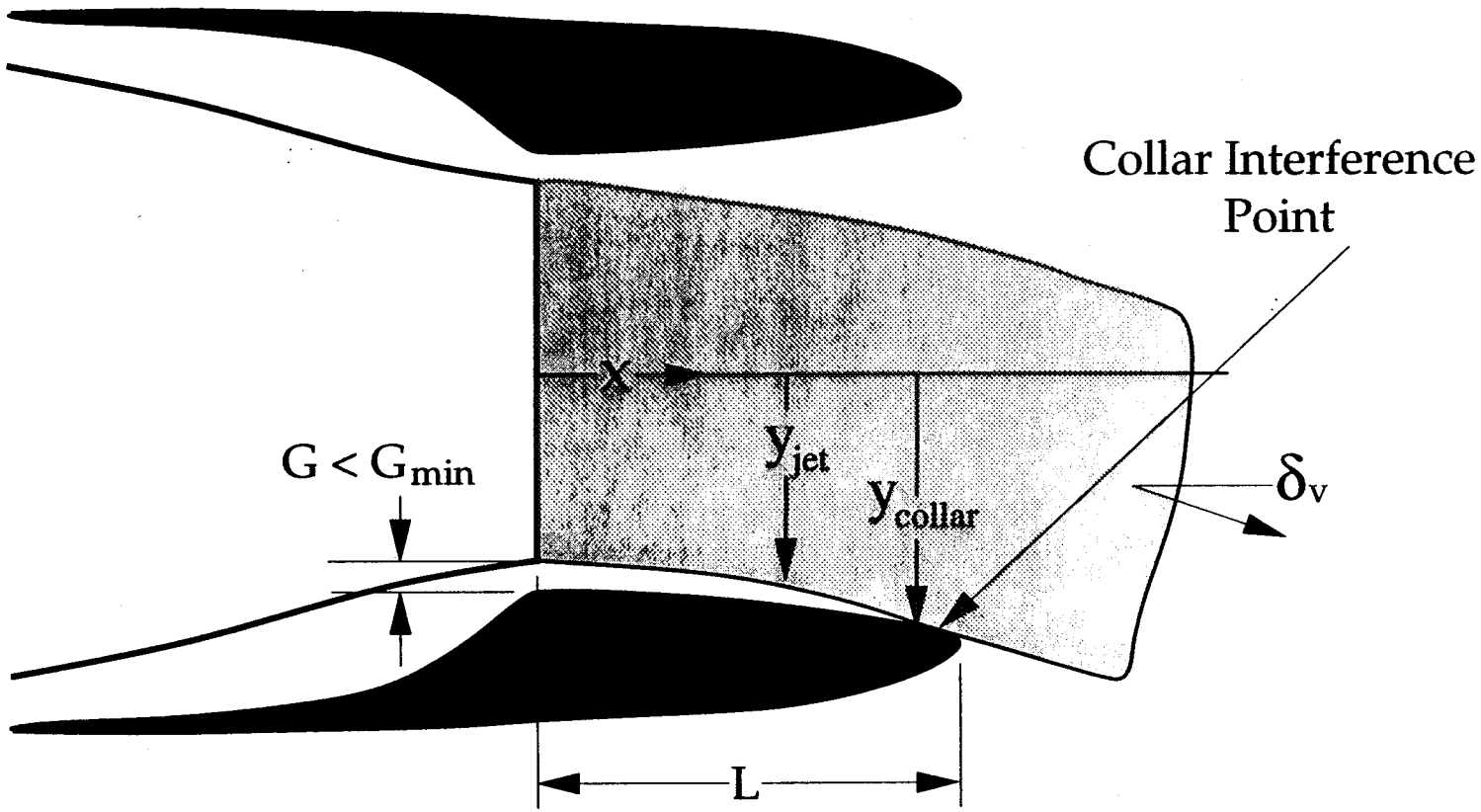

Figure 5.1 Schematic of jet to collar interference which occurs when $G < G_{min}$.

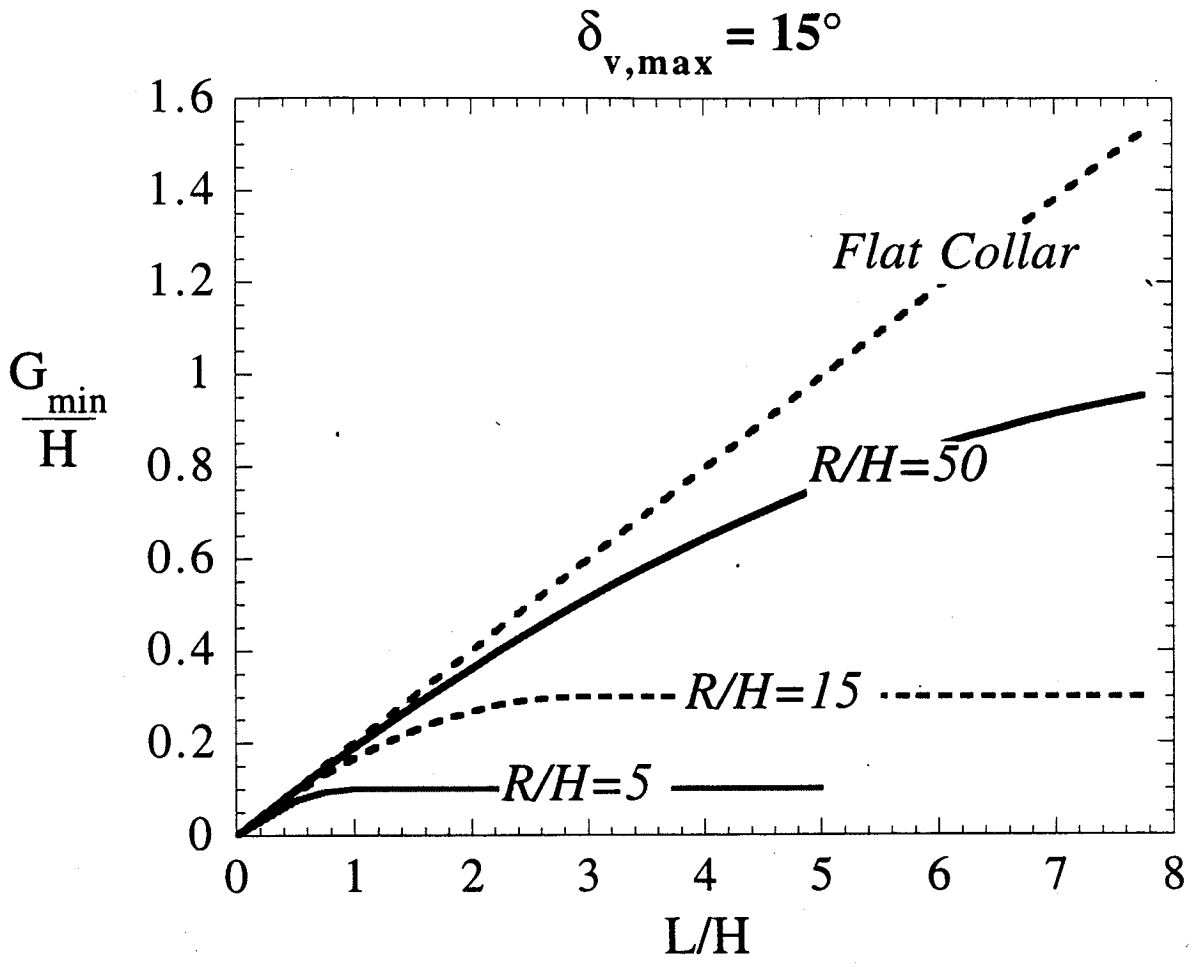

Figure 5.2 Theoretically computed gap width G_{min}, at which jet to collar interference occurs, is plotted as a function of collar length, for various R/H. Conditions represent a vector angle, $\delta_v = 15°$.

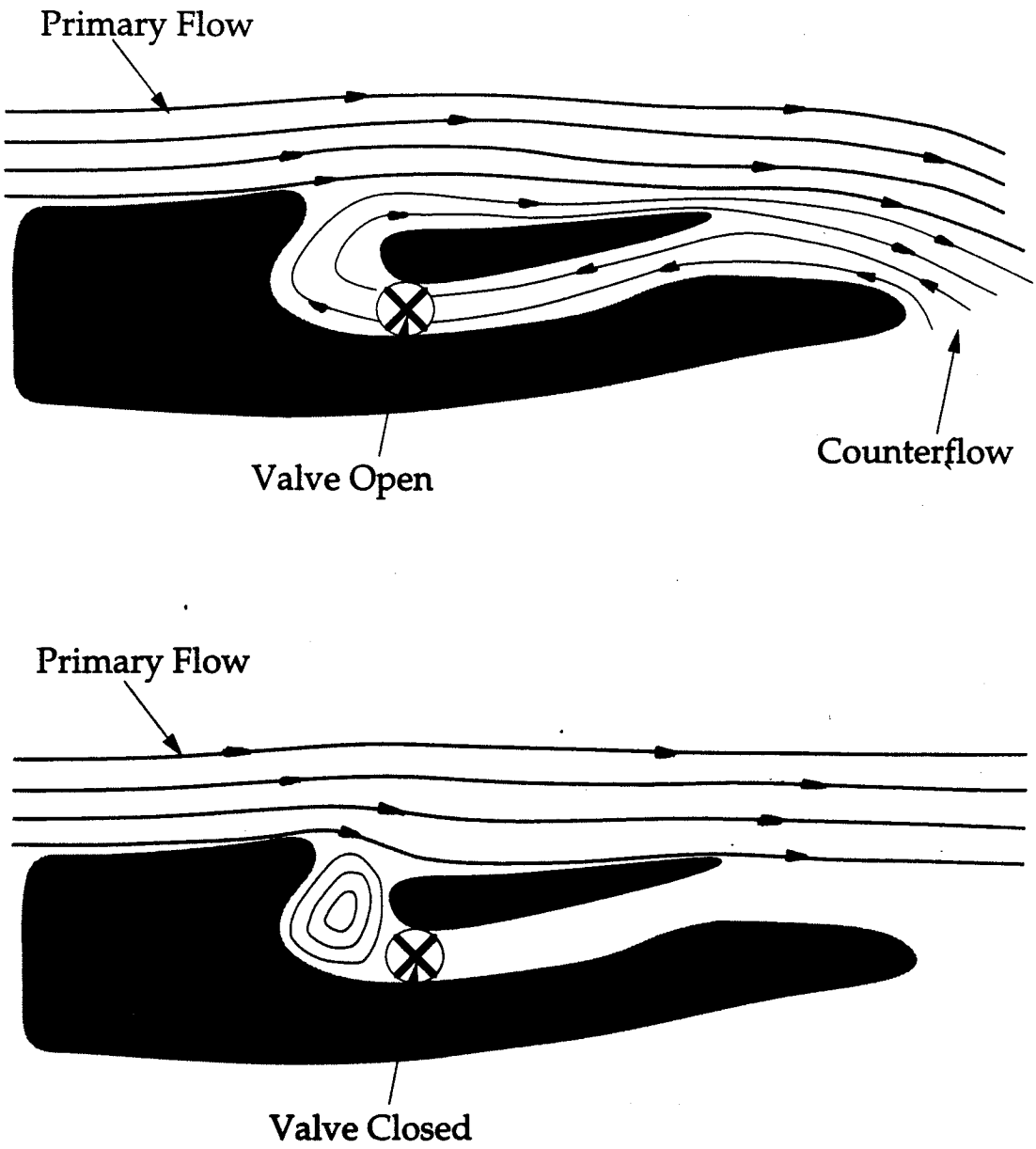

Figure 5.3 Schematic of a passive ejector design that potentially could be used to supply counterflow to CFTV system. When valve are closed, jet flow over abrupt step causes local low pressure zone. Low pressure may be used to pull vacuum when valve opens.

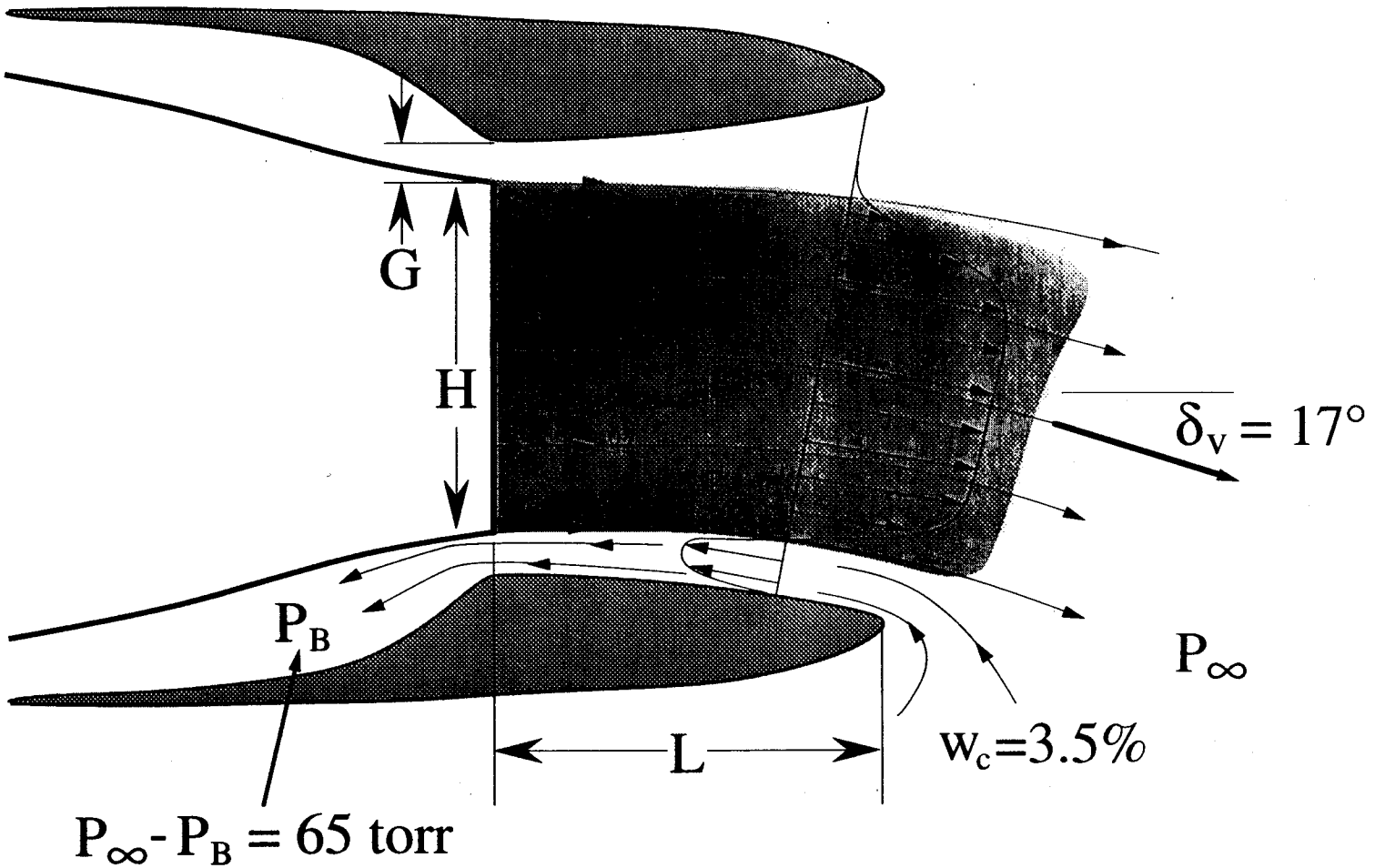

Figure 5.4 Scaled drawing of "optimal" geometry based on drag minimization, and secondary pumping power requirements: L/H=1.15, R/H=6, G/H=0.2.

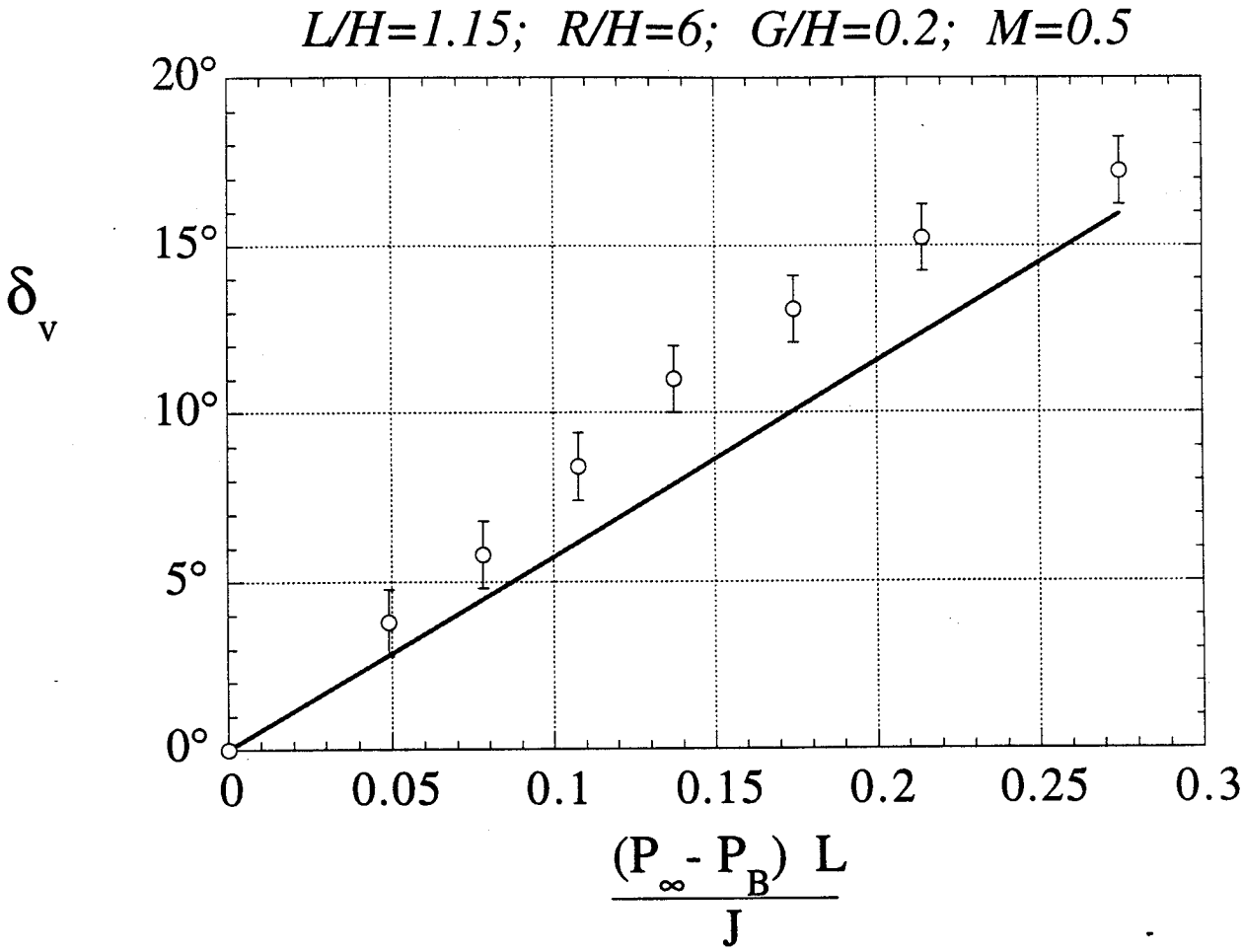

Figure 5.5 Experimentally measured operating curve for "optimal" geometric case: L/H=1.15, R/H=6, G/H=0.2. Collar was designed to vector M=0.5 jet continuously up to δ_v = 17°

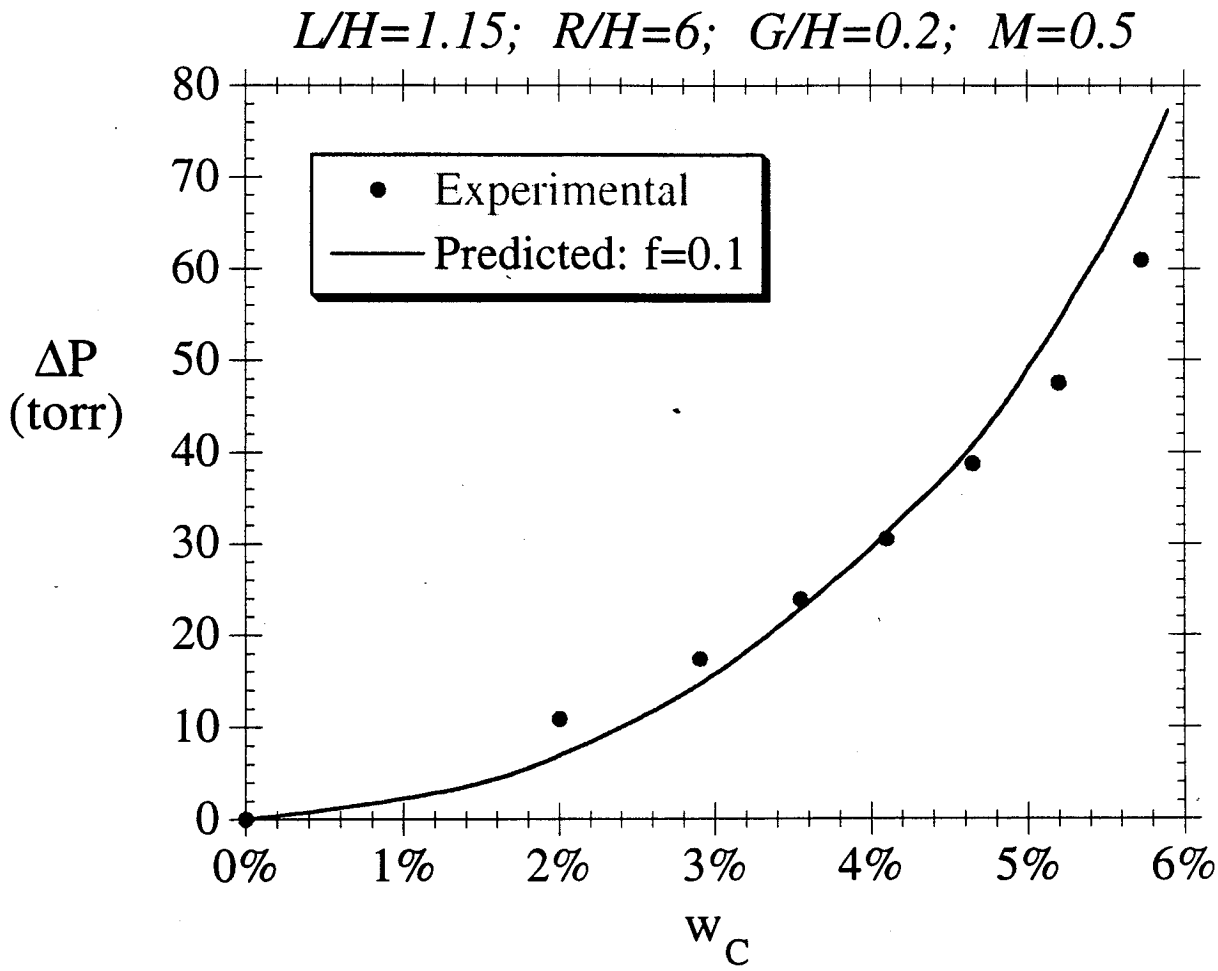

Figure 5.6 Control pressure, $\Delta P = P_\infty - P_B$, is plotted vs. experimentally measured counterflow ratio for "optimal" geometric case: L/H=1.15, R/H=6, G/H=0.2. Solid line represents prediction given by model using f=0.1.